Spatiotemporal Mapping of Electrochemical Diffusion Layers

A Thesis Submitted to the College of
Graduate Studies and Research
In Partial Fulfillment of the Requirements
For the Degree of Masters of Science
In the Department of Chemistry
University of Saskatchewan, Saskatoon

By:
Michael James Lardner

PERMISSION TO USE

In presenting this thesis in partial fulfillment of the requirements for a Postgraduate degree from the University of Saskatchewan, I agree that the Libraries of this University may make it freely available for inspection. I further agree that permission for copying of this thesis in any manner, in whole or in part, for scholarly purposes may be granted by the professor or professors who supervised my thesis work or, in their absence, by the Head of the Department or the Dean of the College in which my thesis was completed. It is understood that any copying or publication or use of this thesis or parts thereof for financial gain shall not be allowed without my written permission. It is also understood that due recognition shall be given to me and to the University of Saskatchewan for any scholarly use of any material in my thesis.

Requests for permission to copy or to make other use of material in this thesis in whole or in part should be addressed to:

Head of the Department of Chemistry

University of Saskatchewan

Saskatoon, Saskatchewan

S7N 5C9

Canada

Abstract

Although pure electrochemical techniques can provide substantial knowledge about electrochemical reaction mechanisms, they lack the ability to provide direct molecular structure information about the species involved. This inability to extract molecular information can result in mechanistic ambiguity with respect to the identity of the reaction intermediates. This information can be obtained by coupling *in situ* spectroscopic methodologies with electrochemical techniques. This is known as spectroelectrochemistry.

A particularly problematic area of study with spectroelectrochemical techniques is the analysis of the mass transport of species within the diffusion layer of the electrode. The visualization of the diffusion layer surrounding electrodes allows for the unambiguous determination of electrode processes. However, a high degree of spatial and temporal resolution is needed as the diffusion layer in a typical electrochemical reaction extends to a thickness of hundreds of microns in tens of seconds.

While traditional infrared spectroelectrochemical techniques have been valuable for the study of electrochemical processes, they do not provide the spatial and/or the temporal resolution that is needed to examine the diffusion layers produced at electrodes. This thesis focuses on the development of an IR technique that couples synchrotron based IR radiation (SIR) with electrochemistry, allowing for the concentrations of species present within the diffusion layer of an electrode to be mapped during an electrochemical reaction.

The reduction of ferricyanide and oxidation of hydroquinone (HQ) are used as test redox systems to study the ability of SIR to map electrochemical diffusion layers. The resulting diffusion coefficients of ferricyanide, ferrocyanide, hydroquinone and benzoquinone are extracted using the IR method developed here and compared to those determined independently by hydrodynamic linear sweep voltammetry (HLSV). The diffusion coefficients of all species as determined by SIR diffusion layer mapping will be shown to be consistent with the diffusion coefficients determined by HLSV. This validates the ability of SIR diffusion layer mapping to monitor electrochemically generated diffusion layers.

Acknowledgements

I would like to thank Dr. Ian Burgess for all of his help, support, guidance and patience and for making my graduate studies an enjoyable experience. Without him, I would have not been exposed to the wonderful world of spectroelectrochemistry, known the joy of running experiments at the Canadian Light Source, nor would the thesis you are about read have been possible.

I would like to thank the other members of the Burgess Empire and its associated members for making every day in the Burgess lab amazing.

A huge thanks to Ted Toporowski, Blair Chomyshen and Jill Cornish of the Physics Machine Shop at the University of Saskatchewan who turned my designs into reality. Without their skillz none of this work would have been possible.

This project would also not be possible without all the support, guidance and suggestions of the Mid-IR beamline scientists, Dr. Ferenc Borondic, Tim May, Dr. Xia Liu and Dr. Scott Rosendahl. Shout out to Dr. Ferenc Borondic for shooting down my first cell design within 5 seconds of seeing it.

Thanks to Dr. Vicki Meli for all her help and support and for suggesting that I pursue graduate studies in the Burgess Group.

I would also like to thank my parents who have given me their love and support every step of the way. I am blessed have you two, your advice and encouragement has been of an unimaginable help throughout these last couple of years. I promise one day you'll understand what I do.

Finally I need to thank my fiancé Emily who came across Canada to join me on this adventure. Having you here has been a blessing. I don't think I would have been able to get through this without you.

Table of Contents

List of Figures

List of Tables

List of Abbreviations

BQ	1,4-Benzoquinone
CV	Cyclic Voltammetry
CμXRF	Confocal MicroX-Ray Fluorescence
D-SC	Double-Step Chronoamperometry
ECL	Electrochemiluminescence
ECSA	Electrochemical Active Surface
EDX	Energy Dispersive X-Ray Fluorescence Microscopy
FEEM	Fluorescence-Enabled Electrochemical Microscopy
HLSV	Hydrodynamic Linear Sweep Voltammetry
HQ	Hydroquinone
IL	Ionic Liquid
IR	Infrared
MCT	Mercury Cadmium Telluride
NA	Numerical Aperture
NMR	Nuclear Magnetic Resonance
OPL	Optical Path Length
PEEK	Polyether Ether Ketone
PMT	Photomultiplier Tube
PVC	Polyvinyl Chloride
RDE	Rotating Disk Electrode
S/N	Signal-to-Noise

SEC	Spectroelectrochemical Cell
SECM	Scanning Electrochemical Microscopy
SEM	Scanning Electron Microscopy
SICM	Scanning Ion Conductance Microscopy
SIR	Synchrotron Infrared Radiation
STXM	Scanning Transmission X-Ray Microscopy
TAA	Trianisylamine
TCNQ	Tetracyanoquinodimethane
UPD	Underpotential Deposition

Chapter 1: Introduction

1.1: Spectroelectrochemistry

Traditionally, electrochemistry involves the measurement of electrical responses such as current, voltage, charge, and capacity as a function of either time or another electrical variable. Although such measurements provide powerful kinetic and/or thermodynamic information concerning chemical processes occurring at electrified interfaces, it has long been recognized that electrochemical measurements do not carry any direct molecular information. Consequently, the molecular identity of species must be inferred based on the values measured in electrochemical experiments. This lack of direct molecular identification of species is a significant weakness of electrochemical methods. The capability to probe the nature of the redox and other species on and near the electrode surface would be of great benefit to understanding electrochemical processes. In order to extract molecular information about the nature of the species present, electrochemical methods must be coupled with additional analytical techniques.

In principle, spectroscopy is ideal for such purposes as molecular and atomic spectroscopies have evolved into highly sensitive tools that are employed ubiquitously in analytical laboratories. This has been recognized in the electrochemical community and electrochemists often use spectroscopy in order to extract important molecular information about electrochemical processes. When the coupling of spectroscopy and electrochemistry occurs in-situ it is called spectroelectrochemistry. However, spectroelectrochemistry is technically very challenging for the simple reason that experimental conditions that support high-quality electrochemical measurements are often diametrically opposed to ideal spectroscopy conditions. Nevertheless there is a diverse range of spectroelectrochemical techniques that employ various spectroscopies including X-ray absorption*(1, 2)*, nuclear magnetic resonance (NMR)*(3-5)*, UV-Vis*(6)*, fluorescence*(7)*, Raman*(8, 9)* and infrared (IR).*(10, 11)*

1.2: IR Spectroelectrochemistry

Of particular interest here and in other studies has been the coupling of IR techniques with electrochemistry.*(12-14)* A major advantage of infrared spectroelectrochemical studies is its sensitivity to both surface and solution species.

The majority of spectroelectrochemical techniques using IR have focused on two major methodologies: internal IR reflection and external IR reflection. As discussed above, a major problem when combining spectroscopy with electrochemistry is technique compatibility. In the case of IR this is manifested in the need to have an electrolyte (often an aqueous solution) which strongly absorbs infrared radiation. Decreasing the concentration of electrolyte leads to highly resistive cells and greatly distorted electrochemical responses. Internal reflection techniques garnered attention for spectroelectrochemical use due to two main factors. The first is the fact that internal reflection techniques eliminate the attenuation of the IR beam by the water solvent. This is accomplished by having the beam impinge from the back side of an IR transparent crystal that supports the electrode. The second is the ability to incorporate surface enhancement*(14)*, which drastically decreases the detection limits. These low detection limits have made this particular technique very attractive for surface sensitive spectroelectrochemical experiments. These techniques are limited by the fact that the electrode must be made of a thin layer of metal deposited on a high refractive index IR transparent substrate, limiting the metals and electrode shapes that can be employed.

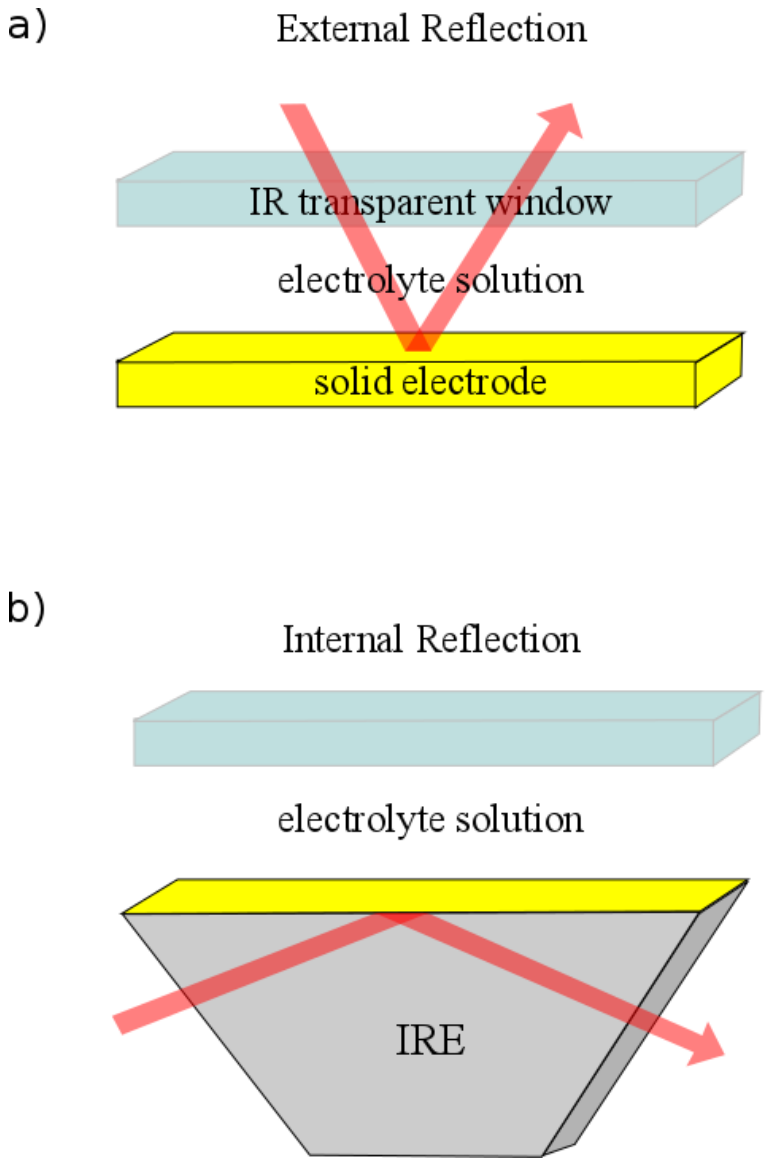

Figure 1.1: External reflection spectroscopy (a) and internal reflection spectroscopy (b) optical geometries. IRE is infrared element, which is a high refractive index IR transparent material.

External IR reflection does not eliminate the absorption by the water solvent and thus requires the use of thin cavity cells to ensure sufficient signal. It does, however, allow for the use of preferred electrode shape and structure and can be used to study process occurring on the surfaces of well-defined single crystal electrodes.*(15, 16)*

While these techniques have proved to be very robust in providing molecular information about species present in electrochemical processes, they are limited by the fact that they only probe the

electrode surface as is the case for internal IR reflection techniques or the entire region near the electrode simultaneously in the case for external IR reflection. Furthermore, for both types of experimental configurations a large spot size is used resulting in spatially unresolved average signals over a large area. This makes these techniques unsuitable for studying speciation within the diffusion layer of the electrochemical interface.

The ability to resolve the spatial distribution of species within the diffusion layer created at the electrode can give valuable information not only about fundamental aspects and the measured response (voltage, current), but also other processes occurring within the vicinity of the electrode. Processes of particular interest are coupled homogenous chemical reactions that occur within the diffusion layer. Broadly speaking, coupled electrochemical and chemical reactions fall into two categories: where the electrochemical process precedes the chemical reaction, called ***EC*** reactions (Figure 1.2a) and where the chemical reaction precedes the electrochemical step called ***CE*** reactions (Figure 1.2b).*(17)* These coupled chemical reactions can have a large effect on overall electrode kinetics. For example, intermediates in these coupled reactions can absorb on the electrode surface, passivating it. This is known as electrode poisoning.*(18)* A spatial and temporal map of the diffusion space around the electrode provides fundamental information such as the diffusion coefficients of the redox and other reactive species as well as reaction rates of the coupled chemical reactions.

a) $A + e^- \rightarrow B$
$B \rightarrow C$

b) $A \rightarrow B$
$B + e^- \rightarrow C$

Figure 1.2: EC reaction scheme (a) and CE reaction scheme (b).

1.3: Diffusion

The diffusion of species to and from the electrode plays an integral role in the responses that are measured and is of great interest for the studies herein. If the rate of electron transfer between the electrode and the redox-active species is sufficiently fast then the observed current will be mass-transport controlled. In the absence of convection and electromigration, the only

mechanism for mass-transport is diffusion. The concentration of any species under diffusion control is a function of both space and time. As the current flowing through the cell is defined by the flux of the redox material at the electrode surface it is apparent that diffusional mass-transport defines the time-dependent current.

The nature of the diffusion layer produced at an electrode is dependent on the electrode geometry which in turn causes differences in the recorded electrochemical responses. The focus here will be the diffusion space around an inlaid band electrode as this is the electrode shape employed in the present study. Fick's second law of diffusion provides the diffusion at an inlaid band electrode*(17)*:

$$\frac{\partial C(x,z,t)}{\partial t} = D\left[\frac{\partial^2 C(x,z,t)}{\partial x^2} + \frac{\partial^2 C(x,z,t)}{\partial z^2}\right] \tag{1.1}$$

With the following boundary conditions:

$$C_{reactant}(x,z,0) = C^*_{reactant} \tag{1.2}$$

$$C_{product}(x,z,0) = 0 \tag{1.3}$$

$$\lim_{x\to\infty} C(x,z,t) = C^*_{reactant} \tag{1.4}$$

$$\lim_{z\to\infty} C(x,z,t) = C^*_{reactant} \tag{1.5}$$

$$C(x,0,t) = 0 \ (t > 0, x \leq W) \tag{1.6}$$

Where $C_{reactant}$ is the concentration of the reactant redox species present, $C_{product}$ is the concentration of product redox species, $C^*_{reactant}$ is the initial concentration of the original redox species present, *z* is the distance perpendicular to the electrode surface, *x* is the distance parallel to the electrode surface and *W* is the width of the electrode. The diffusion space is shown in Figure 1.3.

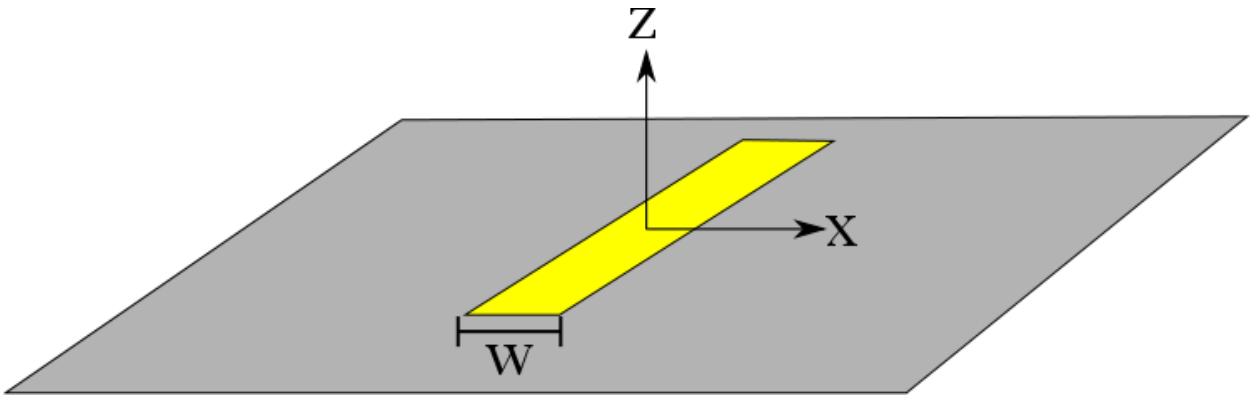

Figure 1.3: Diffusion space for an inlaid band electrode (gold) in an insulating material (grey).

At short times, the thickness of the diffusion layer is very small compared to the length scale of the electrode and the diffusion space grows linearly along the z-direction (perpendicular to the electrode surface). In this limiting case the resulting current can be approximated using the Cottrell equation:

$$i(t) = \frac{nFAD^{1/2}C^*}{\pi^{1/2}t^{1/2}} \tag{1.7}$$

Where *n* is the number of electrons transferred, *F* is Faraday's constant, *D* is the diffusion coefficient of the original redox species present and C^* is the initial concentration of the original redox species present. At longer time, diffusion along the x-direction can no longer be ignored, which results in a diffusion layer that is hemispherical in nature. The current from hemispherical diffusion around an in-laid band electrode is given by:*(17)*

$$i(t) = \frac{2\pi nFADC^*}{w \cdot \ln(64Dt/w^2)} \tag{1.8}$$

Where *w* is the width of the electrode, *ln* is the natural logarithm and all other variables have the same designation. This shows that the current developed at band electrodes never reaches a steady-state and is always dependent on time.

The above boundary conditions and resulting solutions to Fick's equation apply when semi-infinite conditions exist in the z and x directions. As will be discussed later in this thesis, diffusion at band electrodes is complicated if the cell volume is small and asymmetrically restricted. Restricted geometries result in no obtainable analytical solution to Fick's second law. Numerical methods are then required for diffusion analysis of complicated cell geometries.

1.4: Thesis Goals

The focus of the work presented in this thesis is the development and verification for the use of synchrotron infrared radiation (SIR) as a spectroscopic probe for monitoring the spatiotemporal evolution of diffusion layers created at an electrode surface during an electrochemical reaction. The thesis aims to verify the hypothesis that SIR provides a powerful and unique means to accurately map the spatiotemporal evolution of electrochemical diffusion layers.

In order to realize SIR as a probe to monitor these diffusion layers many technical aspects had to be overcome. In particular a major challenge has been the design of a spectroelectrochemical cell (SEC) that would allow the IR beam to be placed adjacent to the electrode of interest without obstructing the beam. To realize this, a divergence from the usual internal and external reflection IR techniques was required, as transmission of the IR beam through the solution is needed rather than reflection from the electrode surface is required.

The designed SEC had to also allow for highly reproducible measurements. Infrared spectroscopy is inherently a low signal to noise technique and requires the co-addition of many replicate experiments (ensemble averaging). To be effective, every individual measurement in the ensemble must be highly reproducible such that only the noise and not the signal is degraded in the co-addition process. In a spectroelectrochemical experiment this amounts to ensuring that the electrochemical response is invariant over the course of many (several hundred) replicate measurements.

The motivation for using SIR as the IR source for diffusion layer mapping is the fact that it can be focused to diffraction limited spot sizes (~10 μm), while still having substantial photon throughput. This gives SIR the spatial resolution that is required to probe electrochemical diffusion layers that are typically in the range of 250 μm. To utilize the spatial resolution capabilities of SIR required the synchronous triggering of time resolved IR measurements with the onset of the electrochemical reaction. This synchronous triggering needed to be done in such a way that several hundred replicate measurements could be done without variation in either the electrochemical or IR response. Details of the extensive method development required to achieve the synchronous triggering of the electrochemical reaction with the acquisition of IR data in such a way that the spectroscopic data can be used to monitor the spatial and temporal evolution of the diffusion layer is described in this body of work.

1.5: Scope of the Thesis

Chapter 2 endeavors to give an overview of the previous techniques that have been implemented to monitor the evolution of diffusion layers created during electrochemical processes. This chapter is broken into three sections. The first section discusses electrochemical methods that have been previously used to examine diffusion layers, in particular scanning electrochemical microscopy (SECM). Electrochemical methods have revolved around the use of SECM because it provides the required spatial resolution needed to perform diffusion layer mapping. A comparison between potentiometric and amperometric measurements used in SECM will be discussed. The second section will examine optical techniques that have been successfully implemented to probe diffusion layers. These techniques include UV-Vis spectroscopy, Raman spectroscopy and fluorescence spectroscopy. The various methods and specific techniques that are used to implement these different spectroscopies will be discussed. The advantages and disadvantages of these methods will be considered. The third section examines X-ray techniques. X-ray methods to probe diffusion layers are the most recent addition to the available methods for diffusion layer mapping. The first use of scanning transmission X-ray microscopy, which offers unparalleled spatial resolution, to follow an electrochemical reaction will be discussed. The work by Peng *et al(19)* on the development of

confocal micro-X-ray microscopy of diffusion layer mapping will be examined along with Uematsu *et al's(20)* use of energy dispersive X-ray fluorescence microscopy.

Chapter 3 will look at the electrochemical and infrared spectroscopic techniques that were used to implement diffusion layer mapping via SIR. The theory behind the electrochemical techniques of cyclic voltammetry, hydrodynamic linear sweep voltammetry and chronoamperometry will be discussed at the beginning of this chapter. From there the focus will shift to infrared spectroscopy, with the theoretical foundations of vibrational spectroscopy being initially laid out. The associated instrumentation used in infrared spectroscopy, in particular the Michelson interferometer and infrared microscopy will be subsequently examined. The aspects of the time resolved measurements used here will likewise be examined. The final section will discuss globar and synchrotron sources of infrared radiation. The goal of this chapter is to give the reader the required background information needed in order to understand the diffusion layer mapping technique developed here.

The method and details of the IR measurements used to obtain the diffusion layer maps, along with the analysis of the measured IR data that results in the final concentration profiles for the redox species at various distances from the electrodes will be discussed in Chapter 4. Considerations in the design of a spectroelectrochemical cell (SEC) that allows for the IR beam to be positioned adjacent to a working electrode will be provided. The various SEC designs will also be discussed.

This chapter will also look at the use of hydrodynamic linear sweep voltammetry (HLSV) to independently determine the diffusion coefficients of ferricyanide, ferrocyanide, benzoquinone (BQ) and hydroquinone (HQ). Additionally, the determination of the molar extinction coefficients of both BQ and HQ in D_2O used in the analysis of the oxidation of HQ data will be described. Afterward, the technical aspects involved in the diffusion layer mapping will be discussed in some detail. This discussion will focus on the importance of reproducible electrochemistry within the SEC. Furthermore, the investigation into the IR beam shape and the way in which the use of a slightly defocused beam and blade aperture instead of circular aperture leads to improved spatial resolution will be described.

A treatise of the numerical simulations of the diffusion space that are needed to model the experimental concentration transients within the SEC will be given. This will include details

concerning how diffusion coefficients of the redox species are extracted and the comparison of experimental and simulated concentration *versus* time curves.

Chapters 5 and 6 will focus on the diffusion layer mapping studies of the two sample redox systems: the reduction of ferricyanide to ferrocyanide and the oxidation of hydroquinone to benzoquinone. These two redox couples were used as the test redox cases for diffusion layer mapping by SIR. The ferri/ferrocyanide redox was the first redox couple to be investigated. Diffusion layer mapping of the ferri/ferrocyanide redox couple shows that SIR can spatially and temporally resolve the redox species within the diffusion layer. However, the simulation of the resulting concentration transients resulted in diffusion coefficients for ferricyanide and ferrocyanide that were considerably lower than the literature values. The details behind this discrepancy are discussed at length. The oxidation of HQ was studied using an improved cell design to test if the discrepancy was systematic.

In Chapter 7 the diffusion coefficients of both the redox couples will be considered in considerable depth in an effort to reconcile the resulting discrepancy between diffusion coefficients determined by the diffusion layer mapping here and those previously done by Arvia *et al.(21)* It will be shown that the diffusion coefficients determined independently by HLSV and those determined by diffusion layer mapping are, in fact self-consistent, validating the use of the SIR methodology to extract quantitative data about the molecular species.

Finally, in Chapter 8 the improvements that could be made to the SEC and the methodology that would result in the ability to study a wider range of electrochemical systems as well as improve the spatial resolution of this SIR methodology will be discussed. Of particular interest is the use of this diffusion layer mapping to study EC type reactions. This will be a large focus of the suggested future work for the further growth of the diffusion layer mapping methodology developed here.

1.6: References

1. Kondo, T.; Masuda, T.; Aoki, N.; Uosaki, K. Potential-Dependent Structures and Potential-Induced Structure Changes at Pt(111) Single-Crystal Electrode/Sulfuric and Perchloric Acids Interfaces in the Potential Region between Hydrogen Underpotential Deposition and Surface Oxide Formation by In situ Surface X-ray Scattering. *J. Phys. Chem. C* **2016,** Just Accepted, **DOI:** 10.1021/acs.jpcc.5b12766.

2. Grunder, Y.; Mosselmans, J. F.; Schroeder, S. L. M.; Dryfe, R. A. W. In Situ Spectroelectrochemistry at Free-Standing Liquid-Liquid Interfaces: UV-vis Spectroscopy, Microfocus X-ray Absorption Spectroscopy, and Fluorescence Imaging. *J. Phys. Chem. C* **2013,** *117*, 5765-5773.

3. Klod, S.; Ziegs, F.; Dunsch, L. In Situ NMR Spectroelectrochemistry of Higher Sensitivity by Large Scale Electrodes. *Anal. Chem.* **2009,** *81*, 10262-10267.

4. Wu, J.; Day, J.,B.; Franaszczuk, K.; Montez, B.; Oldfield, E.; Wieckowski, A.; Vuissoz, P. o. m.; Ansermet, J. Recent progress in surface NMR-electrochemistry. *J. Chem. Soc. , Faraday Trans.* **1997,** *93*, 1017-1026.

5. Bussy, U.; Giraudeau, P.; Silvestre, V.; Jaunet-Lahary, T.; Ferchaud-Roucher, V.; Krempf, M.; Akoka, S.; Tea, I.; Boujtita, M. In situ NMR spectroelectrochemistry for the structure elucidation of unstable intermediate metabolites. *Analytical & Bioanalytical Chemistry* **2013,** *405*, 5817-5824.

6. Pruiksma, R.; McCreery, R. L. Observation of electrochemical concentration profiles by absorption spectroelectrochemistry. *Anal. Chem.* **1979,** *51*, 2253-2257.

7. Yu, Z. L.; Casanova-Moreno, J.; Guryanov, I.; Maran, F.; Bizzotto, D. Influence of Surface Structure on Single or Mixed Component Self-Assembled Monolayers via in Situ Spectroelectrochemical Fluorescence Imaging of the Complete Stereographic Triangle on a Single Crystal Au Bead Electrode. *J. Am. Chem. Soc.* **2015,** *137*, 276-288.

8. Jeanmaire, D. L.; Van Duyne, R. P. Surface Raman Spectroelectrochemistry. *Journal of Electroanalytical Chemistry and Interfacial Electrochemistry* **1977,** *84*, 1-20.

9. Fleischmann, M.; Hendra, P. J.; McQuillan, A. J. Raman spectra of pyridine adsorbed at a silver electrode. *Chemical Physics Letters* **1974,** *26*, 163-166.

10. Bewick, A.; Kunimatsu, K.; Stanley Pons, B. Infrared spectroscopy of the electrode-electrolyte interphase. *Electrochim. Acta* **1980,** *25*, 465-468.

11. Pons, S.; Davidson, T.; Bewick, A. Vibrational spectroscopy of the electrode-solution interface. 2. Use of Fourier transform spectroscopy for recording infrared spectra of radical ion intermediates. *J. Am. Chem. Soc.* **1983,** *105*, 1802-1805.

12. Pons, S.; Datta, M.; McAleer, J. F.; Hinman, A. S. Infrared spectroelectrochemistry of the Fe(CN)64−/Fe(CN)63− redox system. *Journal of Electroanalytical Chemistry and Interfacial Electrochemistry* **1984,** *160*, 369-376.

13. Jin, B.; Liu, P.; Wang, Y.; Zhang, Z.; Tian, Y.; Yang, J.; Zhang, S.; Cheng, F. Rapid-Scan Time-Resolved FT-IR Spectroelectrochemistry Studies on the Electrochemical Redox Process. *J Phys Chem B* **2007,** *111*, 1517-1522.

14. Miyake, H.; Okada, T.; Samjeske, G.; Osawa, M. Formic acid electrooxidation on Pd in acidic solutions studied by surface-enhanced infrared absorption spectroscopy. *Phys. Chem. Chem. Phys.* **2008,** *10*, 3662-3669.

15. Prieto, F.; Su, Z.; Leitch, J. J.; Rueda, M.; Lipkowski, J. Quantitative Subtractively Normalized Interfacial Fourier Transform Infrared Reflection Spectroscopy Study of the Adsorption of Adenine on Au(111) Electrodes. *Langmuir* **2016,** *32*, 3827-3835.

16. Martinez-Hincapie, R.; Berna, A.; Rodes, A.; Climent, V.; Feliu, J. M. Surface Acid-Base Properties of Anion-Adsorbed Species at Pt(111) Electrode Surfaces in Contact with CO2-Containing Perchloric Acid Solutions. *J. Phys. Chem. C* **2016,** Just Accepted, **DOI:** 10.1021/acs.jpcc.6b00589.

17. Bard, A. J.; Faulkner, L. R. *Electrochemical Methods: Fundamentals and Applications*, 2nd ed.; John Wiley and Sons Inc: New York, New York, 2001.

18. Seidel, Y. E.; Schneider, A.; Jusys, Z.; Wickman, B.; Kasemo, B.; Behm, R. J. Mesoscopic mass transport effects in electrocatalytic processes. *Faraday Discuss.* **2009,** *140*, 167-184.

19. Peng, S.; Liu, Z.; Sun, T.; Ma, Y.; Ding, X. Spatially Resolved In Situ Measurements of the Ion Distribution Near the Surface of Electrode in a Steady-State Diffusion in an Electrolytic Tank with Confocal Micro X-ray Fluorescence. *Anal. Chem.* **2014,** *86*, 362-366.

20. Uematsu, T.; Han, J.; Tsuda, T.; Kuwabata, S. Metal-Ion Diffusion in Ionic Liquid Studied by Electrochemical Scanning Electron Microscopy with X-ray Fluorescence Spectrometry. *J. Phys. Chem. C* **2012,** *116*, 20902-20907.

21. Arvía, A. J.; Bazán, J. C.; Carrozza, J. S. W. The diffusion of ferro- and ferricyanide ions in aqueous potassium chloride solutions and in solutions containing carboxy-methylcellulose sodium salt. *Electrochim. Acta* **1968,** *13*, 81-90.

Chapter 2: Literature Review

2.1: Introduction

Electrochemists have known for a long time that purely electrochemical techniques cannot provide molecular information about the species involved in electrochemical process. Therefore, the nature of the species involved in the electrochemical process must be inferred based on the resulting electrochemical signal (current, potential, etc.) measured. Furthermore, it is known that the current produced at the electrode is dependent on the concentration gradient of the species in the area adjacent to the electrode. Determining the exact concentration of redox species can be complicated due to the presence of coupled chemical reactions. Electrochemical analysis can be complicated further by the fact that some of the species can affect the electrochemical reaction through poisoning of the electrode.*(1)* Being able to determine the distribution of the individual species in the area adjacent to the electrode (known as the diffusion layer) during an electrochemical reaction would allow for the unambiguous determination of the processes occurring therein.

This chapter will examine existing literature reporting various methods that have been used to map diffusion layers that are produced at an electrode during electrochemical processes.

2.2: Scanning Electrochemical Microscopy

Scanning electrochemical microscopy (SECM) is a powerful electrochemical technique developed in the 1980's that uses a special four electrode setup. Two electrodes serve as the conventional counter and reference electrodes. The two others act as the probe and working electrode. In SECM a small probe electrode whose potential/current is controlled/monitored is placed adjacent to a working electrode (Figure 2.1).*(2)*

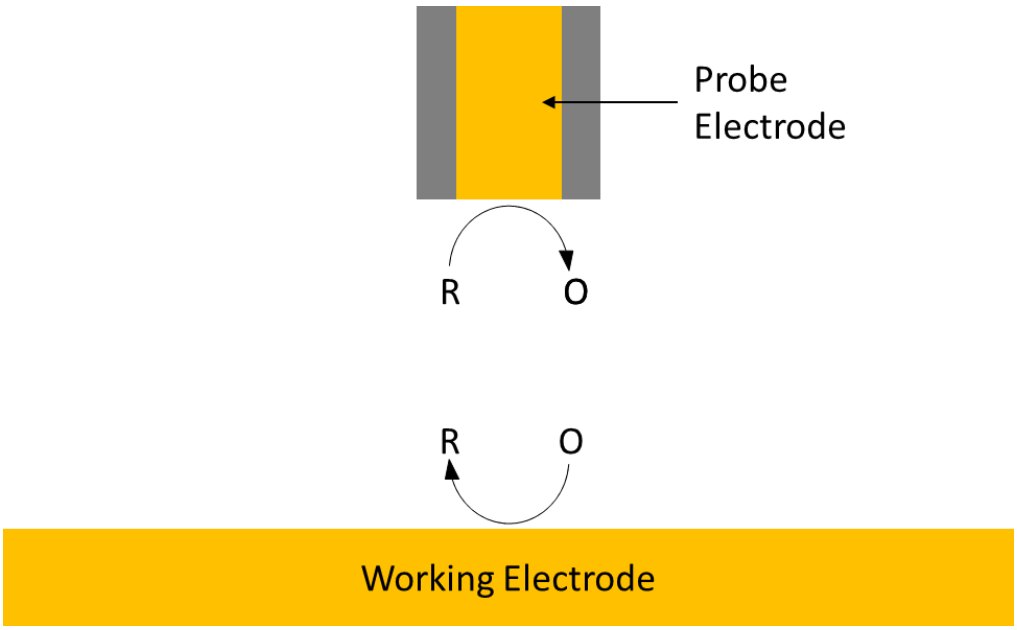

Figure 2.1: Scanning electrochemical microscopy setup running in amperometric measurement mode.

The probe electrode allows for the monitoring of species within the vicinity of the working electrode. With SECM there are two measurements that are typically done for the mapping of diffusion layers, potentiometric and amperometric. In potentiometric measurements an electrochemical reaction is triggered and the potential at the probe electrode is monitored. This potential is related to the relative amount of redox species present at the probe electrode surface. In amperometric measurements, like potentiometric measurements an electrochemical reaction at the working electrode is triggered. However, the probe electrode is set to a potential where the reverse electrochemical reaction occurs and the current resulting from this reverse reaction is monitored. The resulting current can be related to the concentration of the species present at the probe electrode.*(2)* As seen in Figure 2.1 the probe electrode is placed near the working electrode, the presence of the probe can restrict diffusion of species to the working electrode surface. As such care must be taken to use a probe that is of a sufficiently small size so that its presence does not disrupt the resulting diffusion layer. This clearly represents a disadvantage for diffusion layer mapping

It was realized by Engstrom and co-workers that if the probe electrode position could be precisely controlled in the direction normal to the working electrode surface that the diffusion

produced at the working electrode could be spatially monitored.*(3)* Engstrom and co-workers' initial study employed a 10 µm probe electrode and analyzed the oxidation of ferrocyanide using the amperometric measurement method.*(3)* They were able to improve their method by employing a carbon fiber probe electrode with a considerably smaller diameter. The use of smaller working electrodes allowed for faster amperometric measurements as a steady state current is reached in a shorter amount of time.*(4)* This improved method allowed for the accurate measurement of redox species concentrations and time scales between 50 ms and 500 ms. Impressively, they were able to probe the EC reaction of dopamine, where they were able to follow various species concentrations. This allowed for the differentiation between two proposed mechanisms for the overall process.*(4)*

From these initial studies the use of SECM has been adapted to study not only diffusion layers produced at solid electrodes, but also those produced at polarized liquid-liquid interfaces of two immiscible fluids.*(5)* Monitoring the concentrations near the interface, Zhang *et al* were able to visualize the ion transport of ferrocenium ions across the interface. The ability to monitor this transfer allowed the contributions of electron transfer and ion transfer to the overall current measured to be separated. This decoupling between the current contributed by electron transfer and that contributed by ion transport is not distinguishable using conventional electrochemical methods.*(5)*

Another adaptation of SECM has allowed for the diffusion of oxygen across the air-water interface with a monolayer of 1-ocatanol present at the interface.*(6)* This study was able to monitor the diffusion of oxygen across the interface at varying surface pressures of the 1-octanol, showing that the ability of oxygen to cross the interface decreased as the surface pressure of the 1-ocatanol monolayer increased.

All of the SECM methods discussed so far have utilized amperometric measurements. These amperometric measurements may not always be the appropriate choice. This is due to the fact that some of the species produced at the working electrode may not be redox active or if they are, the potential at which they are redox active lies outside the potential window of the solvent. Amperometric measurements can also disrupt the diffusion layer at the working electrode, as the composition of the solution in the vicinity of the probe electrode is altered from that of the surrounding solution. This change in composition can disrupt the diffusion of species in the

local vicinity leading to anomalous currents. This is particularly problematic at small interelectrode distances as the probe electrode reproduces the initial redox species, providing positive feedback to the working electrode.

To solve this problem many groups have used potentiometric measurements and have coupled them with ion selective membranes. Potentiometric measurements prevent the disruption of the diffusion layer and the ion selective membranes allows only the ion of interest to be probed. Ion selective potentiometric SECM analysis of diffusion layers have been applied to selectively monitor NH_4^+, K^+, Zn^{2+} and H^+ ions.*(7-9)* While these measurements eliminate the problems of the amperometric measurements, they do suffer from two major drawbacks. The first being the technical difficulty in producing the ion selective probe electrode at sufficiently small size such that it does not interfere with diffusion to the working electrode. The other is the difficulty in determining the interelectrode distance between the working electrode and the probe electrode. In amperometric measurements the measured current at the probe along with the known diffusion coefficients of the redox species are used to determine the interelectrode distance. These potentiometric measurements do not have access to this method of determination of the interelectrode distance as the resistance of the ion selective membrane is too large to allow accurate determination. Bard *et al* produced a probe tip that consisted of an ion selective membrane electrode and a silver/silver chloride electrode typically used as a reference electrode for the determination of interelectrode distance.*(7)*

Momotenko *et al* have used a variation on SECM called scanning ion conductance microscopy (SICM), where a change in the conductance of the solution is used to probe the presence of ions in the diffusion layer. SICM avoids the technical problems of producing a probe electrode as it only requires a glass capillary to be pulled to a sufficiently small diameter, typically ~10 μm.*(10)* This is simple compared to the capillary pulling, silanization and deposition of the ion selective membrane that is needed to produce ion selective electrodes.*(7)* The fact that SICM measures a change in conductance means that it does not provide any selectivity. Thus, the resulting conductance change is proportional to the total change of ions within the tip and not just the ions of interest. This greatly complicates the analysis of the distribution of the species of interest, but can be simplified if no supporting electrolyte is present.

Amatore and co-workers have extensively studied the use of SECM to map diffusion layers. These studies focus on the comparison of potentiometric and amperometric methods to effectively probe the concentration of species with the diffusion layers generated at electrodes. These studies examined the oxidation of ferrocyanide and the reduction of tetracyanoquinodimethane (TCNQ).*(11, 12)* The motivation for using TCNQ is its interesting electrochemical behavior. TCNQ can be first reduced to $TCNQ^{\bullet-}$ and subsequently to $TCNQ^{2-}$, however TCNQ and $TCNQ^{2-}$ readily conproportionate to form two $TCNQ^{\bullet-}$ molecules. This added homogenous reaction complicates the distribution of species within the diffusion layer, making it a very interesting system.

Both potentiometric and amperometric measurements have been shown to be capable of monitoring the speciation of molecules within the diffusion layer for the oxidation of ferrocyanide and the reduction of TCNQ.*(11, 12)* Both methods have independently shown that in the case where the potential at the working electrode is set to trigger the second reduction of TCNQ, the diffusion layer is split into two regions: an inner diffusion layer and an outer diffusion layer. In the inner diffusion layer close to the electrode, only $TCNQ^{\bullet-}$ and $TCNQ^{2-}$ exist. In the outer region of the diffusion layer only TCNQ and $TCNQ^{\bullet-}$ exist. At the intersection of these two layers there is a small overlap of both TCNQ and $TCNQ^{2-}$ where they react to form $TCNQ^{\bullet-}$. As such $TCNQ^{\bullet-}$ reaches its maximum concentration at this point.*(11, 12)* It is clear that both measurement types are capable of monitoring distribution of species within the diffusion layer, but both techniques suffer from drawbacks. In the case of potentiometric detection the main problem is the fact that it only produces ratios of the concentrations and additional information is needed to extract precise concentrations. Potentiometric measurements also suffer from the fact that the measurement times are on a length scale such that only steady state diffusion at the working electrode can be probed, so transient processes cannot be studied.*(11)*

In the case of amperometric measurements, the reverse reaction at the probe electrode disrupts the diffusion layer of the working electrode, which can lead to artificially high currents as discussed above. Amperometric measurements also require that both species in the redox couple be redox active.*(12)* However, the current amperometric measurements are directly related to species concentration and the measurement times are short enough that transient processes can

be observed. These features make amperometric measurements more attractive than potentiometric measurements and became the focus of further studies.*(12)*

Amatore and co-workers noticed during potentiometric measurements that the current would deviate from the expected result, particularly at longer times when the diffusion layer extended into solution beyond 60-70 µm.*(12)* Similar behavior was also seen by Engrstrom in his initial work using amperometric measurements. Engstrom suggested that this deviation could arise from three factors; the recycling of redox species between the probe and working electrode, shielding of the working electrode from the probe electrode, preventing diffusion of species to the electrode and natural convection.*(4)* Natural convection is the microscopic movement of solution in a macroscopically still solution. This fluid movement is difficult to characterize as it arises from sources that are not easily quantified, such as vibrations, air current and thermal gradients. Amatore and co-workers were able to eliminate the first two causes for the current deviation proposed by Engstrom and attributed the deviation solely to natural convection. To account for natural convection Amatore developed a model that incorporates the effect of enhanced mass transport with an apparent diffusion coefficient. This apparent diffusion coefficient increases with increased distance from the electrode to account for the presence of natural convection.*(13)* The incorporation of this apparent diffusion coefficient has been used to successfully model diffusion layers out to several hundred microns.*(13-15)*

It is clear that SECM techniques offer a powerful set of methods to spatially resolve the distribution of species within the diffusion layer, but they do suffer drawbacks. In the case of ion selective membrane electrodes, it is technically demanding to produce electrodes of a sufficiently small size and there are issues with determining the interelectrode distance. SICM lacks molecular specificity as the measurement takes into account the change in the overall ion concentration and not just the ion of interest. Amatore and co-workers have highlighted the issues with potentiometric measurements in that they only produce concentration ratios and cannot study transient processes. For amperometric measurements problems arise from disruption of the diffusion layer of the working electrode as well as the fact that in order to be detected, the species must be redox active.

2.3: UV-Vis

Initial studies of diffusion layers produced at electrodes using UV-Vis spectroscopy involved imaging the interference pattern produced by a refractive index gradient at the electrode during an electrochemical reaction.*(16-18)* This method does provide an effective means of monitoring the deposition or corrosion of metals*(19, 20)*, but the resulting interference pattern produced by the refractive index gradient is a product of the overall concentration change at the electrode and thus this method like SICM does not provide specificity. If the redox species also doubles as the electrolyte species then the interference pattern is produced purely from the species of interest.*(19, 20)* Also, in order to produce sufficient refractive index gradients a concentration in the molar range of the redox species must be used instead of the millimolar range typically employed in electrochemical studies.

McCreery and co-workers developed a method based on absorption spectroscopy to monitor species in a diffusion layer rather than the previous methods based on interference.*(21)* In these studies a micron sized beam that was positioned at various distances from the electrode surface within the diffusion layer and the resulting absorbance was detected by a photomultiplier tube (PMT). This was achieved by using light from a laser source, micron width slits and a micro positioner to direct the beam parallel to the electrode surface.*(21)* In these initial studies McCreery and co-workers were able to follow the concentration changes of the cation radical of N,N,N', N'-tetramehtylparaphenylenediamine during its production at the electrode, but the resulting concentrations did not show agreement with those predicted for a diffusion limited process via Fick's second law. This deviation was particularly pronounced at distances less than 50 μm and greater than 200 μm from the electrode. This method was improved by using a cell design with smaller slits as well as better alignment of the beam. Nevertheless, large deviations still appeared at 20 μm from the electrode and the overall concentration changes still did not agree well with those predicted by a diffusion limited electrode reaction. It was found that this deviation was systematic as similar results were found when the solvent and redox couple were changed.*(22)*

Suspecting that diffraction/refraction effects of light were causing the deviation, simulation of the absorbance data was done when the slit was placed at the electrode surface. Various slit widths were used to account for the larger volume that would be interrogated due to these

effects. It was found that the absorbance corresponded to a slit width of ~ 25 μm, which is significantly larger than the 3 μm slits used. This indicates that a larger volume is probed than that selected by the slits.*(22)* These diffraction/refraction effects will be particularly problematic at positions close to the electrode, but should be negligible at larger distances. As such, the deviation at larger distances was attributed to natural convection.

From these studies, McCreery and co-workers recognized that the electrode size must be reduced in order to limit these effects. The new cell employed a radical new design. The electrode in the new design had a thickness of 15 μm (compared to the 500 μm used in the older design) and a photodiode array was utilized instead of a PMT. In this configuration a wider collimated beam is passed by the electrode. It is then magnified and imaged by the photodiode array, resulting in each pixel of photodiode interrogating a 1.25 μm segment of the beam and allowing for the entire diffusion layer to be imaged simultaneously.*(23, 24)* This design resulted in significantly better agreement between the resulting concentration changes and those predicted by theory. This agreement also extended over a greater range with agreement being seen as close as 8 μm away from the electrode. At closer distances the diffraction/refraction effects are present and result in deviation.

The ability of the photodiode array to image the entire diffusion layer simultaneously was used to image the change of absorbance of trianisylamine (TAA) during a cyclic voltammogram (CV). Select points on the CV curve were probed, showing the changes in the TAA absorbance as the potential was varied.*(24)* This indicates that concentrations of redox species can be followed during dynamic processes.

To enhance the capabilities of the UV-Vis absorbance spectroelectrochemical method they developed, McCreery and co-workers opted to use a xenon lamp instead of a laser. The xenon lamp continuum source allowed for multiple species to be observed. This ability to monitor multiple species does come at the cost of spatial resolution and also a decrease in temporal resolution as the xenon arc lamp's lower power requires longer acquisition times.*(25)*

Efforts have been made to probe the diffusion layers around electrodes of various shapes via this UV-Vis method. These studies have focused on the diffusion layers produced at cylindrical and hemispherical electrodes.*(26, 27)* The analysis of diffusion layers at these electrodes is complicated by the fact that the beam will interrogate a gradient of concentrations as it passes

through the diffusion layer produced at these electrodes as depicted in Figure 2.2. The analysis of the resulting absorbance requires that each of the different concentrations the beam interrogates as it passes through the diffusion layer to be accounted for.

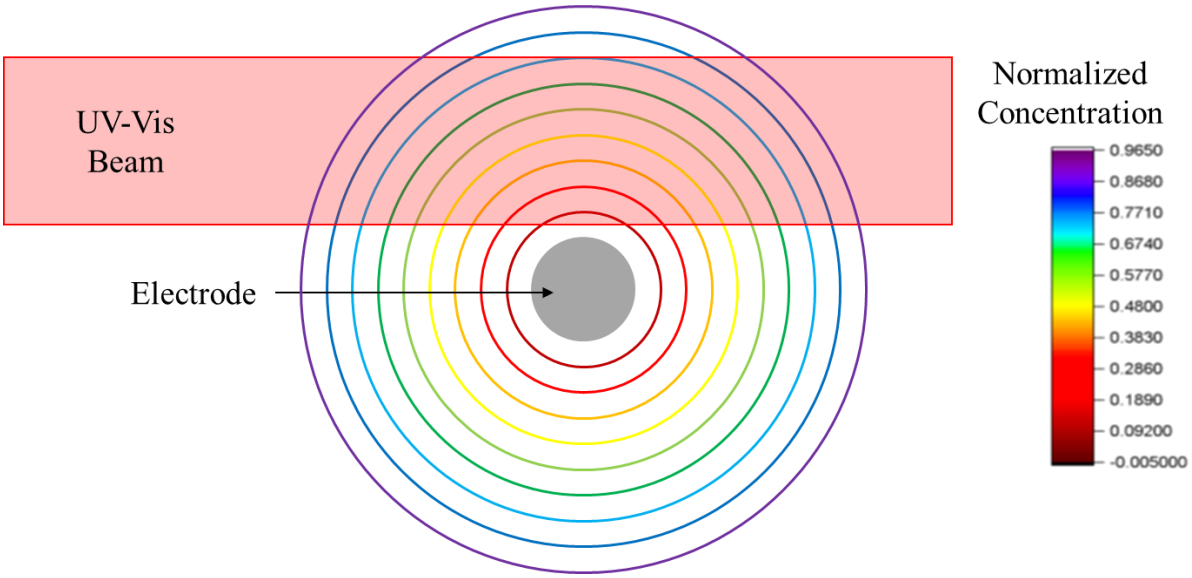

Figure 2.2: UV-Vis beam passing through the diffusion layer of a cylindrical electrode.

The analysis of the diffusion layers at spherical and cylindrical electrodes show a much greater deviation between predicted and experimental concentrations. Studies by Wu *et al*, a lateral movement of the diffusion layers around a cylindrical electrode was noticed. This movement varied in the time of onset as well as in magnitude and direction between each individual experiment.*(26)* It was found that smaller diameter electrodes resulted in greater movement and faster onset, with the onset being noticed in as little as 100 ms after triggering the electrochemical reaction at a cylindrical electrode of 12 µm diameter.*(26)* Using larger diameter electrodes, placing the cell and components on a vibration isolation table along with waiting 5 to 10 minutes after stirring the solution to ensure quiescence was found to increase the stability of the diffusion layer. This increase in stability was not very reproducible with deviations still seen at short times.*(26)* Wu *et al* attributed this lateral movement to the presence of natural convention within the solution, which is enhanced in the case of cylindrical electrodes, because unlike planar electrodes there is no large surface surrounding the electrode that impedes fluid movement.*(26)* Interestingly, Posdorfer *et al* did not observe this large movement of fluid at

cylindrical electrodes nor did they see it in their studies of diffusion layers at hemispherical electrode. However, this could be due to the fact that the diameter of the cylindrical electrode they used was much larger.*(27)* It is possible that the larger electrode impedes fluid motion in the vicinity of the electrode leading to a more stable system.

The advancement of imaging and optics technology has allowed the seminal work by McCreery on diffusion layer mapping using UV-Vis absorption spectroscopy to be adapted to a variety of systems of interest. Olbrich-Stock *et al* have used this method to monitor the growth of diffusion layers during the electropolymerization of thiophene.*(28)* Ruiz and co-workers have used it to look at ion transfer across polarized liquid-liquid interfaces as well as the deposition of platinum nanoparticles at polarized liquid-liquid interfaces.*(29, 30)* It has even been adapted for use with optical microscopy in order to follow the diffusion of protons across An ion-selective membrane.*(31)*

UV-Vis absorption spectroelectrochemistry has been developed into a powerful technique for the study of diffusion in electrochemical reactions. It offers a major advantage over SECM methods in that it is non-invasive, therefore it does not disrupt the evolving diffusion layer at the electrode. In UV-Vis absorbance spectroscopy, however the absorption bands in solution are quite broad, which can lead to difficulty in identifying the species present and knowing their concentrations accurately if there is significant overlap of the signals.

2.4: Raman

Studies of electrochemically generated diffusion layers using Raman spectroscopy have centered around the use of confocal microscopy in order to provide the spatial resolution needed to monitor the evolution of a diffusion layer produced at an electrode. The first attempt to monitor diffusion layers was by Ozeki *et al*, who used Raman microscopy. In these studies the microscope was used to place the focal point of the laser at various distances from the electrode surface and to monitor the resulting Raman signal during an electrochemical reaction. While this method did show a change in concentration of the electroactive species, that change was not as expected; a strong signal was still seen when the focal point was set beyond the electrode surface.*(32)* They attribute these recorded signals to reflection of the laser from the electrode and into solution, with the recorded signal arising due to this reflected beam. This indicates that

the spatial resolution of this method is quite poor, resulting in averaging of the Raman signal over large areas.

Through the use of confocal Raman microscopy the resolution is greatly enhanced as it allows for a select volume to be interrogated. Amatore and co-workers successfully utilized the spatial resolution capabilities of confocal Raman microscopy to monitor the distribution of $TCNQ^{\bullet-}$ during the reduction of TCNQ.*(33, 34)* This method like SECM was able to monitor the distribution of $TCNQ^{\bullet-}$ within the diffusion layer and show that when the potential was set to the second reduction of TCNQ, that the diffusion layer was segregated into two segments as described above. However, unlike SECM this method could only probe the presence of $TCNQ^{\bullet-}$, as a laser source was used so that it exhibited Resonant Raman Effect in order to produce enough signal to be monitored at the millimolar concentrations used. As a result, the concentrations of TCNQ and $TCNQ^{2-}$ had to be determined by using conservation of fluxes, which can be an issue, as the diffusion coefficients must be known. They also encountered a problem with the accurate positioning of confocal volume due to the changes in the refractive index of the solution that occur at the electrode during an electrochemical reaction. This effect is more pronounced as the length of solution that the beam passes through increases. At a path length of 170 μm the vertical resolution was found to be 4 μm and around 10 μm for a 1 mm path length.*(33)* Despite these issues, Amatore and co-workers were able to monitor the distribution of TCNQ, $TCNQ^{\bullet-}$ and $TCNQ^{2-}$ with excellent agreement to those that are predicted from Fick's second law.

Confocal Raman microscopy has also been used to monitor the electrodeposition of copper. This work unlike the work by Amatore did not require the movement of the confocal volume to monitor the diffusion layer. Instead, the volume was positioned just beyond the electrode and the composition within the volume recorded as the electrode grew during the deposition.*(35)* Through this analysis Texier *et al* were able to break the deposition into three phases. An initial slow growth stage, a fast growth phase and finally a relaxation phase. They were also able to observe the adsorption of H_2 and elucidate its role in the electrodeposition process.*(35)*

The use of Raman spectroscopy has not received as much attention for monitoring diffusion layers as either SECM or UV-Vis spectroscopy, mainly because of the fact that the signals produced by the analytes at concentrations typically used in electrochemical experiments would be too small.

2.5: Fluorescence

Similar to Raman spectroscopy, some fluorescence techniques have taken advantage of the spatial resolution of confocal microscopy to monitor diffusion layers. These studies have used fluorescence to monitor the pH profiles produced at electrodes during an electrochemical reactions that involves coupled proton transfer. (Figure 2.3)

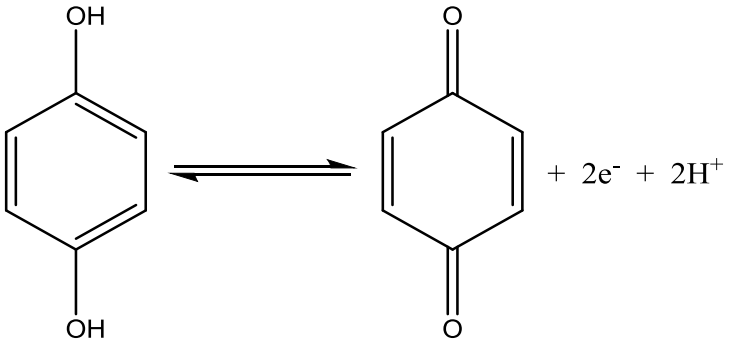

Figure 2.3: Example of an electrochemical reaction that involves coupled proton transfer. Oxidation of hydroquinone to benzoquinone.

The growth of the pH gradient was monitored using a pH sensitive fluorophore whose fluorescence intensity varied as a function of pH.*(36-39)* Unwin and co-workers have used this method to examine the pH gradients produced at disk electrodes during the reduction of benzoquinone and the reduction of water. They also implemented it to look at pH gradients of water reduction at ring electrodes.*(36, 37)* During their analysis of the reduction of water at disk and ring electrodes they simulated the resulting pH profile and found that good agreement could be obtained by incorporating natural convection using the method developed by Amatore.*(37)* Unwin extended this work to monitor the diffusion of organic acids across a lipid bilayer.*(38)* The visualization of the pH gradient in this work allowed the transport of various organic acids across the lipid membrane to be monitored and the resulting permeation coefficient of each of the acids to be determined.*(38)*

Leenheer *et al* have taken advantage of this method to monitor the effectiveness of water splitting catalysts.*(39)* They show that under galvanostatic conditions (constant current) that an increase in electrode area results in a much larger area of pH change. They were also able to

examine the catalytic ability of various metals for water splitting, as well as the effects of electropolishing the electrodes. They prepared parallel electrodes consisting of nickel, platinum, silver and gold. The pH gradient around the electrodes was monitored before and after electropolishing. The conditioning consisted of cycling the potential to a point where the metal surface was oxidized to remove surface contaminates. Before electropolishing, silver and platinum show activity for water reduction, with no activity for nickel and gold. After electropolishing the platinum electrode showed a large increase in activity, the gold electrode showed some activity, but the silver and nickel electrodes showed no activity. This decrease in the silver activity is due to the fact that the oxidation caused dissolution of the silver electrode.*(39)*

Leenheer *et al* discuss the fact that the switch from low fluorescence intensity to high fluorescence of the fluorophore only occurs over a narrow pH range. Only if the pH change spans the values where the fluorophore alters its fluorescence intensity can the profiles be monitored. This requires that the initial pH of the solution be selected so that the change in pH occurs over the narrow range such that fluorescence intensity varies.*(39)*

Another related method that utilizes fluorescence confocal microscopy is electrochemiluminescence (ECL). The main difference between ECL and fluorescence confocal microscopy is that the resulting fluorescence is a result of the ECL reaction in solution. The studies by Amatore *et al* use the ECL to map the reaction between $Ru(bpy)_3^+$ and $Ru(bpy)_3^{3+}$ that produce two $Ru(bpy)_3^{2+}$, with one being in an excited state that fluoresces.*(40)* By following this fluorescence they were able to monitor the spatial distribution of this reaction at various distances from the electrode. However, this is not very useful as only the reaction can be followed and not the entire diffusion layer.

Zhang and co-workers have developed a fluorescence technique that does not utilize confocal microscopy to provide spatial resolution for monitoring diffusion layers. Their fluorescence-enabled electrochemical microscopy (FEEM) method couples the electrochemical reaction with the electrochemical production of the fluorophore via a bipolar electrode, shown in Figure 2.4. Using this setup they have been able to correlate the intensity of the fluorescence produced on one side of the bipolar electrode to the electrochemical reaction on the other side of the electrode.*(41)*

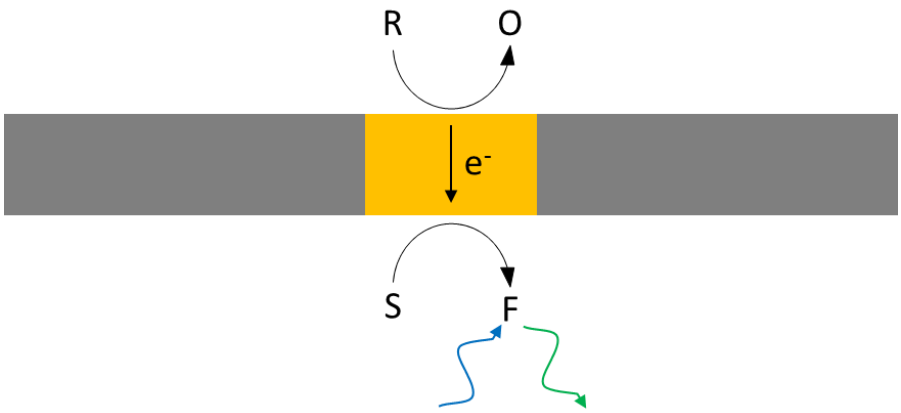

Figure 2.4: Coupling of an electrochemical reaction and electrochemical production of an active fluorophore via a bipolar electrode as used in FEEM. O is the oxidized species, R is the reduced species, S is the inactive form of the fluorophore and F is the active form of fluorophore.

To implement this for diffusion layer mapping they used an array of bipolar electrodes in an insulator that separates two solutions. One side contains only the precursor to the fluorophore and the other side contains the redox species for the electrochemical reaction of interest. Similar to SECM, a small electrode is placed adjacent to the bipolar electrode array and the electrochemical reaction is triggered at the same time the bipolar electrode is polarized. The reverse electrochemical reaction happens at the bipolar electrode on the side containing the redox species and the production of the fluorophore is produced on the other side (Figure 2.5). In this setup the fluorescence produced can be related to the concentration of the redox species at the bipolar electrode. Furthermore, by adjusting the distance between the bipolar array and the electrode, the diffusion layer around the electrode can be mapped.*(42)*

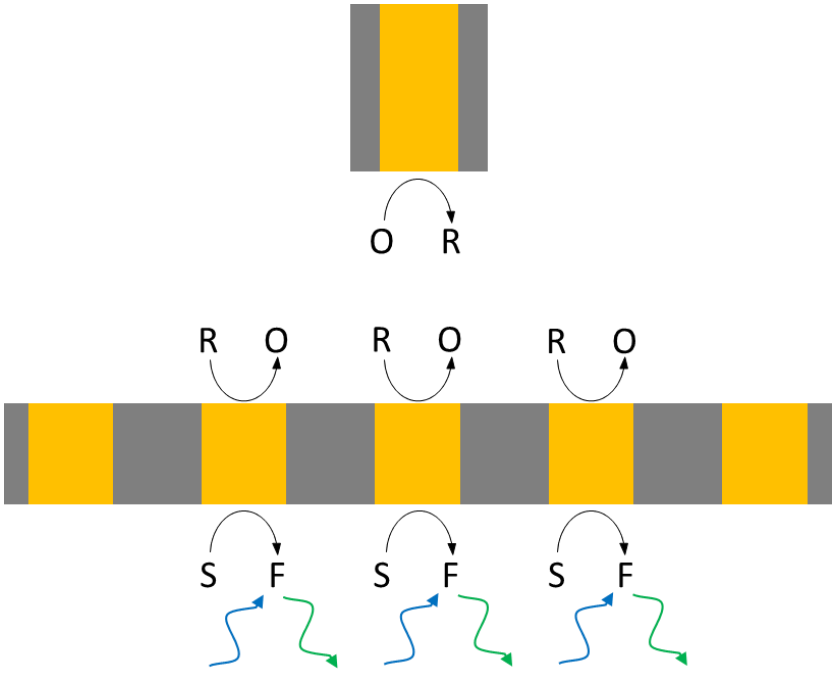

Figure 2.5: FEEM setup used to monitor diffusion layers.

Oja *et al* were able to monitor the concentration during the reduction of ferrocyanide at a small 10 µm diameter carbon fiber electrode. The use of the bipolar electrode array also allowed discrimination between the diffusion layers produced by two 10 µm diameter carbon fiber electrodes that were placed 147 µm apart and were at slightly different distances to the array.*(42)*

This method suffers from the problem of disruption of the diffusion layer at the working electrode, similar to the case of SECM. This arises at distances between the electrode and the array of less than 20 µm as the large bipolar electrode array impedes diffusion of ferrocyanide to the electrode. Beyond 20 µm there does not appear to be any interference from the array on the diffusion to the electrode.*(42)*

The final fluorescence method that will be discussed has been developed by Amatore *et al*, where they use an optical fiber bundle to trigger and monitor the fluorescence of diffusing species at an electrode.*(43)* In this method the optical fiber bundle is placed on a large 3 mm diameter disk electrode, with the individual 3-4 µm optical fibers in the bundle providing the needed spatial resolution to monitor the diffusing species during the electrochemical reaction. In this study the fluorescent $Ru(bpy)_3^{2+}$ is oxidized to the non-fluorescent $Ru(bpy)_3^{3+}$. Unlike

fluorescence confocal microscopy or FEEM this method is used for the direct observation of the redox species, which allows for much easier determination of the concentrations of the redox species as the fluorescence is directly related to the concentrations of the redox species.

Through this method, Amatore *et al* were able to follow the production of the $Ru(bpy)_3^{3+}$ and the consumption of $Ru(bpy)_3^{2+}$, with the concentration profiles showing good agreement to those predicted by Fick's second law beyond 7 μm from the electrode surface.*(43)* In order to get this good agreement, optical fibers with low numerical aperture (NA) and high concentrations of $Ru(bpy)_3^{2+}$ were needed. This was required because each optical fiber probes a cone of volume and at high NA and low concentrations the cones of two adjacent optical fibers overlap, leading to an artificially large signal. Decreasing the NA decreases the angle of acceptance of the cone and the increased concentration of $Ru(bpy)_3^{2+}$ decreases the depth into solution that is interrogated, which eliminates the overlap as shown in Figure 2.6.*(43)*

This method is advantageous compared to the two previous methods in that it allows for the direct observation of the redox species, but unlike the previous methods it does require one of the redox species to be fluorescent. Large electrodes are also needed as the placement of the optical fiber bundle would disrupt the evolution of the diffusion layers produced by smaller electrodes. Large electrodes were also needed so that the bundle could be placed such that it probes the linear diffusion at the middle of the electrode without any edge effects.*(43)*

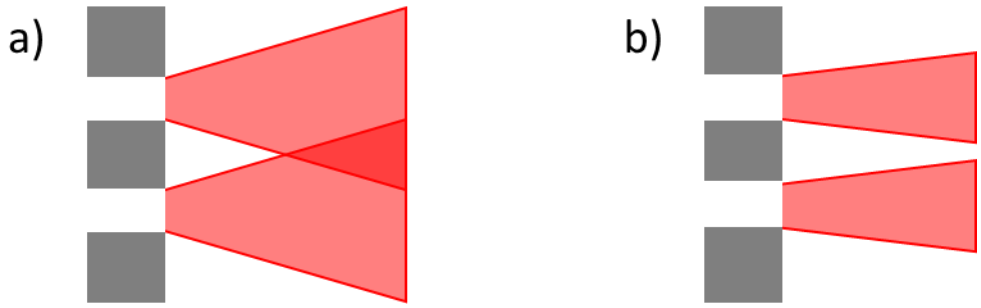

Figure 2.6: Cone of volume (red) probed by (a) optical fibers of high NA, with low redox species concentration and (b) optical fiber of low NA, with high redox species concentration.

Overall fluorescence techniques provide the ability to monitor diffusion layers, but fluorescence confocal laser microscopy and FEEM do not directly monitor the redox species, instead the

concentrations of the redox species are coupled to secondary signals. Fluorescence confocal laser microscopy is limited, in that it requires the appropriate selection of a pH sensitive fluorophore and restricted electrolyte pH. The pH change is also only visible over the small range determined by the fluorophore. FEEM is limited by the fact that the large bipolar electrode array disrupts diffusion to the electrode so that the closest distance that can be probed is 20 μm form the electrode. While Amatore's optical fiber bundle avoids the problems of the first two techniques by directly monitoring the redox species, it does mean that one of the redox species must be fluorescent. It also suffers from the fact that only large electrodes can be used, so that fast processes cannot be probed.

2.6: X-ray

The first recorded use of an X-ray technique to spatially and temporally monitor an electrochemical reaction was done by Guay *et al*, where they used scanning transmission X-ray microscopy (STXM) to look at the changes in oxidation state of a polyaniline layer on a gold electrode.*(44)* By monitoring changes in the N 1s edge at 398.7 eV, which appears upon oxidation of the polymer, the change in oxidation state of the entire polyaniline layer could be monitored. While this is not diffusion layer mapping, it does showcase that STXM can provide 50 nm spatial resolution, which is far superior to any of the other techniques previously discussed. However, Guay *et al* encountered technical problems with the spectroelectrochemical cell as they were not very robust. This was due to the fact that very small electrochemical cells of mircron thickness were needed to allow sufficient X-ray throughput. Using electrodes of the desired size and shape required deposition of thin layers of metal on an X-ray transparent substrate. As a result, the gold layers were not stable over long periods and would peel away from the substrate or crack when a potential was applied most likely due to poor adhesion to the substrate.*(44)*

Besides STXM, a method based on confocal micro-X-ray fluorescence (CμXRF) has also been developed and allows for the spatial and temporal monitoring of diffusion layers during copper deposition.*(45, 46)* Using this method Peng et al were able to observe the depletion of copper at the electrode surface at various potentials and copper concentrations.*(46)* While successful, this method can only probe concentrations above 0.1 M and its spatial resolution is only 26.4 μm.

This is much worse than many of the previous methods discussed. These studies do, however, use a conventional X-ray source and the limit of detection and resolution could be improved upon by using a much brighter X-ray source, such as a synchrotron.

The final X-ray technique that will be discussed is energy dispersive x-ray fluorescence microscopy (EDX). This technique utilizes a small electron beam (<100 nm) produced by a scanning electron microscope (SEM) for spatial resolution and to produce x-ray fluorescence. Uematsu *et al* were able to follow the dissolution of silver ions in an ionic liquid (IL).*(47)* Through mapping the diffusion of silver ions from the electrode, they were able to show that the increase in the silver ion concentration caused an increase in the IL viscosity. This increase in viscosity caused large decreases in the diffusion of silver ions near the electrode. By taking into account the increase in viscosity, the experimental diffusion of the silver ions was measured and found to agree well with that predicted by theory.*(47)* The obvious hindrance to the use of this techniques is the fact that SEM requires vacuum and electrochemistry requires a solution. This incompatibility makes this method useful only in very select cases, such as in ionic liquids as they have negligible vapour pressures.

While X-ray methods are fairly recent additions to those available to map diffusion layers they do show promise. In particular, STXM is a promising method, due to its spatial resolution. In order to achieve this, a spectroelectrochemical cell needs to be produced that has stable electrodes as well as the required thin cavity to allow sufficient X-ray throughput. For CμXRF a synchrotron source is needed to improve upon the spot resolution and detection limit in order to be applicable to a wider range of electrochemical reactions. The method based on EDX measurement is the most restrictive and it is unlikely to find broad application.

2.7: IR

There have been no reports of diffusion layer mapping using IR partly due to the difficulty of combining IR spectroscopy and electrochemistry, as discussed in Chapter 1. However, if these drawbacks can be removed or mitigated, then IR spectroscopy is an ideal candidate to probe the evolution of diffusion layers as a large number of molecules have observable IR signals.

Like UV-Vis and the other optical methods, it is a non-invasive technique so that the evolving diffusion layer will not be perturbed. However, unlike UV-Vis, IR absorption signals have much narrower bandwidths, providing better specificity. IR provides benefits over Raman techniques, as it doesn't rely on inherent signal enhancement to detect analytes at typical concentrations used in electrochemical experiments. Compared to fluorescence techniques, IR doesn't require tagging analyte molecules with specific reporters and can, therefore, directly follow the redox species. IR also has advantages over X-ray techniques, the most notable being the fact that it does not require a vacuum which facilitates cell design. Surprisingly, diffraction-limited IR has greater spatial resolution compared to CμXRF.

2.8: References

1. Seidel, Y. E.; Schneider, A.; Jusys, Z.; Wickman, B.; Kasemo, B.; Behm, R. J. Mesoscopic mass transport effects in electrocatalytic processes. *Faraday Discuss.* **2009,** *140*, 167-184.

2. Bard, A. J.; Fan, F. R. F.; Kwak, J.; Lev, O. Scanning electrochemical microscopy. Introduction and principles. *Anal. Chem.* **1989,** *61*, 132-138.

3. Engstrom, R. C.; Weber, M.; Wunder, D. J.; Burgess, R.; Winquist, S. Measurements within the diffusion layer using a microelectrode probe. *Anal. Chem.* **1986,** *58*, 844-848.

4. Engstrom, R. C.; Meaney, T.; Tople, R.; Wightman, R. M. Spatiotemporal description of the diffusion layer with a microelectrode probe. *Anal. Chem.* **1987,** *59*, 2005-2010.

5. Zhang, J.; Slevin, C.,J.; Unwin, P.,R. Resolution of coupled electron transfer-ion transfer processes at liquid/liquid interfaces by visualisation of interfacial concentration profiles. *Chem. Commun.* **1999,** *16*, 1501-1502.

6. Slevin, C. J.; Ryley, S.; Walton, D. J.; Unwin, P. R. A New Approach for Measuring the Effect of a Monolayer on Molecular Transfer across an Air/Water Interface Using Scanning Electrochemical Microscopy. *Langmuir* **1998,** *14*, 5331-5334.

7. Wei, C.; Bard, A. J.; Nagy, G.; Toth, K. Scanning Electrochemical Microscopy. 28. Ion-Selective Neutral Carrier-Based Microelectrode Potentiometry. *Anal. Chem.* **1995,** *67*, 1346-1356.

8. Klusmann, E.; Schultze, J. W. pH-microscopy—theoretical and experimental investigations. *Electrochim. Acta* **1997,** *42*, 3123-3134.

9. Schröck, K.; Schulte, A.; Schuhmann, W. Visualization of the Reaction Zones Between Two Miscible Solutions with Potentiometric and Amperometric Microsensors. *Electroanalysis* **2005,** *17*, 489-494.

10. Momotenko, D.; McKelvey, K.; Kang, M.; Meloni, G. N.; Unwin, P. R. Simultaneous Interfacial Reactivity and Topography Mapping with Scanning Ion Conductance Microscopy. *Anal. Chem.* **2016,** *88*, 2838-2846.

11. Amatore, C.; Szunerits, S.; Thouin, L. Mapping concentration profiles within the diffusion layer of an electrode: Part II. Potentiometric measurements with an ultramicroelectrode. *Electrochemistry Communications* **2000,** *2*, 248-253.

12. Amatore, C.; Szunerits, S.; Thouin, L.; Warkocz, J. Mapping concentration profiles within the diffusion layer of an electrode: Part III. Steady-state and time-dependent profiles via amperometric measurements with an ultramicroelectrode probe. *Electrochemistry Communications* **2000,** *2*, 353-358.

13. Amatore, C.; Szunerits, S.; Thouin, L.; Warkocz, J. The real meaning of Nernst's steady diffusion layer concept under non-forced hydrodynamic conditions. A simple model based on Levich's seminal view of convection. *J Electroanal Chem* **2001,** *500,* 62-70.

14. Baltes, N.; Thouin, L.; Amatore, C.; Heinze, J. Imaging Concentration Profiles of Redox-Active Species with Nanometric Amperometric Probes: Effect of Natural Convection on Transport at Microdisk Electrodes. *Angewandte Chemie International Edition* **2004,** *43,* 1431-1435.

15. Amatore, C.; Knobloch, K.; Thouin, L. First direct experimental evidence of migration contributions through monitoring of concentration profiles at low supporting electrolyte concentration. *Electrochemistry Communications* **2004,** *6*, 887-891.

16. Muller, R. H. Double beam interferometry for electrochemical studies. In *Advances in electrochemistry and electrochemical engineering;* Wiley-Interscience New York: 1973.

17. O'Brien, R. N.; Rosenfield, C. A.; Kinoshita, K.; Yakymyshyn, W. F.; Leja, J. The Dependence of Concentration Gradient on Current Density at Working Electrodes. *Can. J. Chem.* **1965,** *43*, 3304-3310.

18. Knox, C.; Sayano, R. R.; Seo, E. T.; Silverman, H. P. Holographic interferometry in electrochemical studies. *J. Phys. Chem.* **1967,** *71*, 3102-3104.

19. Fukunaka, Y.; Denpo, K.; Iwata, M.; Maruoka, K.; Kondo, Y. Concentration Profile of Cu2+ Ion near a Plane Vertical Cathode in Electrolytes Containing CuSO4 and an Excess of H_2SO_4 as a Supporting Electrolyte . *J. Electrochem. Soc.* **1983,** *130*, 2492-2499.

20. Yuan, B.; Chen, S.; Yang, X.; Wang, C.; Li, L. Mapping the transient concentration field within the diffusion layer by use of the digital holographic reconstruction. *Electrochemistry Communications* **2008,** *10*, 392-396.

21. Pruiksma, R.; McCreery, R. L. Observation of electrochemical concentration profiles by absorption spectroelectrochemistry. *Anal. Chem.* **1979,** *51*, 2253-2257.

22. Pruiksma, R.; McCreery, R. L. Spectroelectrochemical observation of diffusion profiles by the parallel absorption method. *Anal. Chem.* **1981,** *53*, 202-206.

23. Jan, C. C.; McCreery, R. L.; Gamble, F. T. Diffusion layer imaging: spatial resolution of electrochemical concentration profiles. *Anal. Chem.* **1985,** *57*, 1763-1765.

24. Jan, C. C.; McCreery, R. L. High-resolution spatially resolved visible absorption spectrometry of the electrochemical diffusion layer. *Anal. Chem.* **1986,** *58*, 2771-2777.

25. Wu, H.; McCreery, R. L. Spatially Resolved Absorption Spectroelectrochemistry: Spectra and Concentration Profiles of Species Generated and Consumed at Single and Twin Electrodes. *J. Electrochem. Soc.* **1989,** *136*, 1375-1379.

26. Wu, H. P.; McCreery, R. L. Observation of concentration profiles at cylindrical microelectrodes by a combination of spatially resolved absorption spectroscopy and the Abel inversion. *Anal. Chem.* **1989,** *61*, 2347-2352.

27. Posdorfer, J.; Olbrich-Stock, M.; Schindler, R. N. Spatially resolved UV—VIS absorption measurements in planar, cylindrical and spherical diffusion layers. Kinetic investigations of a heterogeneous electron transfer reaction. *Electrochim. Acta* **1994,** *39*, 2005-2013.

28. Olbrich-Stock, M.; Posdorfer, J.; Schindler, R. N. UV—visible spectroscopic studies in the diffusion layer during electropolymerization of thiophene. *J Electroanal Chem* **1994,** *368*, 173-181.

29. Martínez, A.; Colina, A.; Dryfe, R. A. W.; Ruiz, V. Spectroelectrochemistry at the liquid|liquid interface: Parallel beam UV–vis absorption. *Electrochim. Acta* **2009,** *54*, 5071-5076.

30. Izquierdo, D.; Martinez, A.; Heras, A.; Lopez-Palacios, J.; Ruiz, V.; Dryfe, R. A. W.; Colina, A. Spatial Scanning Spectroelectrochemistry. Study of the Electrodeposition of Pd Nanoparticles at the Liquid/Liquid Interface. *Anal. Chem.* **2012,** *84*, 5723-5730.

31. Gyurcsanyi, R. E.; Lindner, E. Spectroelectrochemical Microscopy: Spatially Resolved Spectroelectrochemistry of Carrier-Based Ion-Selective Membranes. *Anal. Chem.* **2005,** *77*, 2132-2139.

32. Ozeki, T.; Irish, D. E. Estimation of the concentration-distance profile within the electrochemical diffusion layer by Raman microprobe spectroscopy. *Journal of Electroanalytical Chemistry and Interfacial Electrochemistry* **1990,** *280*, 451-455.

33. Amatore, C.; Bonhomme, F.; Bruneel, J.; Servant, L.; Thouin, L. Mapping dynamic concentration profiles with micrometric resolution near an active microscopic surface by confocal resonance Raman microscopy. Application to diffusion near ultramicroelectrodes: first direct evidence for a conproportionation reaction. *J Electroanal Chem* **2000,** *484*, 1-17.

34. Amatore, C.; Bonhomme, F.; Bruneel, J.; Servant, L.; Thouin, L. Mapping concentration profiles within the diffusion layer of an electrode: Part I. Confocal resonance Raman microscopy. *Electrochemistry Communications* **2000,** *2*, 235-239.

35. Texier, F.; Servant, L.; Bruneel, J. L.; Argoul, F. In situ probing of interfacial processes in the electrodeposition of copper by confocal Raman microspectroscopy. *J Electroanal Chem* **1998,** *446*, 189-203.

36. Cannan, S.; Douglas Macklam, I.; Unwin, P. R. Three-dimensional imaging of proton gradients at microelectrode surfaces using confocal laser scanning microscopy. *Electrochemistry Communications* **2002,** *4*, 886-892.

37. Rudd, N. C.; Cannan, S.; Bitziou, E.; Ciani, I.; Whitworth, A. L.; Unwin, P. R. Fluorescence Confocal Laser Scanning Microscopy as a Probe of pH Gradients in Electrode Reactions and Surface Activity. *Anal. Chem.* **2005,** *77*, 6205-6217.

38. Grime, J. M. A.; Edwards, M. A.; Rudd, N. C.; Unwin, P. R. Quantitative visualization of passive transport across bilayer lipid membranes. *Proceedings of the National Academy of Sciences* **2008,** *105*, 14277-14282.

39. Leenheer, A. J.; Atwater, H. A. Imaging Water-Splitting Electrocatalysts with pH-Sensing Confocal Fluorescence Microscopy. *J. Electrochem. Soc.* **2012,** *159*, H752-H757.

40. Amatore, C.; Pebay, C.; Servant, L.; Sojic, N.; Szunerits, S.; Thouin, L. Mapping Electrochemiluminescence as Generated at Double-Band Microelectrodes by Confocal Microscopy under Steady State. *ChemPhysChem* **2006,** *7*, 1322-1327.

41. Oja, S. M.; Guerrette, J. P.; David, M. R.; Zhang, B. Fluorescence-Enabled Electrochemical Microscopy with Dihydroresorufin as a Fluorogenic Indicator. *Anal. Chem.* **2014,** *86*, 6040-6048.

42. Oja, S. M.; Zhang, B. Imaging Transient Formation of Diffusion Layers with Fluorescence-Enabled Electrochemical Microscopy. *Anal. Chem.* **2014,** *86*, 12299-12307.

43. Amatore, C.; Chovin, A.; Garrigue, P.; Servant, L.; Sojic, N.; Szunerits, S.; Thouin, L. Remote Fluorescence Imaging of Dynamic Concentration Profiles with Micrometer Resolution Using a Coherent Optical Fiber Bundle. *Anal. Chem.* **2004,** *76*, 7202-7210.

44. Guay, D.; Stewart-Ornstein, J.; Zhang, X.; Hitchcock, A. P. In Situ Spatial and Time-Resolved Studies of Electrochemical Reactions by Scanning Transmission X-ray Microscopy. *Anal. Chem.* **2005,** *77*, 3479-3487.

45. Tsuji, K.; Yonehara, T.; Nakano, K. Application of Confocal 3D Micro-XRF for Solid/Liquid Interface Analysis. *Analytical Sciences* **2008,** *24*, 99-103.

46. Peng, S.; Liu, Z.; Sun, T.; Ma, Y.; Ding, X. Spatially Resolved In Situ Measurements of the Ion Distribution Near the Surface of Electrode in a Steady-State Diffusion in an Electrolytic Tank with Confocal Micro X-ray Fluorescence. *Anal. Chem.* **2014,** *86*, 362-366.

47. Uematsu, T.; Han, J.; Tsuda, T.; Kuwabata, S. Metal-Ion Diffusion in Ionic Liquid Studied by Electrochemical Scanning Electron Microscopy with X-ray Fluorescence Spectrometry. *J. Phys. Chem. C* **2012,** *116*, 20902-20907.

Chapter 3: Techniques and Theory

3.1: Cyclic Voltammetry

In Cyclic Voltammetry (CV) a triangular potential wave is applied using a potentiostat to an electrode of interest. The nature of the potential wave applied depends on the two potential limits (most negative and most positive potentials) and the potential scan rate (V/s). The current as a result of the potential wave is measured and plotted versus potential (Figure 3.1).

CV is typically done in a three-electrode electrochemical cell and the potential is applied between the working and reference electrodes. The resulting current is measured between the working and counter electrode.

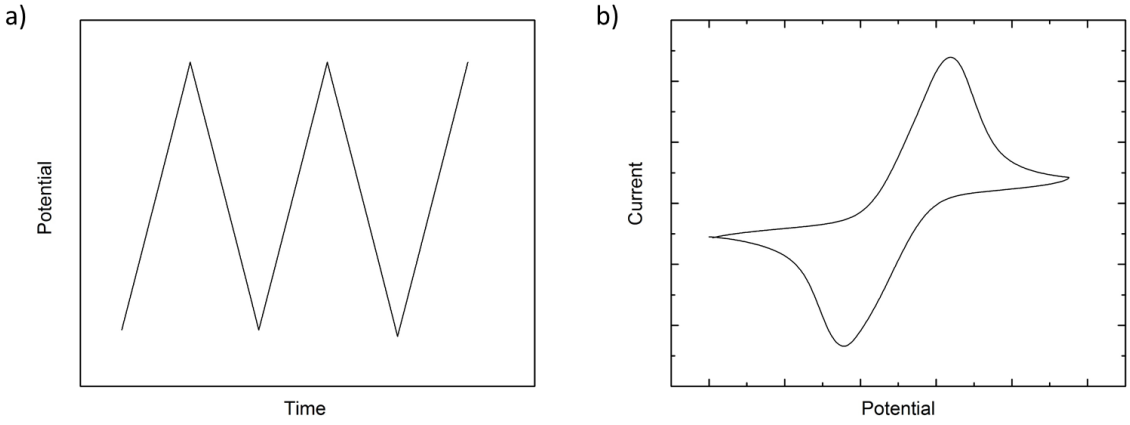

Figure 3.1: (a) Potential wave and (b) the resulting voltammogram for a one electron transfer.

3.2: Hydrodynamic Linear Sweep Voltammetry

Hydrodynamic linear sweep voltammetry like CV is a voltammetric technique in that it is a controlled potential method where the current is measured as a function of potential. Linear sweep voltammetry differs from CV in that the potential is ramped linearly from some initial potential (E_i) to a final potential (E_f) then the measurement is stopped, whereas with CV where the potential cycles between the two potential limits.

Hydrodynamic electrochemical experiments are electrochemical experiments where the electrode or the electrolyte are motion.*(1)* Hydrodynamic techniques, unlike many stationary electrode techniques, allow for a steady state to be obtained at the electrode at relatively short times. The hydrodynamic technique employed here is hydrodynamic linear sweep voltammetry (HLSV) using rotating disk electrode (RDE). A RDE is composed of a disk electrode that is embedded into a cylinder of insulating material. The disk face is the electroactive surface and is then placed in the liquid and spun at varying speeds. The spinning motion of the cylinder in the liquid causes flow of the solution outward along the surface of the disk face. This outward flow in turn causes inward flow towards the disk face. The fluid flow towards the electrode surface brings material to a distance δ_0 from the electrode. Solution is stagnant beyond this distance, in what is called the Nernst stagnation layer. At distances beyond the Nernst stagnation layer ($> \delta_0$), the concentration is equal to the bulk concentration of the redox active species. This steady state results in a limiting current at potentials sufficiently far from the formal potential of the redox active species. The limiting current is described by the Levich equation:

$$i_{lim} = 0.62nFAD^{2/3}\omega^{1/2}v^{1/6}C^{*} \qquad (3.1)$$

Where n is the number of electrons transferred, *F* is Faradays constant, *A* is the area of the electrode, *D* is the diffusion coefficient of the redox active molecule, ω is the rotation speed in radians per second, *v* is the kinematic viscosity of the solution and C^{*} is the bulk concentration of the electroactive molecule.

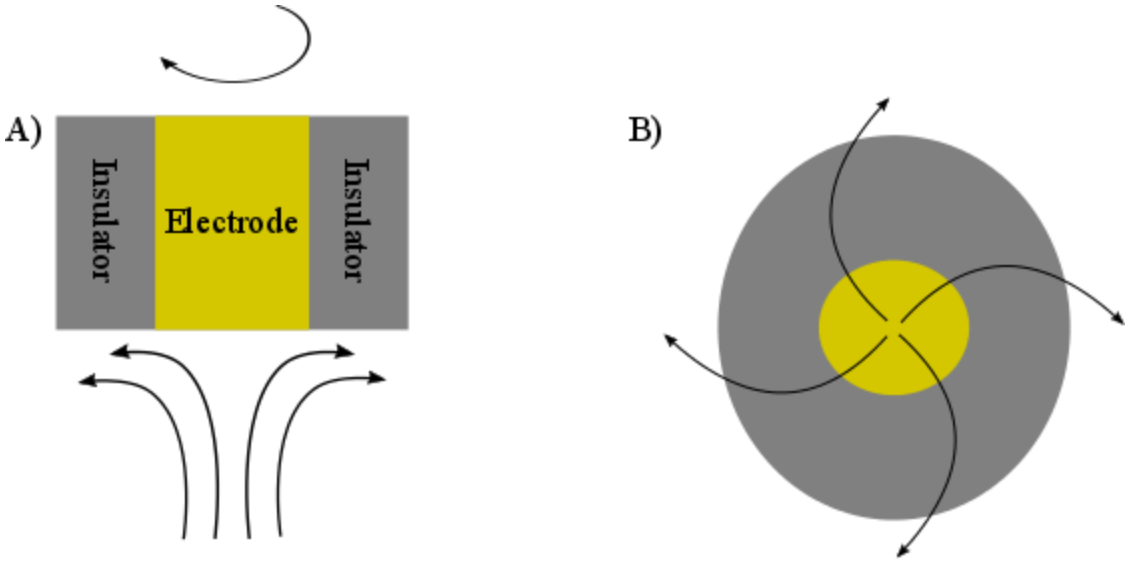

Figure 3.2: (a) Cross-section showing flow of fluid to the surface of a RDE, (b) plan view showing flow of fluid at the surface of a RDE.

3.3: Chronoamperometry

Chronoamperometry is a potential step technique where the potential is stepped from a reference potential (E_{ref}) to a new values (E_{step}). The current as a function of time during the potential step is monitored and plotted as current *versus* time.

Typically, in chronoamperometry experiments the reference potential is chosen such that one electroactive species is stable at the electrode. The potential after the step is chosen such that the electroactive species is unstable at the electrode and undergoes oxidation or reduction depending on the electrode potential.

A common chronoamperometric method is to step the potential from E_{ref} to E_{step} and hold at E_{step} for a specific amount of time then back to E_{ref}. The current is monitored for the entire experiment, resulting in a current response from the forward and backward reactions. This is known as double step chronoamperometry.

3.4 Infrared Spectroscopy

3.4.1: Infrared Radiation

Infrared (IR) radiation is electromagnetic radiation that corresponds to the wavelengths from ~0.70 μm to 1000 μm. IR spectroscopy looks at the interaction of IR radiation with matter. The energy range of IR radiation corresponds to the energies of vibrational and rotational transitions in molecules. IR radiation is typically split into three regions: near-IR (~0.7 – 2.5 μm), mid-IR (2.5 – 25 μm) and far-IR (25 – 1000 μm). The mid IR region results in vibrational transitions, whereas the near and far IR regions can involve electronic transitions and rotations respectively. These can make the spectra in the near and far IR regions hard to interpret. As such, mid IR is used in these studies and is an ideal technique to study electrochemical processes, as almost all molecules absorb IR radiation. The IR spectrum provides molecular information and can be used with Beer's law to provide quantitative information.

The interaction between mid IR radiation and molecules results in transitions between quantized vibrational states. To explore the nature of vibrations and how molecular information can be determined, the vibration of a diatomic molecule will be demonstrated briefly. The vibration of a diatomic molecule can be considered as the vibration of two masses connected by a spring. In this case the vibration can be approximated as a harmonic oscillator. In this approximation the vibration of the two masses will obey Hooke's law where the vibrational frequency is described by:

$$\omega = \frac{1}{2\pi}\sqrt{\frac{k}{\mu}} \tag{3.2}$$

Where k is the spring constant and μ is the reduced mass. Intuitively this shows that the frequency of molecular vibrations will be dependent on the two atoms that decide the reduced mass and the bonding between atoms that decide the spring constant. The quantum mechanical treatment of the harmonic oscillator results in discrete energy levels for vibration given by:

$$E_n = \left(n + {}^1/_2\right)h\omega \tag{3.3}$$

Where $n = 1,2,3\ldots$, h is Plank's constant and ω is the vibrational frequency. From equation 3.2 and 3.3, it can be seen that only radiation of specific energy can be absorbed and that it can be related back to molecular information as the energy absorbed is dependent on the bonding between the atoms that determines ω.

In the previous example, a diatomic molecule was used to describe vibrations because it has only one possible vibration. Most of the molecules of interest consist of a number of atoms and by increasing the number of atoms the number of possible vibrational modes also increases. The number of vibrational modes a molecule can have is dependent on the number of atoms within the molecule. Each atom will have three degrees of freedom, so that a molecule with N atoms will have 3N degrees of freedom. Not all of these are vibrational degrees of freedom; three are due to the translational motion of the atoms and another three are the rotational degrees of freedom around the axes. The remaining degrees of freedom are the vibrational degrees of freedom (vibrational modes), meaning that a molecule will have 3N-6 vibrational (modes) degrees of freedom.*(2)* This is a little different for linear molecules, as they will have 3N-5 degree of freedom.

Although a molecule will contain a number of vibrational modes, not all of these modes will be IR active (i.e. not all vibrations will appear in the IR spectrum of the molecule). In order for a vibration to be IR active, the vibration must cause a change in the dipole moment of the molecule.*(2, 3)* As an example, the vibrational modes of CO_2 will be examined. CO_2 is a linear molecule that contains 3 atoms, so it will have 4 vibrational modes, which are depicted in Figure 3.3. The vibrations of CO_2 consist of two stretching modes and two bending modes. The symmetric stretch depicted in Figure 3.3a does not cause a change in the dipole moment of the CO_2 molecule and as such this vibration is not present in the IR spectra of CO_2. The stretch depicted in Figure 3.3b is an asymmetric stretch that does change the dipole moment of the CO_2 molecule and is therefore present in the IR spectrum. The two bending vibrations of CO_2 shown in Figure 3.3c and 3.3d are IR active and are also degenerate. This means that although four vibrational modes are present for CO_2, only two can be seen by IR spectroscopy as the degenerate signals overlap. This is typical and shows that care must be taken when interpreting IR spectra.

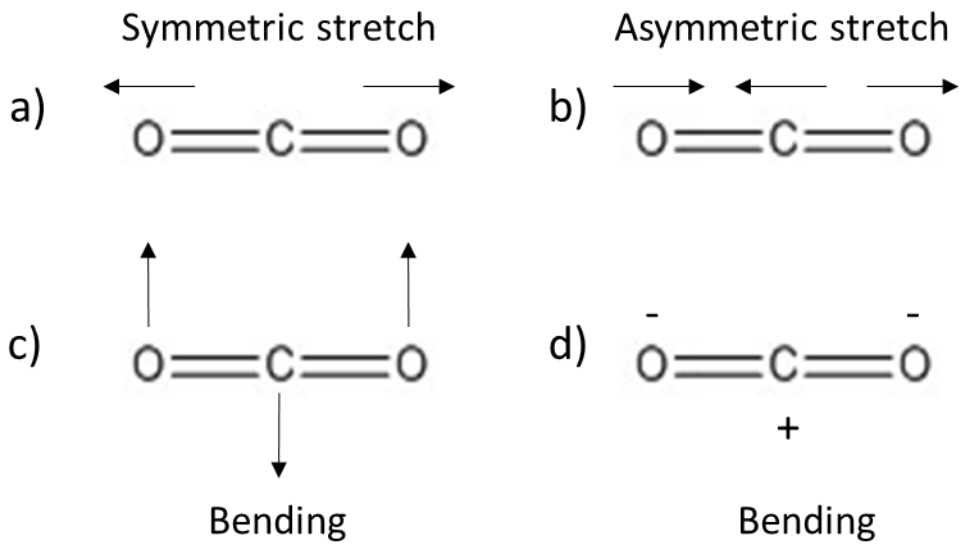

Figure 3.3: Bending modes of CO_2, (a) Symmetric stretch (IR inactive), (b) Asymmetric stretch (IR active, 2350 cm^{-1}), (c) Bending (IR active, 666 cm^{-1}), (d) Bending (IR active, 666 cm^{-1}).

3.4.2: Michelson Interferometer

Modern IR spectroscopy measurements are done using a Michelson interferometer. In a Michelson interferometer the IR beam from the source impinges on a beam splitter and separates the IR beam into two beams. One IR beam is sent to a fixed mirror and the other is sent to a moveable mirror. The IR beams are reflected off these mirrors and back to the beam splitter where the two reflected beams are combined and then sent to reflect or pass through the sample, where the detector finally measures the resulting signal.

The movable mirror allows the optical path length (OPL) between the mirror and the beam splitter to be varied, this change in OPL results an interference pattern between the IR radiation reflected off the stationary and moveable mirrors.*(3)* This interference pattern is called an interferogram. This interferogram is then Fourier transformed from time space to frequency space, thus producing the IR spectrum.

3.4.3: Infrared Microscopy

IR microscopy utilizes an optical microscope as seen in Figure 3.5. An IR microscope can be used to do both reflectance and transmission IR measurements. In reflectance experiments the IR beam comes from the top. The objective then focuses the beam where it is

reflected off the sample back to the objective and then the radiation is measured by the detector. In transmission mode the IR beam comes from the bottom where the condenser focuses the beam. The beam passes through the sample to the objective and is then measured by the detector. In an IR microscope the area probed by the IR beam size can be selected by choosing the appropriate aperture and condenser/objective, thus IR microscopes can provide spatial resolution of the sample.

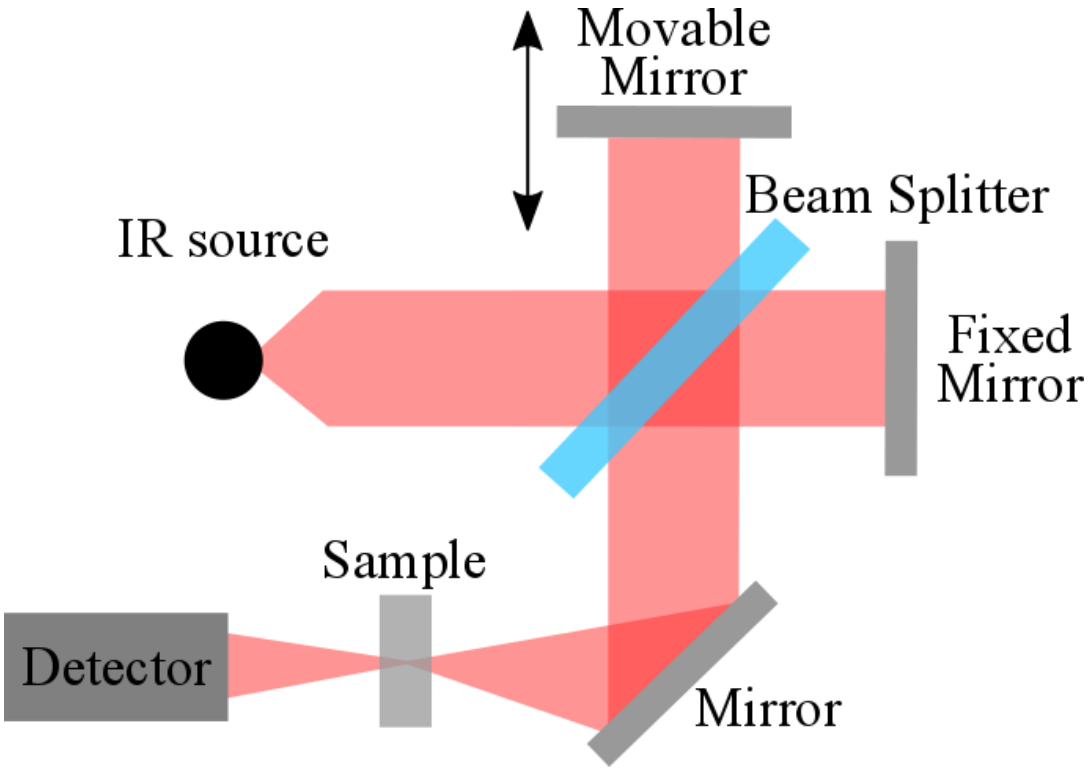

Figure 3.4: Diagram of a Michelson Interferometer.

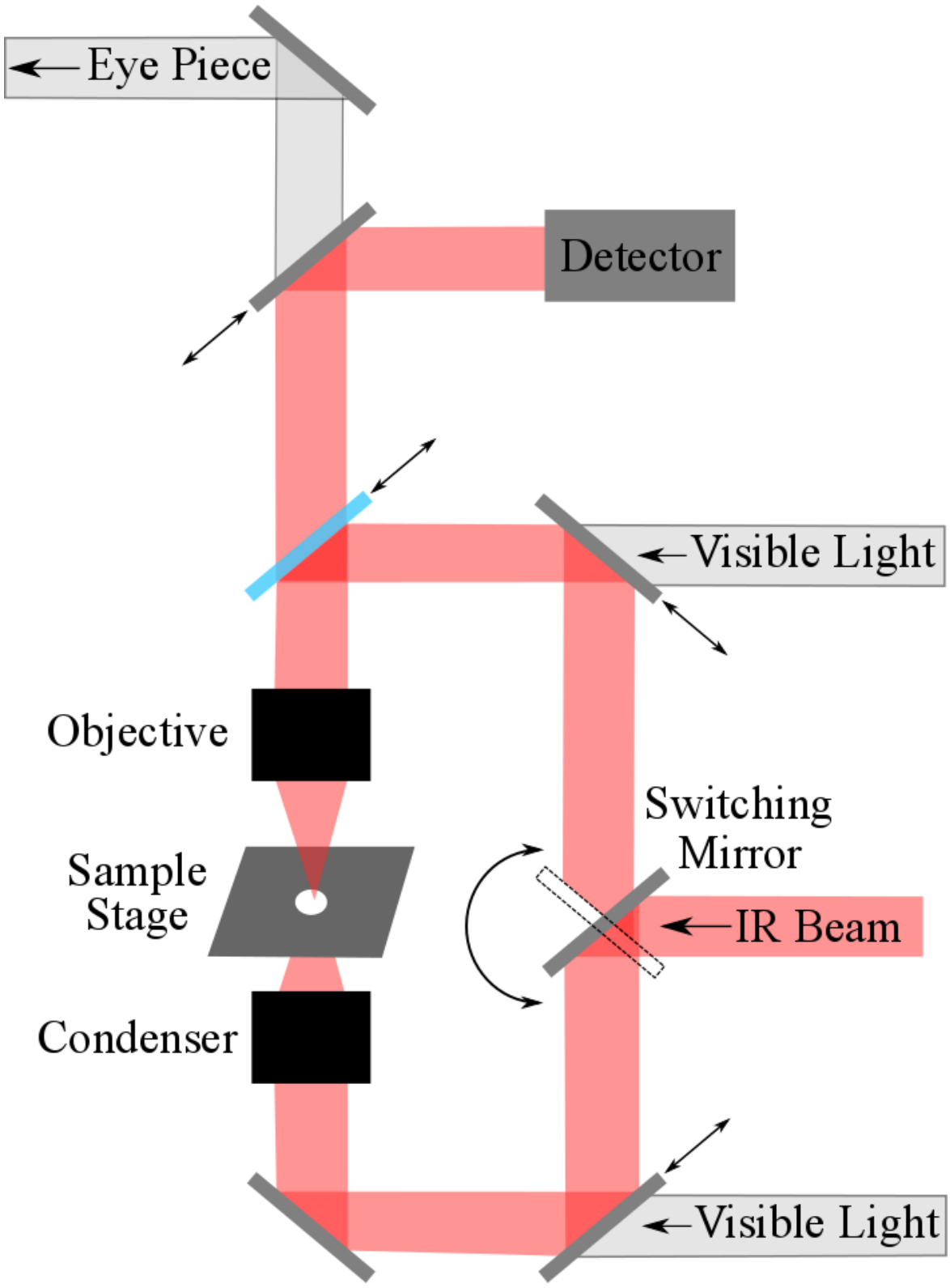

Figure 3.5: Diagram of an IR microscope. The switching mirror allows for use of either transmission or reflectance modes.

3.4.4: Time Resolved Measurements

The time resolution of an IR interferometer is dependent on the speed at which an interferogram can be collected. This depends on the mirror speed and the path length of the movable mirror. Typically, in order to gather information on a dynamic process the time to gather 1 interferogram must be 10x faster than the time of the dynamic process.*(3)* Time resolved measurements will be considered in detail in Chapter 4.7.

3.5: Infrared Sources

3.5.1: Globar

Traditional IR sources in the mid IR region for IR spectroscopy are thermal emissive materials typically made of silicon carbide and often-called Globars.*(3)* Globars are blackbody radiators and the IR radiation is given off in all directions. Therefore, it must be collected and focused into the interferometer.

3.5.2: Synchrotron Infrared Radiation Sources

Synchrotron sources produces electromagnetic radiation through the interactions of electrons with a magnetic field. An electron beam is bent by a magnetic field, which causes the electron beam to lose energy. Some of this lost energy is released as electromagnetic radiation of various wavelengths. The electromagnetic radiation is given off tangential to the electron beam path and is quite collimated. This results in an IR beam produced with a very high brilliance. Brilliance is a measure of intensity where it is defined as the number of photons per unit area per subtended angle. This means that although a globar has higher total photon output than a synchrotron source, the synchrotron source has greater photon throughput at small IR beam spots as the globar emits photons in all directions. This results in a greater signal from the detector at small spot sizes when a synchrotron source is used compared to a globar.*(4)*

3.6: References

1. Bard, A. J.; Faulkner, L. R. *Electrochemical Methods: Fundamentals and Applications*; Wiley: New York, 2001.

2. Harris, D. C.; Bertolucci, M. D. *Symmetry and Spectroscopy: An Introduction to Vibrational and Electronic Spectroscopy*; Oxford University Press: New York, 1978.

3. Tasumi, M.; Sakamoto, A. *Introduction to Experimental Infrared Spectroscopy: Fundamentals and Practical Methods*; Wiley: Chichester, West Sussex, United Kingdom, 2015.

4. Miller, L. M.; Smith, R. J. Synchrotrons versus Globars, Point-Detectors versus Focal Plane Arrays: Selecting the best Source and Detector for Specific Infrared Microspectroscopy and Imaging Applications. *Vibrational Spectroscopy* **2005,** *38*, 237-240.

Chapter 4: Materials and Methods

4.1: Reagents and Solutions

Potassium ferricyanide ($K_3Fe(CN)_6$ ≥99.99% trace metals basis), potassium ferrocyanide trihydrate ($K_3Fe(CN)_6 \bullet 6H_2O$ ≥99.99% trace metals basis) and sodium fluoride (NaF ≥99.98%) were purchased from Sigma-Aldrich and used as received. 1,4-benzoquinone (98+%) was purified by sublimation. Hydroquinone (99%) was used as received. Potassium phosphate monobasic (KH_2PO_4, ACS grade) and Potassium phosphate dibasic (K_2HPO_4, ACS grade) were purchased from EMD as used a received. Deuterium oxide (D, 99%) was purchased from Cambridge Laboratories, Inc. (Andover, MA). All aqueous solutions were prepared using Milli-Q water(≥18.2 $M\Omega cm^{-1}$), except those using D_2O as the solvent.

4.2: Spectroelectrochemical cell

SIR experiments were done using a custom built spectroelectrochemical cell (SEC) that was based on a previous reflectance cell designed by Scott Rosendahl during his PhD work in the Burgess group.*(1)* The new cell allowed for transmission of IR radiation through the cell.*(2)*

4.2.1: Spectroelectrochemical Cell Design Considerations

The main obstacle with the design of the new SEC was compatibility with the IR microscope. In order for the SEC to be used for diffusion layer mapping studies it had to allow for transmission of the focused IR beam through the SEC at positions adjacent to the electrode (20 – 100 µm). Additionally, the SEC had to allow for potential control, have a thin cavity so that there would be sufficient photon throughput (signal), allow for fluid to flow through the cell, and fit within the working distance of the objective and condenser. The problems of potential control, thin cavity and fluid flow in the cell were dealt with in previous SEC designs. *(2, 3)*

As described below, the appeal of diffusion layer mapping using SIR is the ability to focus the IR beam to small spot sizes at known distances from the electrode edge. These distances are typically 15-100 µm. Part of the problem arises from the fact that the IR beam from the

condenser is conical in shape, and the angle between the IR beam and the normal to the surface is ~24 degrees. This means that the working electrode must be oriented such that it can be positioned within 15 – 100 μm from the focused IR beam spot, but also in a way that the working electrode and other parts of the SEC do not obstruct the IR beam as it diverges from the focal point. The first cell design depicted in Figure 4.1a consisted of a square calcium fluoride (CaF_2) window embedded in polyvinyl chloride (PVC) puck with the working electrode along one edge of the window. This initial SEC design did not allow for the IR beam to be positioned adjacent to the working electrode as a large portion of the IR beam would be obstructed by the working electrode along the edge of the CaF_2 window as seen in Figure 4.1a.

The second cell design (Figure 4.2b) eliminated the problem of positioning the IR beam adjacent to the working electrode by placing a thin platinum (Pt) foil (12 μm thickness) over half the CaF_2 window. This allows for the IR beam to be positioned within the diffusion layer without obstructing the IR beam. While this design has allowed for the positioning of the IR beam in the desired location it results in a more complicated diffusion space that was very difficult to model. Having the Pt foil protruding into solution also causes edge effects that cannot be easily accounted for in numeric simulations (see below). An embedded band electrode such as the one shown (Figure 4.1a) in the first design is desired as diffusion at an embedded band electrode is analytically well described.*(4, 5)*

To produce a SEC cell that employed an embedded band electrode while allowing the IR beam to be positioned adjacent to the IR beam, a CaF_2 window with one edge beveled at a 45º angle was utilized. The working electrode was placed on the beveled edge as seen in Figure 4.1c.

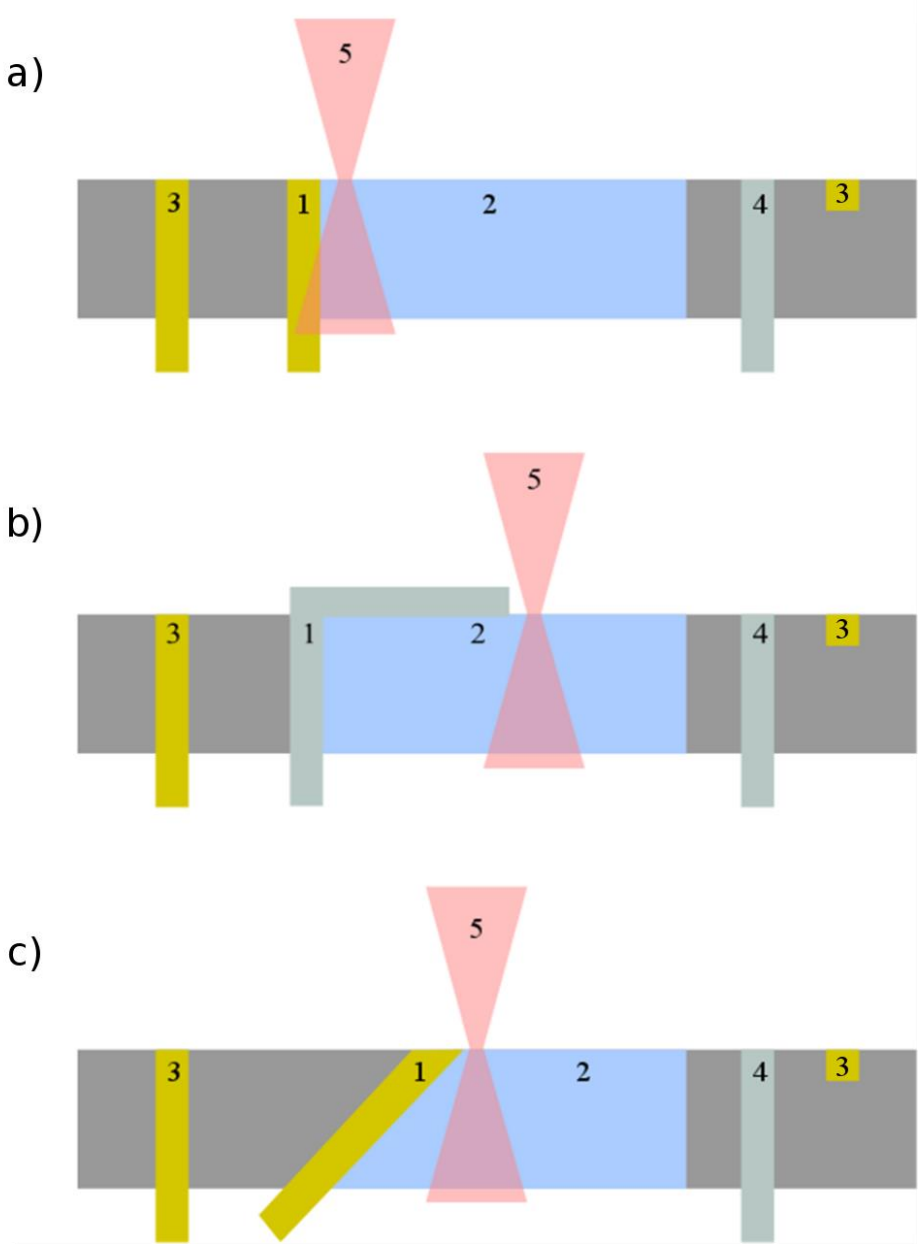

Figure 4.1: Cross sections through the spectroelectrochemical cells, 1: working electrode, 2: CaF_2 window, 3: counter electrode, 4: reference electrode, 5: IR beam. (a) First design with the working electrode along the edge of a square CaF_2 window. (b) Second design with the Pt foil overlaid on the CaF_2 window serving as the working electrode, (c) Third design with the working electrode on the beveled edge of the CaF_2 window.

The first two SEC designs are also limited in that they are only compatible with the 15x objective and condenser. This limitation arises because the electrical and fluid connections extend out perpendicular from the back face of the PVC puck. This makes the cell too large to fit within the working distance of the larger magnification objectives and condensers. While the

15x objective and condenser are sufficient for diffusion layer mapping, higher magnification objectives and condensers will increase photon throughput through the same size spot. The current SEC design (Figure 4.1c and Figure 4.2) provides compatibility with the 36x objective and condenser by having the fluid and electrical connections extend out from the side of the PVC puck instead of from the bottom face.

4.2.2: SEC Assembly

As discussed above, the SECs used for diffusion layer mapping consisted of a PVC puck with an inlaid 10 mm x 10 mm x 2mm CaF_2 window (Crystran, UK) bevelled at 45 º along one edge. The working electrode was a ~150 µm x ~700 µm x ~10 mm gold foil. A 0.25 mm diameter silver wire (99.9985%, Alfa Aesar) served as a pseudo-reference electrode and a 1 mm diameter gold wire (99.9985%, Alfa Aesar) acted as the counter electrode. The gold foil working electrode was secured to the beveled edge of the CaF_2 window with a minimal amount of cyanomethacrylate glue (Elmer's Products, USA). The bottom of the bevelled edge and the middle of the gold foil were roughened with 1200P grit sand paper to ensure good adhesion between the CaF_2 and gold. The gold foil modified CaF_2 window was secured in the PVC puck with a fiberglass resin (3M, USA) along with the silver pseudoreference and gold counter electrode (Figure 4.2). The working face of the cell was then polished to a mirror finish using successively finer diamond polish, the finest being 1 µm (Pace Technologies, USA). The working, counter and reference electrodes were connected to individual D-subminiature female connector pins. These connectors were secured to the back side of the cell with cyanomethacrylate glue.

The fluid inlet/outlet tubes were secured into holes pre-drilled in the PVC puck with cyanomethacrylate glue. Quarter inch tube adapters (McMaster-Carr, USA) were affixed to the opposite ends to allow facile connection to the fluid tubing. This cell design allowed the IR beam to be positioned to within ~20 µm of the working electrode edge. It is also compatible with both the 15x and 36x objectives on the IR microscope (Bruker, Hyperion 3000) at the 01B1 beamline at the Canadian Light Source.

A thin cavity cell was produced by sandwiching a 25 µm PTFE (Goodfellow, USA) gasket (inner diameter of 19 mm) between the cell and a second, larger (25 mm diameter x 1 mm thick) CaF_2 window. The nominal cell volume was thus 7.1 µL. The exact window to window thickness was determined from the interference fringes produced in the empty cell caused by reflection from the CaF_2 windows. The following equation relates the wavenumber position of the interference fringes to the cavity thickness:

$$b = n \Big/ \left(2\Delta \tilde{\upsilon} \right) \tag{4.1}$$

Where *b* is the cavity thickness, *n* is the number of fringes and $\Delta \tilde{\upsilon}$ is wavenumber difference between the maxima of *n* fringes.

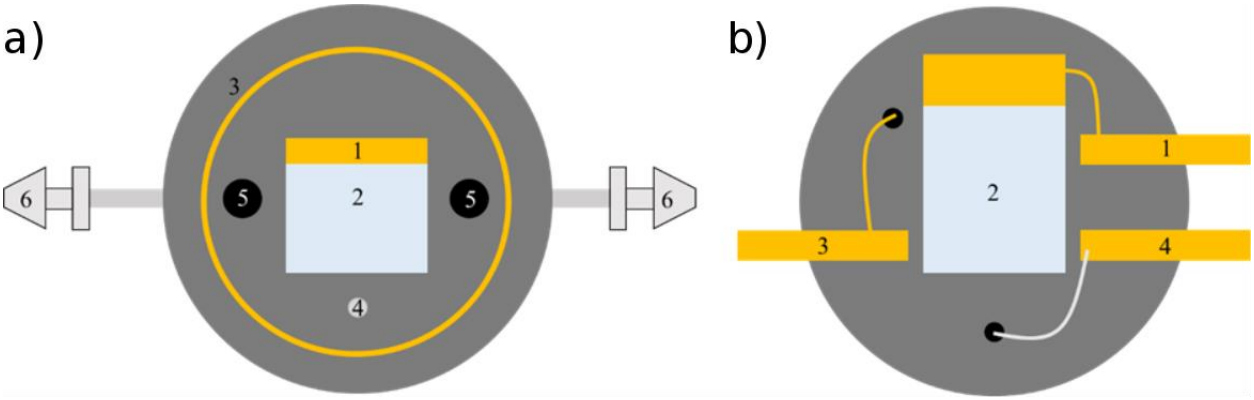

Figure 4.2: (a) Active face of the spectroelectrochemical cell used in experiments;(1) Working electrode, (2) CaF_2 window, (3) Counter electrode, (4) Reference electrode, (5) inlet/outlet holes, (6) Tube connectors. (b) Back face of spectroelectrochemical cell; (1) Working electrode connector, (2) CaF_2 window, (3) Counter electrode connector, (4) Reference electrode connector.

4.3: Determination of Diffusion Coefficients by Hydrodynamic Linear Sweep Voltammetry

Hydrodynamic linear sweep voltammetry was done using a rotating disc electrode (RDE), which consisted of a 3 mm diameter platinum disc electrode embedded in a polyether ether ketone (PEEK) support. An Autolab PGSTAT302N with RDE controller was used to control the working electrode voltage and the RDE rotation speed, as well as monitor the current-

potential responses. The RDE was placed in a glass electrochemical cell which allowed the solution to be purged with argon. An overpressure of argon was maintained over the electrolyte during the experiment to minimize interference from the reduction of oxygen. A gold counter electrode was placed in the same cell as the Pt RDE and an Ag/AgCl reference electrode in saturated KCl solution was connected through a salt bridge in order to prevent chloride contamination.

The RDE was first mechanically polished with 3 µm diamond abrasive for 5 minutes. The RDE was then electropolished in a 0.1 M sulfuric acid solution by cycling the potential from the oxide formation to the start of hydrogen evolution for 30 minutes. A cyclic voltammogram of the Pt electrode under quiescent (no rotation) conditions was recorded and the under potential deposition (UPD) of hydrogen was used to determine its electrochemical surface area (ECSA).

Hydrogen UPD is the adsorption of hydrogen atoms on the surface of Pt at potentials that are positive of the thermodynamic hydrogen evolution potential. The adsorption of hydrogen atoms results in the passage of charge as the H^+ ion in solution is reduced to the adsorbed neutral hydrogen atom species. The charge passed within the UPD region is directly related to the amount of hydrogen adsorbed on the surface. The electrode area is determined by integrating the hydrogen UPD region in the CV to determine the total electronic charge passed. The surface area can then be determined using the well-established charge density value for hydrogen UPD of 210 µC cm^{-2}.*(6)* The RDE was rinsed with copious amounts of deionized water before further use.

Rotating disk electrode experiments were then performed for different supporting electrolytes and the various redox species. In all instances, a CV of the RDE in the absence of the redox probe was run to ensure the RDE was clean. Hydrodynamic linear sweep voltammograms (HLSVs) were collected where the potential was swept at a rate of 10 mV/s and the measurements were repeated for at least five different rotation speeds. A typical LSV of the ferri/ferrocyanide redox couple is shown in Figure 4.3.

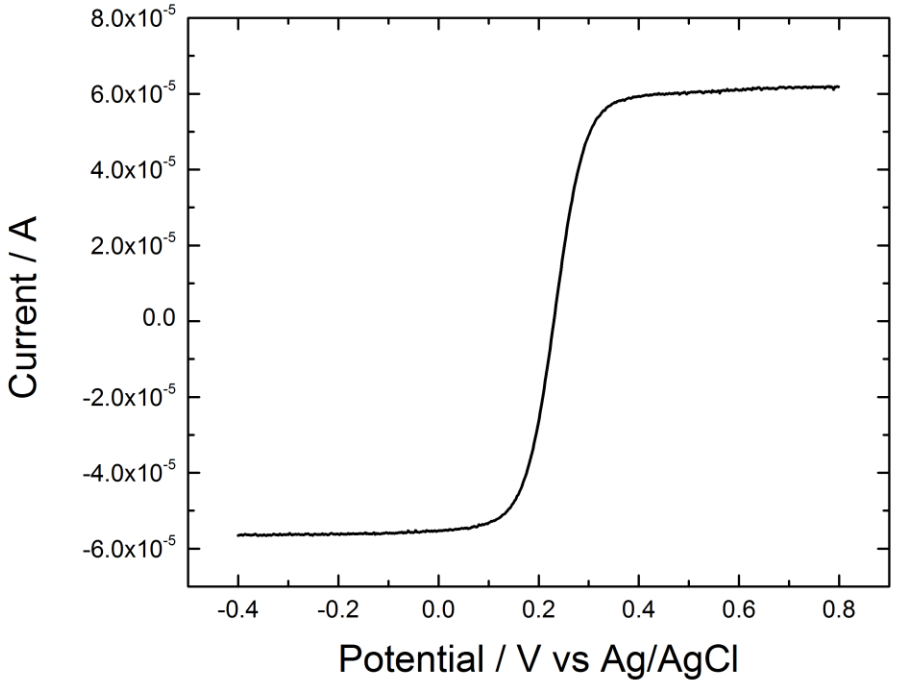

Figure 4.3: Hydrodynamic Linear Sweep Voltammogram of 10 mM ferricyanide and ferrocyanide in aqueous 0.1 M NaF electrolyte at a rotation speed of 3000 RPM.

The limiting current for the reduction (or oxidation) process was readily determined when the current became independent of the applied overpotential. Levich plots were produced by plotting the limiting current, I_L, as a See Figure 4.4. The Levich equation reveals that the slope of this plot should be proportional to the diffusion coefficient, *D*, of the redox species.

$$i_{lim} = 0.62nFAD^{2/3}\omega^{1/2}v^{1/6}C^{*} \quad (4.2)$$

Additional terms in the Levich equation are the Faraday constant, *F*, the electrode area, *A*, the number of electrons transferred in the overall redox reaction, n, the kinematic viscosity of the solution, v, and the concentration of the redox probe, *C*.

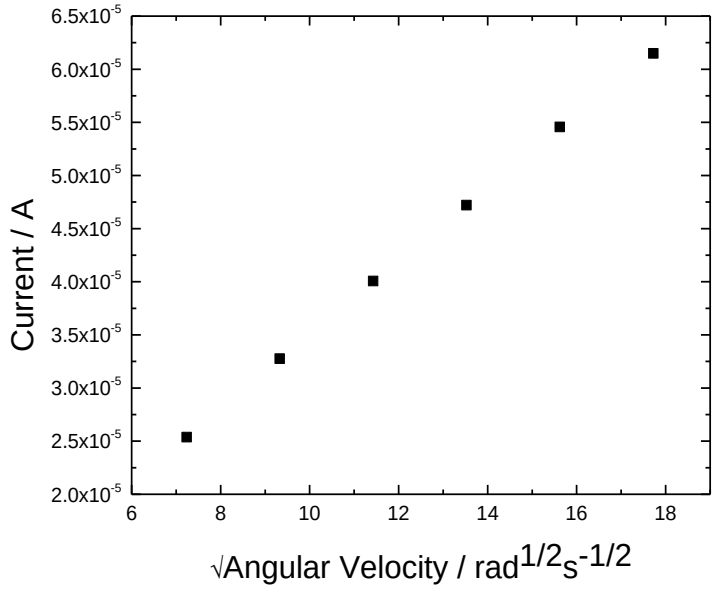

Figure 4.4: Levich plot of the oxidation of 1 mM ferricyanide in 0.1 M NaF electrolyte.

Diffusion coefficients were determined from hydrodynamic voltammetry for all redox species studied in this thesis using essentially the same methodology as described above. It should be noted that in the case of the benzoquinone and hydroquinone the measurements were made in both H_2O and D_2O based electrolyte solutions as SIR measurements for this redox couple were made in heavy water.

4.4: Molar Extinction Coefficients of Hydroquinone and Benzoquinone

As discussed below the evaluation of the diffusion coefficients using IR measurements requires the pre-determination of the molar extinction coefficients of the diffusing (redox) species. IR transmission measurements were taken using a Bruker Vertex 70 spectrometer with a mercury cadmium telluride (MCT) detector. Values were already known for ferricyanide and ferrocyanide,*(7)* so measurements were only required for the hydroquinone (HQ)/benzoquinone (BQ) redox couple.

The determination of the molar extinction coefficients of BQ/HQ were done using D_2O with no electrolyte present as none of the electrolyte species absorb in the same spectral region as the

signals for benzoquinone or hydroquinone. This also avoids other complications due to the electrolyte that will be discussed below. For BQ an initial 15.13 mM solution was made and a serial dilution was used to make solutions with the following concentrations: 10.1 mM, 5.03 mM and 2.52 mM. For HQ, a series of solutions were also made by serial dilution. The solution concentrations of HQ used for the determination of the molar extinction coefficient were; 15.3 mM, 10.2 mM, 5.1 mM and 2.54 mM. These solutions were kept covered and refrigerated until use to minimize photo-oxidation. No discolouration in any of the solutions was noticed during the experiment.

The cell was assembled using a 25 µm thick Teflon gasket and positioned on the sample stage such that the IR beam passed through the cell unobstructed. The cavity thickness was measured at this position. A reference spectrum of D_2O (in the absence of any redox molecules) was made using different spectrometer resolutions (4, 8, and 16 cm^{-1}). Following this, the solution within the cell was replaced with the lowest concentration solution by pumping through 4 mL of the solution. Three spectra at each resolution were then taken. This process was repeated for each concentration starting with the lowest concentration for both BQ and HQ.

As seen in Figure 4.5, the molar extinction coefficient were then determined by plotting the absorbance as a function of concentration and assuming the applicability of Beer's law. The measured molar extinction values for the BQ/HQ species used in this thesis are summarized in Table 4.1.

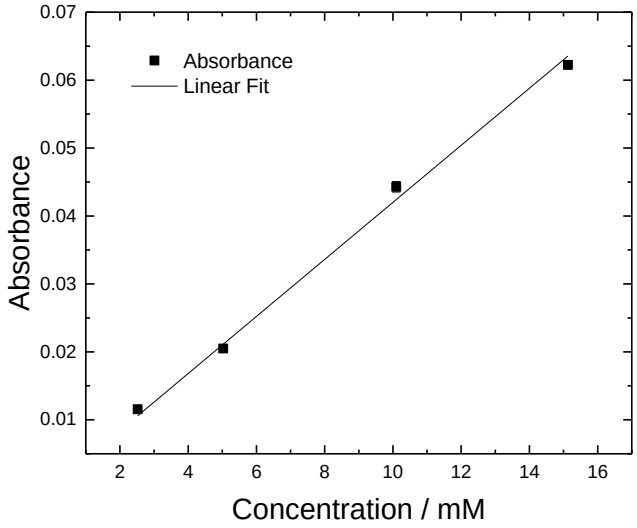

Figure 4.5: Absorbance versus concentration plot to determine molar absorptivity of benzoquinone at a spectral resolution of 8 cm^{-1}.

Spectral Resolution (cm^{-1})	Molar Extinction Coefficients ($M^{-1}cm^{-1}$)	
	Benzoquinone	Hydroquinone
4	1116	1054
8	893	734
16	650	461

Table 4.1: Molar extinction coefficients of Benzoquinone and Hydroquinone at various spectral resolutions.

4.5: Pumping Protocol Optimization

In SIR studies the IR data of the triggered electrochemical reaction is the average of the individual time resolved experiments which are repeated many times until a sufficient signal-to-noise ratio for the IR data is achieved. This requires the electrochemical reaction that is being studied be highly repeatable. To ensure that the IR signal is consistent throughout a SIR diffusion layer mapping study, the initial conditions within the SEC at the start of each time resolved experiment must be identical to ensure the same response. Changes in the initial conditions between individual time resolved experiments would cause a change in the IR response, resulting in a degraded IR signal.

In principle, if the reaction is completely chemically reversible, the initial conditions found in the cell can be re-established by returning the working electrode potential to its base value after a perturbing potential step. This is equivalent to a double-step chronoamperometry experiment. The main concern with obtaining a repeatable electrochemical reaction when doing double-step chronoamperometry is that some of the redox active product diffuses far enough away from the working electrode during the initial potential step that when the potential is returned, not all the product is converted back into reactant.*(4)* Although this "lost charge" is small on an individual basis, if the double-step is repeated numerous times as in the case of the diffusion layer mapping done here there can be a significant change in the composition of the solution. This requires that the solution within the SEC be refreshed after each time resolved experiment to ensure the solution composition is identical at the start of every double-step chronoamperometry experiment.

In order to refresh the solution in the SEC between experiments a pumping system was implemented. The pumping system consisted of a syringe pump (New Era Pump Systems Inc.) used to inject fresh solution into the SEC along with two solenoid valves (Biochem Valves) that close during an experiment to create a closed fluid line, but could be opened to allow solution to flow between time resolved experiments. The system ends with the collection of the used solution (Figure 4.6).

A syringe pump system that could be completely automated was required because refreshing the solution required precise timing such that the fluid in the SEC could be replaced while ensuring that there would be no fluid flow within the SEC during a time resolved experiment. This automation also allows for potential and pumping control via a single LabVIEW program during SIR studies and allows the pumping to be optimized such that the time required to reset the cell is minimized.

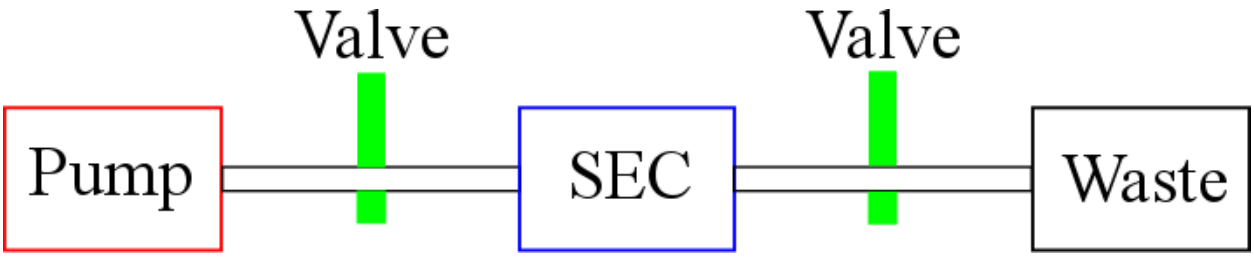

Figure 4.6: Diagram of pumping setup used to fresh the fluid in the SEC.

Custom software written in LabVIEW with a National Instruments 6251 X-series multifunction data acquisition card was used. The software allowed for pump control, valve control, control of quiescence times, as well as control of the solenoid valves in the inlet and outlet fluid lines. In order to determine the optimized conditions for the pumping procedure, a solution of 1 mM ferricyanide in 0.25 M NaF was used as a probe. Ideally, the pump procedure should ensure that the electrolyte within the cell volume is devoid of any turbulent or convective flow, as these mass-transport effects will greatly perturb the expected diffusion-controlled response of the system. In evaluating the pumping protocol, the cell volume was replenished using a given set of conditions (pumping time, pumping rate, timing of valve closing and resting times) and then the electrode potential was stepped to a value where the redox probe gets oxidized. The current-time response was digitally recorded under a limiting set of conditions (extremely long wait times and slow pump rate) to set a bench mark. The specific conditions for the benchmark was the injection of 180 µL of electrolyte at a pump rate of 250 µL/min. The electrolyte was allowed to settle for two minutes after pumping with both the inlet and outlet solenoid valves in the open positions. The valves were sequentially closed with a 30s wait time after each valve closing to allow pressure dissipation within the fluid tubing. Another wait time of two minutes was added to achieve total quiescence within the SEC. The wait times of the various stages in the pumping protocol were then decreased until the transients showed clear deviation from the benchmark. Stability testing was also performed by repeating the chronoamperometry under a given fluid injection protocol for several hours. See Figure 4.7 for an example of the resulting current transients as the wait time is changed.

In order to produce the bench mark described above, a pump rate that would produce a stable system over long times was needed. To reduce the time for pumping, a higher pump rate was used (500 µL/min). This large rate of pumping resulted in high pressures within the SEC. High pressure resulted in solution being forced between the surface of the SEC and the gasket. To avoid this the pump rate was limited to 250 µL/min. While this results in twice the time needed to pump, it provided a stable system where solution could be pumped through the SEC continuously without any solution leaking.

The initial step to optimize the pumping procedure was to adjust the total time that the pump is on (referred to as pump time henceforth). A more intuitive way to think about pump time is to combine it with the pump rate and express it in terms of pumped volume. It should be noted that although the nominal volume with a gasket of 25 µm would be 7.1 µL, the measurement of the cavity by interference fringes resulted in a cavity thickness of 30-40 µm. A cavity thickness of 40 µm results in a volume of 12 µL and was used as the SEC cell volume for the optimization of the pumping protocol. At a minimum, the volume of the SEC needs to be pumped through the SEC to allow the solution to be replaced with no changes in the electrochemical response. A volume that is roughly five times larger than the SEC volume was chosen to ensure that the solution was truly refreshed during the longer SIR studies, which resulted in a pump time of 15 seconds at a rate of 250 $\mu L min^{-1}$. This volume was chosen due to the fact that the placement of the inlet and outlet holes in the SEC results in the majority of the fluid flow in the SEC to be directly from the inlet to the outlet, so a large excess of fluid was required to refresh the solution throughout the SEC.

The pumping of solution caused the buildup of pressure in the fluid tubing. This buildup of pressure within the tubing means that even after the pump has stopped there will be a pressure gradient across the SEC, so fluid will continue to flow for a time after the pump is stopped. This flow required that the solenoid valves not be closed until the pressure on either side had equalized. To ensure pressure dissipation, a 20 second wait time was required. This increases the time required for solution to be refreshed and the overall duration of the SIR diffusion layer mapping study.

The closing of the valves to create a closed system during the SIR experiments causes a small amount of fluid displacement as the valve pinches the tubing. The closing of the valves also causes vibrations. To decrease the fluid movement caused by the closing of the valves, they were closed in sequence with enough delay time to ensure the majority of the flow had subsided. Empirically, it was found that it was critical that the valve between the pump and SEC was closed first. Within three seconds the flow of solution was no longer visible. The electrochemical response was found to be stable when this wait time was set to five seconds.

An additional problem is fluid turbulence within the SEC after the second solenoid valve closes. To ensure that the electrochemistry is mass transport limited, time must be allowed for the

solution to become quiescent. This results in a wait time needed between the closing of the last valve and the start of the SIR experiment to make sure the solution within the cell is stagnant. This time was difficult to determine accurately as non-quiescent conditions resulted in subtle changes in the electrochemical response. The wait time for quiescence was lowered until a 10s quiescence time was reached (Figure 4.7b). Above 10 seconds it was difficult to discern whether or not there was a difference in the transients. To ensure that they system was stable throughout a SIR diffusion layer mapping study the wait time was set to 15s.

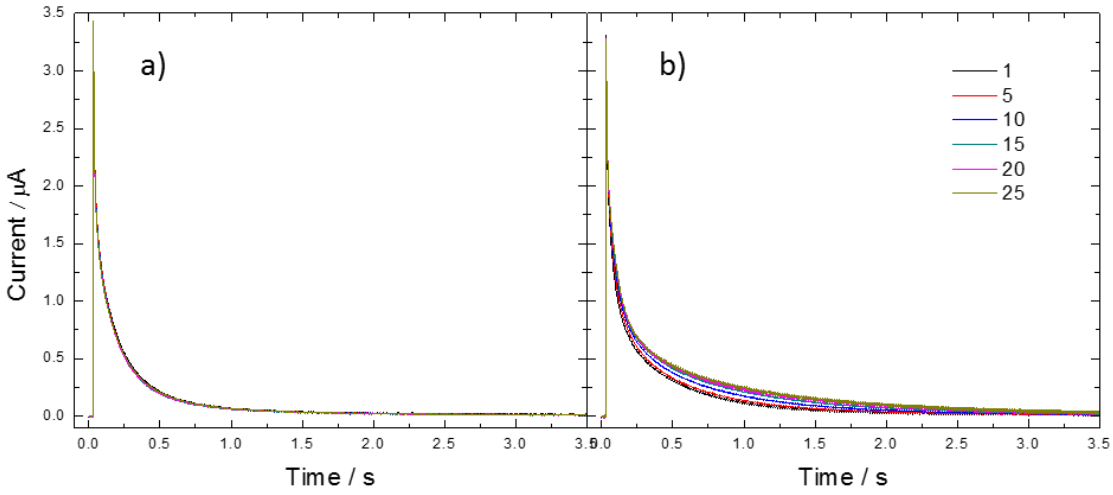

Figure 4.7: Every fifth current transient to 25 of 0.1M NaF electrolyte for (a) benchmark wait times and (b) 10 second wait for quiescence.

The pumping procedure adds an additional 55 seconds to each SIR time resolved experiment and is in fact the majority of time consumption in an SIR diffusion layer mapping study as the collection of IR data only takes ~10 seconds to complete. This demonstrates that SIR diffusion layer mapping studies are limited by the pumping procedure. Any effort that can minimize this time would be hugely beneficial for future experiments.

4.6: SIR beam profile investigation

The SIR beam profile at the 01B1 mid-IR beamline at the Canadian Light Source was investigated using the Bruker 70v spectrometer coupled to a Hyperion 3000 IR microscope using

the 64x64 pixel focal plane array detector with a pixel resolution of 2.7 µm to determine the best configuration of the IR beam for diffusion layer mapping. The data acquired by the focal plane array consists of an IR spectrum at each pixel, where the image of the IR beam at a particular frequency was produced by extracting the IR signal at the desired frequency from every pixel using custom built software in Matlab (MathWorks, USA). The imaging of the beam at the desired frequency revealed that the IR beam was composed of two elliptical beam cross-sections with a roughly Gaussian profile.*(8)* The shape of the beam could be manipulated by slightly defocusing to create an area that was more homogeneously illuminated than the focused beam as seen in Figure 4.8 below.

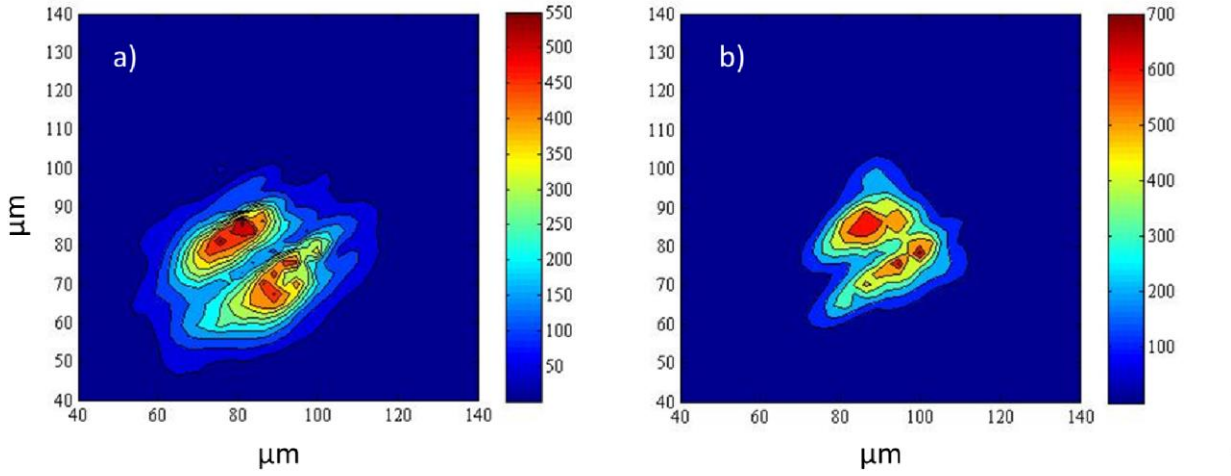

Figure 4.8: Image of the IR beam at a wavenumber of 2040 cm^{-1} with (a) the beam focused and (b) slightly defocused.

4.6.1: Beam Profile and Apertures

The shape of the IR beam (two ellipsoids or a defocused, but more uniform intensity) has implications on the choice of the apertures, as the SEC employed in the SIR studies uses an inlaid band electrode as the working electrode as depicted in Figure 4.2a. In the restricted geometry of the cell, the band electrode results in a quasi-linear diffusion layer perpendicular to the length of the band electrode. Within the time frame of a typical experiment the diffusion layer will extend out ~250 µm from the electrode's edge, but it is expected that only the area that is 100 µm away will produce an appreciable IR signal. This defines the area that can be used for

SIR studies. Within the area available, the closest approach of the IR beam is on the order of 20 μm in the current cell design. This limits the available area to 20 to 100 μm in SIR studies.

The diffusion layer produced in the thin cavity propagates away from the electrode edge over the CaF_2 window (Figure 4.9, 4.11 and 4.13). The following Cartesian coordinates will be defined to assist the subsequent discussion: the direction between the CaF_2 windows will be the z-direction, the length of the electrode is the y-direction, and the x-direction extends away from the electrode edge. As the electrochemical reaction is occurring uniformly along the y-direction, any x-z plane should have the same concentration profile. As such, any change in the IR beam intensity parallel to the edge of the electrode will not affect the resulting IR signal, as the same concentration profile will be interrogated. However, any change in the IR beam intensity perpendicular to the electrode edge (x-direction) will cause bias of the IR signal, with the high intensity portions of the IR beam dominating the overall IR signal produced. The use of blade apertures allows for the beam footprint in the y and x directions to be adjusted to the desired size. This is advantageous over circular apertures as the blade apertures can be set so that the illumination size perpendicular to the electrode is minimized and the illumination area parallel to the electrode edge expanded to encompass the whole beam. The smallest dimension possible with the blade apertures is 10 μm, as smaller sizes causes a stark decrease in signal due to diffraction of the IR beam. It should also be noted that the distance between each set of blade apertures cannot be adjusted with the same accuracy. One can be set to an accuracy of ± 0.5 μm whereas the other set of blade apertures can only be set to an accuracy of ± 7 μm

Figures 4.9 and 4.10 display the advantages of using the blade apertures over the circular apertures. The smallest circular apertures with the 15x objective produces a 20 μm diameter IR illumination spot (Figure 4.10), which would incorporate most of the IR beam whether defocused or focused, resulting in the need for deconvolution of the IR signal based on the two-dimensional intensity of IR illumination within the aperture area. While it is conceivable, it would be impractical, especially when the blade apertures can be used to select the most homogeneous spot of the IR beam as seen in Figure 4.10.

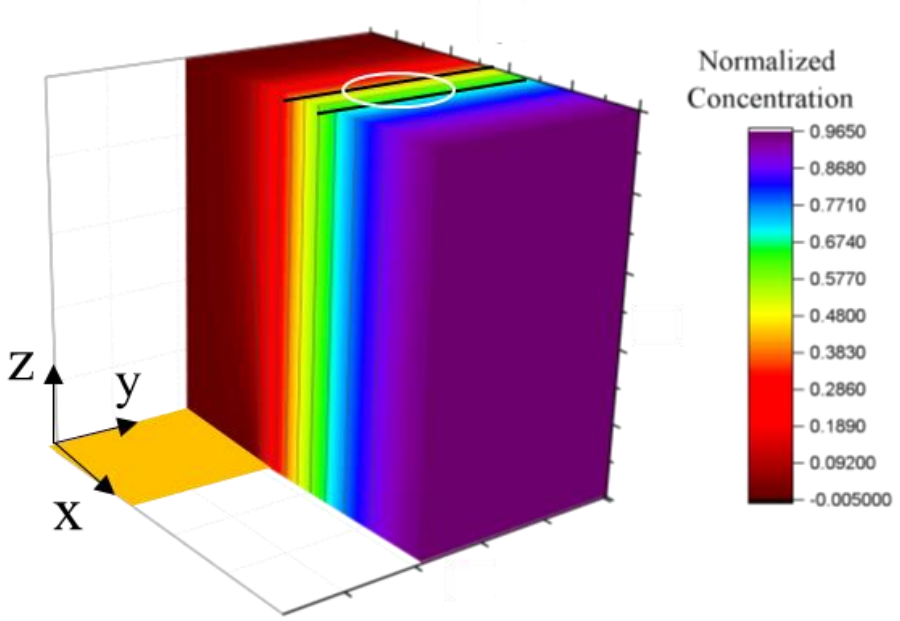

Figure 4.9: Three dimensional contour plot of concentration profile within the SEC, with the blade aperture (white) and circular aperture (black) overlaid and the electrode displayed in yellow. The blade aperture in the y direction is omitted for clarity.

Figure 4.9 shows that by using the blade apertures, a much narrower range of concentrations within the diffusion layer are probed as compared to the 20 µm diameter circular aperture. The ability to probe a narrow range of concentrations further decreases the effects of the non-homogenous IR beam intensity. The blade apertures also allow for more sections of the diffusion layer at distances closer to the electrode to be probed. This is advantageous because the change in concentration of the redox is greater closer to the electrode and produces a stronger IR signal. This in turn decreases the number of repeats of the time resolved experiments to produce adequate signal-to-noise.

4.7: Time-resolved FT-IR measurements

All FT-IR rapid scan measurements were taken at the 01B1 mid-IR beamline at the Canadian Light Source. The resulting rectangular aperture could easily be moved to increasing

distances from the electrode edge. To mitigate the effects of the IR beam heterogeneity as described above, the beam was defocused and the opening of the blade apertures was centered on an area of the IR beam that showed relatively high homogeneity as seen in Figure 4.10. It was assumed that the resulting diffusion profiles would be homogeneous along the electrode's edge and therefore any effects on the measured IR response caused by the inhomogeneities in the IR beam would be minimized.

Figure 4.11 shows the simulated concentration distribution in both the horizontal and vertical directions at short time and short distances from the raised electrode (see below for modelling details). At short times and distances the concertation gradient is large enough that the IR beam will interrogate numerous concentrations within the 10 μm distance (x-direction) selected by the blade apertures. Linear diffusion also has not been established at short time, which results in the IR beam interrogating variable concentrations as it passes through the solution (z-direction), as seen in Figure 4.11b. The resulting IR spectra at short distances and times will report on a distribution of concentrations in both the x and z directions where quantitatively accurate agreement between experimental and simulated results would require rigorous mathematical treatment. However, the error should be significantly less problematic at larger distances due to the increasing linearity of the diffusion front and should result in quantitative agreement.

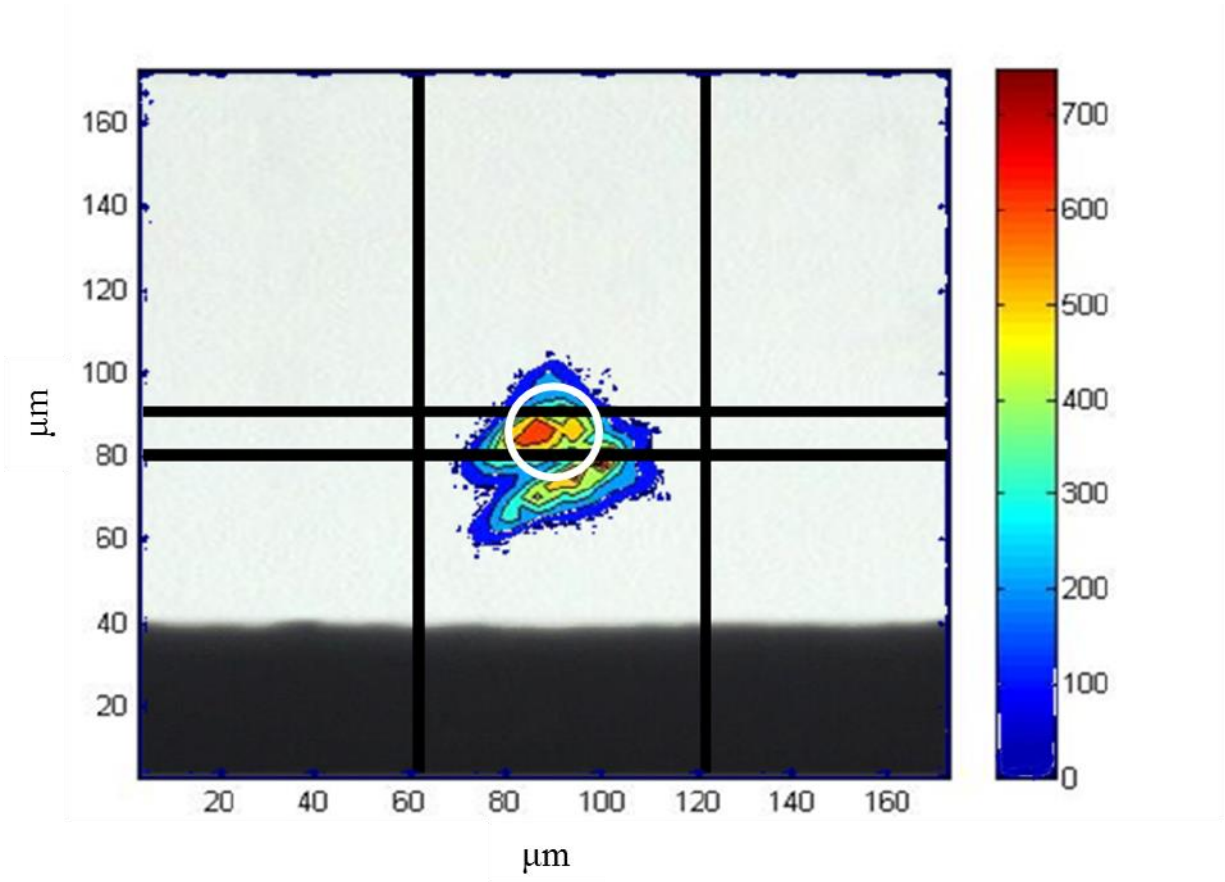

Figure 4.10: Defocused beam with the blade aperture (black) and circular aperture (white) centered on the most homogeneous section of IR beam. The dark grey region is the edge of the working electrode.

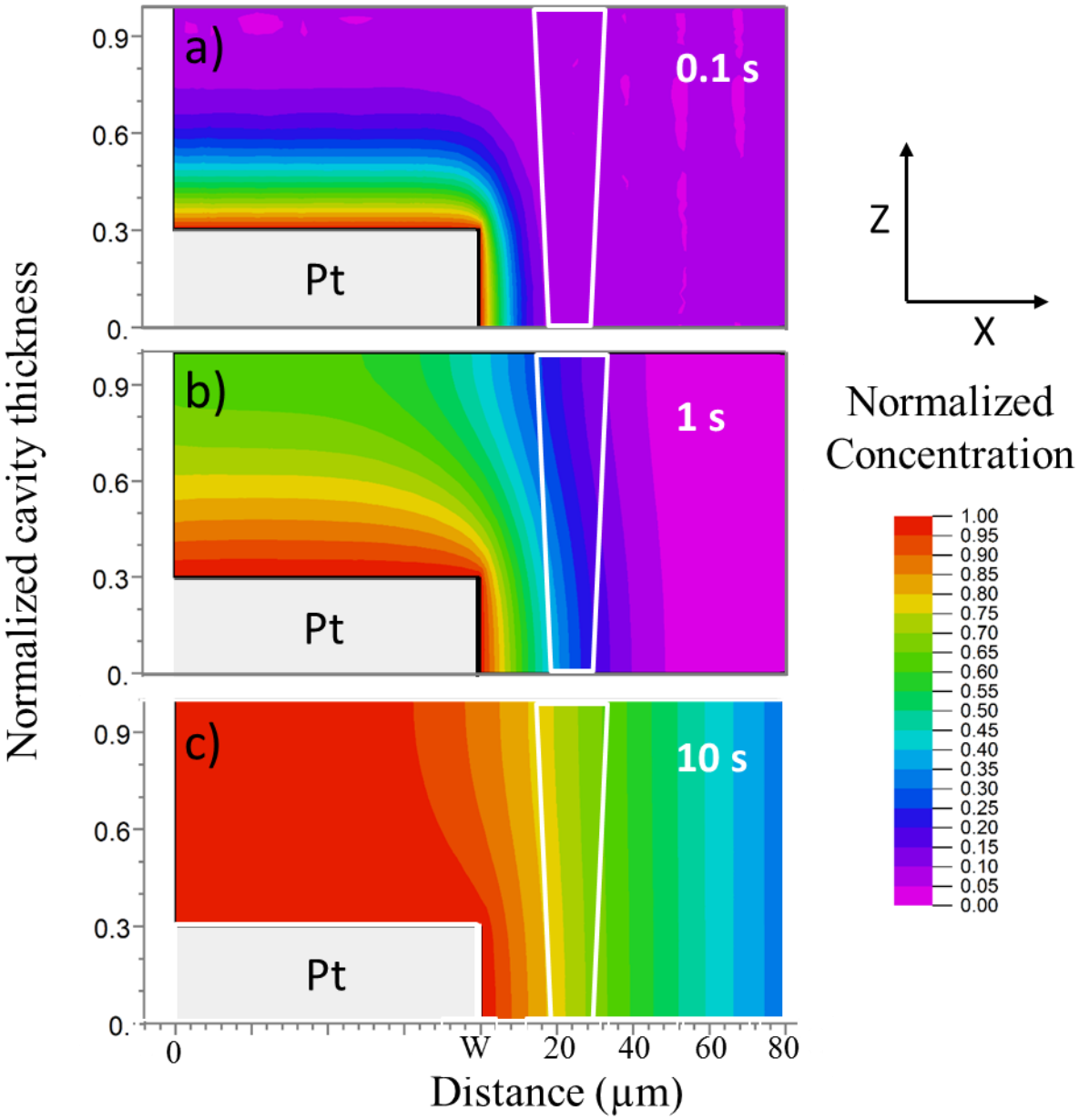

Figure 4.11: Simulated diffusion layer profile at (a) 0.1 second, (b) 1 second and (c) 10 seconds with the IR beam overlaid (white).

For the time resolved IR measurements the mirror speed was 80 Hz and the resolution was set to either 4 cm^{-1} or 8 cm^{-1} depending on the experiment. At 4 cm^{-1} a single interferogram can be collected every ~250 milliseconds and at 8 cm^{-1} every ~170 milliseconds. This allowed for sufficient time resolution to observe the growth of the diffusion layer during the ten second potential step.

Before the start of each SIR diffusion layer mapping study, a cyclic voltammogram was recorded to ensure proper electrochemical behaviour was operative and to determine the reference and step potentials. Step potentials were chosen such that they were sufficiently far from the formal potential of the redox couple to ensure that the electrochemical reaction was diffusion limited. However, too large an overpotential is problematic as secondary redox processes associated with electrolysis of the water or the oxidation of gold need to be avoided.

The setup described in the pumping procedure (Chapter 4.4) was used for double-step chronoamperometry experiments, where the potential was stepped from a reference potential to a sample potential followed, by a potential step back to the reference value with the solution in the SEC being replaced in between experiments. This was performed simultaneously with the time resolved IR measurements. The precise synchronization of the potential step and the start of the individual time resolved IR spectra acquisition was done using custom software written in LabVIEW.

Each rapid scan experiment consisted of 10 inteferograms collected at the reference potential, which were averaged and used as the reference spectrum. This was followed by the collection of either 40 or 60 individual interferograms using the spectrometer's rapid-scan functionality. This resulted in the collection of spectra over approximately 10 seconds with the exact time resolution defined by the chosen spectral resolution. To ensure that the system was properly "reset" after a double potential step, fresh electrolyte was pumped into the cell and allowed to settle. The double-step and pumping process was repeated up to 256 times at each beam position in order to improve the signal-to-noise ratio. This entire procedure was repeated at various positions away from the electrode. The smallest electrode to beam position was determined by how close the IR beam could be placed to the electrode edge without being "clipped" by various components of the cell. The first position measured was the position closest to the electrode edge and the remaining positions measured were increasingly further away so that concentration versus time curves at the various distances could be measured. The term "SIR study" will be used from here on to signify diffusion layer mapping by time resolved IR measurements at positions from the electrode edge.

4.8: Numerical Simulations

To extract the diffusion coefficients, a comparison of the experimental concentration profiles in time and space with those predicted by theory is required. In principle, Fick's second law can be shown to provide an analytical solution for C(x,y,z,t) with the diffusion coefficients being the adjustable parameters. However, there are no analytical solutions for the thin-cavity geometry and numerical simulations are required. Therefore, it was necessary to model the diffusion so that comparisons to the experimental results could be made. The numerical simulations were performed using commercial software (Flex PDE). This software uses finite elements to model space and finite differences to model time. A two dimensional Cartesian geometry was setup with the spatial geometries being the height (Z) and length (X) of the diffusion space (Figure 4.12). Dimensionless variables were used in the numerical simulations. Concentrations are normalized by the bulk concentration of the initial redox species present in the electrolyte and all spatial and temporal parameters are normalized by the cell thickness, *h*. The dimensionless quantities are summarized in Table 4.2.

Variable	*Dimensionless Variables*
Reactant Concentration	$C_{reactant} = {}^{c_{reactant,t}}/_{c_{reactant,initial}}$
Product Concentration	$C_{product} = {}^{c_{product,t}}/_{c_{reactant,initial}}$
Time	$T = {}^{tD_{reactant}}/_{h^2}$
Height	$Z = {}^{z}/_{h}$
Length of the Diffusion Space	$X = {}^{x}/_{h}$
Width of the Electrode	$W = {}^{w}/_{h}$
Diffusion Coefficient of Product	$D = {}^{D_{product}}/_{D_{reactant}}$

Table 4.2: Reduced coordinates used in numerical simulations.

The symmetry of the SEC required that only half of the diffusion space be modelled. The modelled space in the x direction started from the middle (width) of the electrode and extended to a semi-infinite distance. The full cavity thickness, i.e. $0 \leq Z \leq 1$, is modelled. The resulting simulation space is a plane in the cell starting at the middle of the electrode and extending out across the calcium fluoride window and from the face of the cell to the top calcium fluoride window, see Figure 4.12.

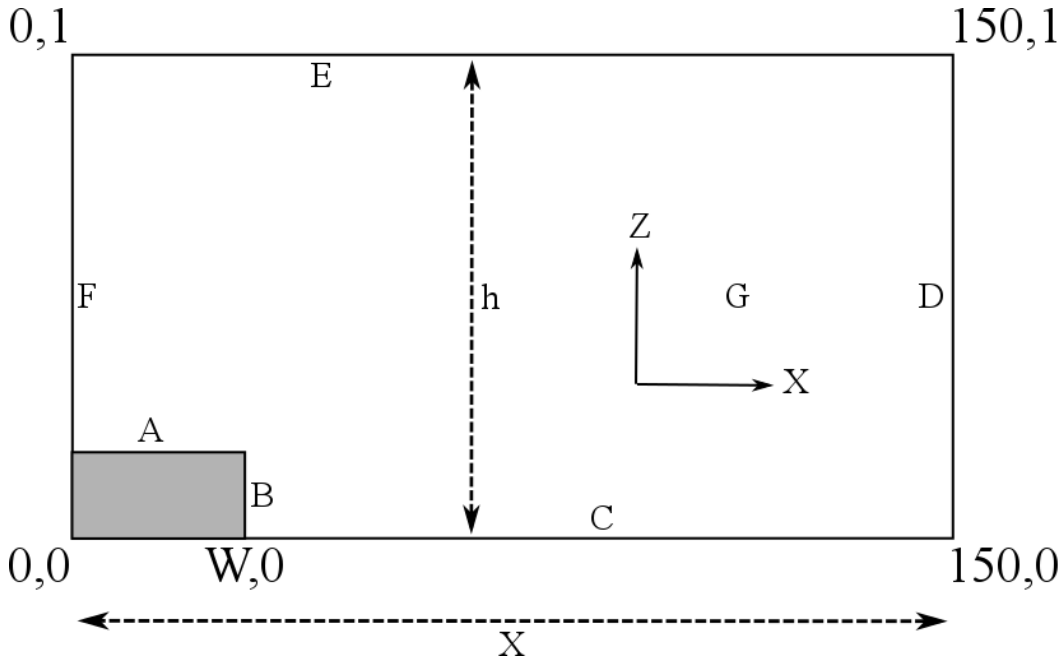

Figure 4.12: Reduced Cartesian coordinates and variables used in the numerical simulations. W is half the width of the electrode in reduced coordinates and B is the height of the electrode in reduced coordinates. (B is zero for the embedded electrode cell design). h is the height of the cell. C, D, E and F are the boundaries where the flux of material is zero

The boundary conditions imposed on the system are summarized in the table below.

Description (Boundary)	*Condition*
Electrode (A and B)	$t = 0, C_{reactant} = 1$
	$t > 0, C_{reactant} = 0$
	$n \cdot \nabla C_{reactant} = -n \cdot D \cdot \nabla C_{product}$
Body of diffusion space (G)	$t = 0, C_{reactant} = 1, C_{product} = 0$
Bottom CaF_2 window (C)	$n \cdot \nabla C_{reactant} = n \cdot \nabla C_{product} = 0$
Top CaF_2 window (E)	$n \cdot \nabla C_{reactant} = n \cdot \nabla C_{product} = 0$
Vertical edge above electrode (F)	$n \cdot \nabla C_{reactant} = n \cdot \nabla C_{product} = 0$
Vertical edge at far end of diffusion space (D)	$C_{reactant} = 1, C_{product} = 0$

Table 4.3: Boundary conditions used in numerical simulations, Letters correspond to the boundary in Figure 4.10.

The signal registered by the IR beam was simulated by selecting a rectangular region at the same distance from the electrode as the experimental data and with the same width as the aperture setting. The normalized concentration in this area is monitored *versus* time and compared to the experimental data. The diffusion coefficient in the simulated data is adjusted until good agreement is obtained between experimental and simulated data diffusion profiles.

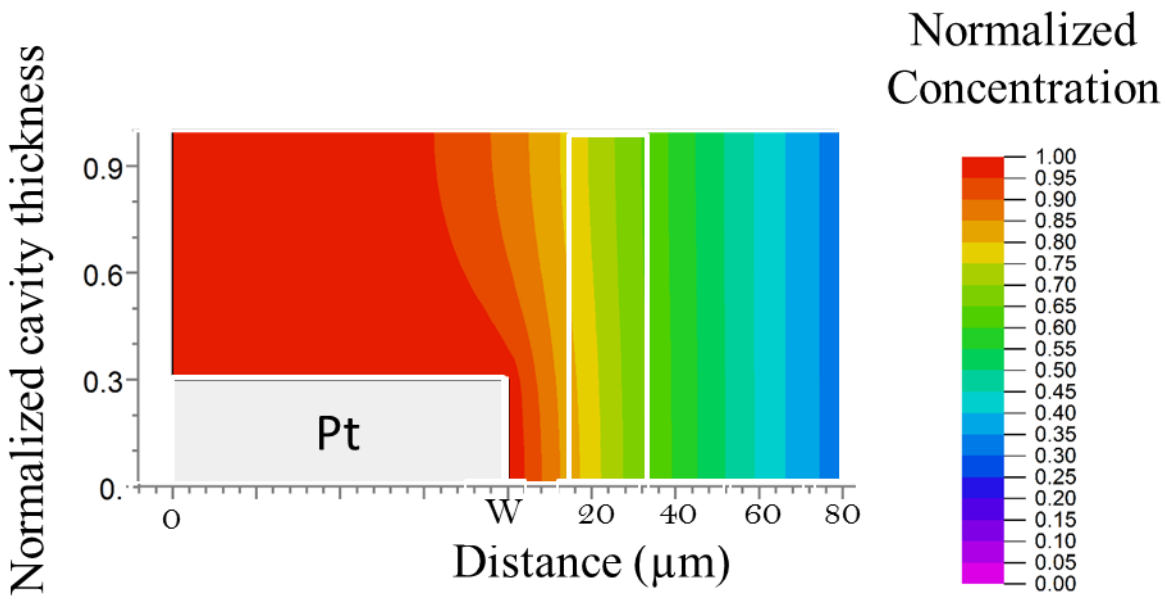

Figure 4.13: Simulation of the diffusion space where the black rectangle is the area interrogated by the IR beam.

4.9: FT-IR Rapid-scan Data Analysis

4.9.1: Ferri/Ferrocyanide

The rapid scan FT-IR spectra collected by the spectrometer's proprietary software (OPUS) are collected as interferograms and digitally Fourier Transformed to provide single-channel spectra. A custom-built routine written in MATLAB was used for further data processing. The routine converted the single channel spectra into absorbance spectra according to equation 4.3.

$$Abs = -Log_{10}\left(\left(S_i / S_{ref}\right)\right) \tag{4.3}$$

Where S_i are the individual spectra at each time and S_{ref} is the reference spectrum collected at the beginning of each time resolved experiment.

These absorbance values were then converted to normalized concentration values via the following equations:

$$\frac{Abs_{(reactant,t)}}{Abs_{(reactant,max.)}} = 1 - \frac{C_{reactant,t}}{C_{reactant,max}} \quad (4.4)$$

$$\frac{Abs_{(product,t)}}{Abs_{(reactant,max.)}} = -\frac{\epsilon_{product}}{\epsilon_{reactant}} \frac{C_{product,t}}{C_{reactant,max}} \quad (4.5)$$

Where Abs is absorption, ε is the molar absorptivity and C is concentration. $Abs_{(reactant,max.)}$ is the maximum absorbance of the reactant species, determined by filling the cell with electrolyte then with the initial reactant solution without applying a potential. The maximum absorbance used in equations 4.4 and 4.5 is calculated using the just electrolyte solution as the reference and the initial reactant solution as the experimental spectra using equation 4.3. To produce the final normalized concentration *versus* time graphs, the absorbance's at the wavelengths of interest (2115 cm^{-1} [ferricyanide], 2040 cm^{-1}[ferrocyanide], 1512 cm^{-1}[hydroquinone] and 1656 cm^{-1}[benzoquinone]) were used.

The absorbance's at the desired wavenumber were then plotted against time, where the time for each point, $t_{spectra,\,i}$ was taken as the mid-point between the start time and end time of the acquisition of each spectra.

4.9.2: Hydroquinone/Benzoquinone

The data analysis for the oxidation of hydroquinone (HQ) to benzoquinone (BQ) uses the same Matlab routine to produce the absorbance spectra.

Every fourth absorbance spectrum was then taken and individually baseline corrected using the peak analyzer function in Origin (OriginLab, USA). A series of straight line fits to each spectra are used as the baseline. From the baseline corrected spectra the maximum absorbance is determined. This absorbance is converted to a normalized concentration and plotted against time by the previously described method.

The error for the experimental data is determined by calculating the standard deviation from a region in the spectra where no signal is present in an individual time resolved spectra at each

distance. The error in absorbance used for all data points at that distance is three standard deviations of the noise value.

4.10 Fitting of Simulation Data

The comparison of the simulated data to the normalized IR data was done using Origin. The reduced simulation data was exported to Origin. The reduced simulation data contains normalized concentrations, but time (t) needs to be extracted from the reduced time (T) in order to be compared to the normalized IR data. Real time was extracted from the reduced time via the following equation:

$$t = {Th^2}/{D_{reactant}} \tag{4.2}$$

The diffusion coefficient of the reactant is varied to adjust the simulation data and plotted versus the experimental IR data. The diffusion coefficient is adjusted until the simulated data and the experimental data showed good visual agreement for the farthest distance from the electrode investigated.

In principle a fitting regression analysis could be implemented, but this would require significant method development.

4.11: References

1. Rosendahl, S.; University of Saskatchewan. *Advances in in-Situ Spectroelectrochemical Fourier Transform Infrared Spectroscopy*, 2013.

2. Rosendahl, S. M.; Borondics, F.; May, T. E.; Pedersen, T. M.; Burgess, I. J. Interface for time-resolved electrochemical infrared microspectroscopy using synchrotron infrared radiation. *Rev. Sci. Instrum.* **2011,** *82*, 083105.

3. Rosendahl, S. M.; Borondics, F.; May, T. E.; Pedersen, T. M.; Burgess, I. J. Synchrotron Infrared Radiation for Electrochemical External Reflection Spectroscopy: A Case Study Using Ferrocyanide. *Anal. Chem.* **2011,** *83*, 3632-3639.

4. Bard, A. J.; Faulkner, L. R. *Electrochemical Methods: Fundamentals and Applications*; Wiley: New York, 2001.

5. Amatore, C.; Pebay, C.; Sella, C.; Thouin, L. Mass Transport at Microband Electrodes: Transient, Quasi-Steady-State, and Convective Regimes. *ChemPhysChem* **2012,** *13*, 1562-1568.

6. Conway, B. E. Electrochemical oxide film formation at noble metals as a surface-chemical process. *Prog Surf Sci* **1995,** *49*, 331-452.

7. Rosendahl, S. M.; Borondics, F.; May, T. E.; Burgess, I. J. Step-Scan IR Spectroelectrochemistry with Ultramicroelectrodes: Nonsurface Enhanced Detection of Near Femtomole Quantities Using Synchrotron Radiation. *Anal. Chem. (Washington, DC, U. S.)* **2013,** *85*, 8722-8727.

8. May, T.; Ellis, T.; Reininger, R. Mid-infrared spectromicroscopy beamline at the Canadian Light Source. *Nuclear Instruments and Methods in Physics Research Section A: Accelerators, Spectrometers, Detectors and Associated Equipment; Proceedings of the 14th National Conference on Synchrotron Radiation ResearchSRI 2007* **2007,** *582*, 111-113.

5: Diffusion Layer Mapping Part 1: Reduction of Ferricyanide

5.1: Introduction

Following the evolution of electrochemical diffusion layers can give insight into the nature of coupled electrochemical reactions. For example, in many electrochemical reactions, including those related to important electrocatalytic reactions such as methanol oxidation, intermediates produced in a heterogeneous charge transfer process diffuse from the electrode surface and undergo a homogeneous chemical reaction in the electrolyte volume adjacent to the electrode. Such processes are known as ***EC*** reactions to designate that an ***E***lectrochemical process precedes a ***C***hemical one. Although it is possible to infer details of the chemical process by measuring its perturbation of the electrochemical reaction, mechanistic insight, the kinetics of the process and even identification of the reaction intermediates requires the collection of analytical information of concentrations in the diffusion layer surrounding the electrode.

There have been many methods developed to probe the growth of electrochemically generated diffusion layers.*(1-6)* As described previously these methods require the use of sensitive and selective analytical techniques. Many of these techniques are limiting due to the fact that they require the analytes to exhibit fluorescence*(4)*, resonant Raman effects*(3)* or require the reaction intermediates and products be redox active.*(7)* IR spectroscopy is an attractive technique for diffusion layer mapping as it should be much more universal as compared to the previous methods used. When coupled with synchrotron radiation, IR microscopy also provides a high degree of spatial resolution.

This chapter will discuss the use of synchrotron infrared radiation (SIR) to investigate the growth of an electrochemically generated diffusion layer within a thin cavity transmission spectroelectrochemical cell (SEC). The thin cavity within the SEC is needed in order to minimize the attenuation of the IR radiation by the solvent. The thin cavity is also responsible for producing a nearly linear diffusion front that extends away from the electrode.

The ferri/ferrocyanide redox couple was the system used to evaluate and develop diffusion layer mapping by SIR. This system is very simple and involves only the reversible one electron transfer redox reaction without a coupled chemical step. It was imperative to study such a simple system to first establish that the SIR-based diffusion layer mapping provides the same diffusion

coefficients for ferricyanide and ferrocyanide that are considered to be well-established in the electrochemistry literature. The ferri/ferrocyanide redox couple was chosen because it had been previous used by the Burgess group to evaluate the use of SIR to probe redox reactions at ultramicroelectrodes with high time resolution.*(8)* The ferri/ferrocyanide is also a well-studied system that has frequently been used in IR spectroelectrochemical studies*(9-11)* owing to the fact that the CN stretches lie outside any interferences from the IR-active modes of water and there is a shift of ~ 75 cm^{-1} in the CN vibration between ferricyanide and ferrocyanide. This spectral shift allows both species to be followed independently by IR.

5.2: Results and Discussion

In order to develop diffusion layer mapping by SIR it was prudent to first characterize the electrochemistry of the ferri/ferrocyanide redox couple in the SEC cell. As discussed above, SIR-based mapping of the diffusion layer requires the co-addition of many individual IR scans during applied potential steps that significantly alter the concentrations of the redox species. As detailed in Chapter 4.4, it is imperative that the system is restored to its initial conditions after each individual measurement to ensure that co-addition of multiple measurements provides improved signal to noise (S/N) ratios. Cyclic voltammetry (CV) and double-step chronoamerometry (D-SC) were done to qualitatively characterize the electrochemistry within the SEC. The CVs of 10 mM ferricyanide within the second version of the SEC cell (Figure 4.1b) were distorted showing that the process was less reversible as indicated by the shift in the peaks to potentials further from the formal potential as seen in Figure 5.1. There also appears to be small waves closer to the formal potential. The current transients produced from D-SC experiments also show abnormal behaviour with a shoulder present in the current transients indicating a secondary process is occurring after about 1 second (Figure 5.2). The nature of this process is unknown, but it is thought that the resistive thin-cavity and large working electrode give rise to this anomalous behaviour. The large electrode and high solution resistance also leads to somewhat large times required to charge the electrode surface (time constant) that could result in a perturbation of the formation and evolution of the diffusion layer. It is also conceivable that the large electrode could give rise to convection at the electrode surface via a density gradient due to the large change in concentration of species at the electrode surface.*(12-14)* Although this

behaviour is anomalous it is consistently seen within the SEC cell with little variation. Due to the unknown origin of this electrochemical behaviour its' effect on the resulting diffusion layer could not be predicted. From the electrochemical description and simulations, it was thought that if there was any effect that it would be most pronounced when the beam was focused to spots close to the working electrode edge and at short times.

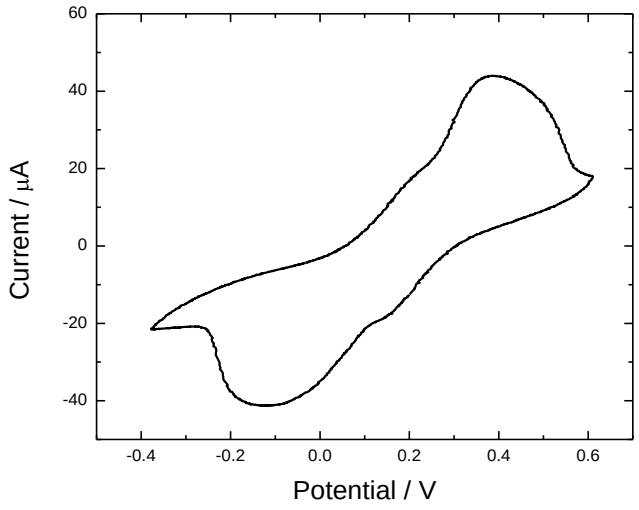

Figure 5.1: Cyclic voltammogram of 10 mM ferricyanide in 0.1 M NaF electrolyte using the second generation SEC (Figure 4.1b).

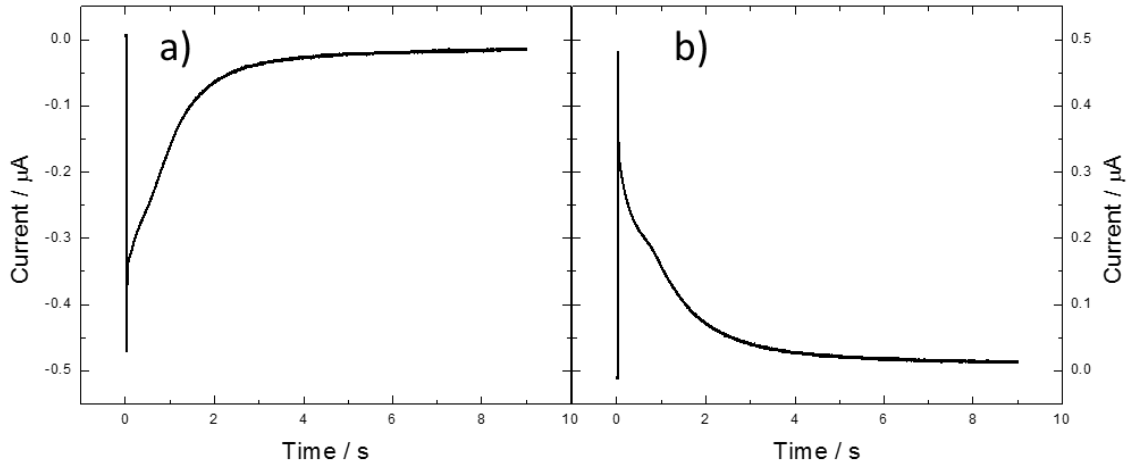

Figure 5.2: Current transients from double-step chronoamperometry experiments, 0.1M NaF, 10 mM ferricyanide within the SEC, with (a) the perturbing potential step followed by (b) the step back to the base potential.

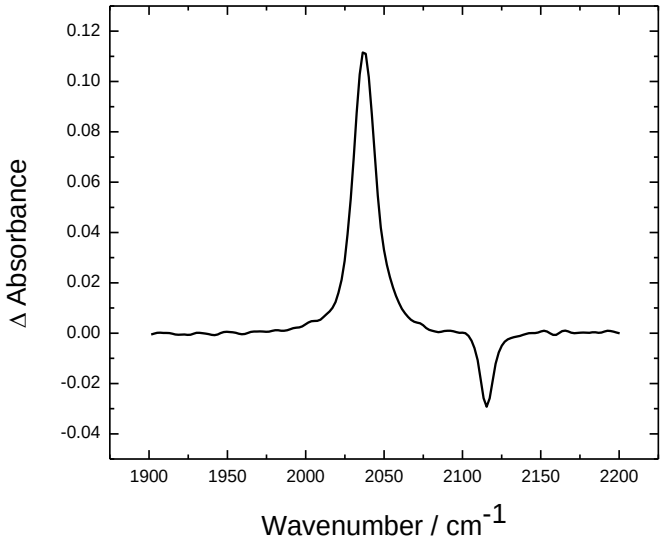

Figure 5.3: Spectrum showing the change in absorbance for the reduction of 10 mM ferricyanide (2115 cm^{-1}) to ferrocyanide (2040 cm^{-1}) in 0.1 M NaF using the SEC cell.

Before SIR studies were performed, the change in IR signal for ferricyanide and ferrocyanide in the SEC were measured. Figure 5.3 shows the change in absorbance for a 10 mM ferricyanide solution after a potential step of from +600 mV to -400 mV. Large changes in the absorbance are observed at 2040 cm^{-1} and a weaker change in absorbance at 2115 cm^{-1}. These bands can be assigned to the conversion of ferricyanide to ferrocyanide. The differences in signal intensity is due to the differences in the molar extinction coefficients of ferricyanide and ferrocyanide.

Figure 5.4 shows the results of this initial qualitative SIR study to investigate the change in ferricyanide and ferrocyanide concentrations following the co-addition of 256 scans. The curves show the expected trend with the change in absorbance at a distance of 25 μm from the electrode showing the largest change. The change in absorbance is smaller for distances further away from the electrode, as expected. This preliminary experiment also demonstrated that when using 10 mM redox species, both the ferricyanide and ferrocyanide IR signatures provide sufficient S/N to allow mapping of the time-dependent diffusion layer concentrations of the species being depleted and the species being produced. The signal for ferricyanide is significantly noisier due to its smaller molar extinction coefficient, but the general trend is visible. With this initial evidence supporting the feasibility of the technique's use in investigating electrochemically generated

diffusion layers, refinements in the measurement described in Chapter 4 were done, specifically the change from circular apertures to the narrow blade apertures with the defocused beam (Chapter 4.5). This allows for higher spatial resolution in the distance perpendicular to the electrode edge and a more homogenous IR illumination. This, along with the ability to refresh the solution within the cell in a timely manner were done to improve the measurement. The refinements in the measurement resulted in the concentration transients shown in Figure 5.5 for both ferri- and ferrocyanide. A qualitative comparison between Figure 5.4 and 5.5 shows that there is an improvement in the S/N, especially for the ferricyanide transients.

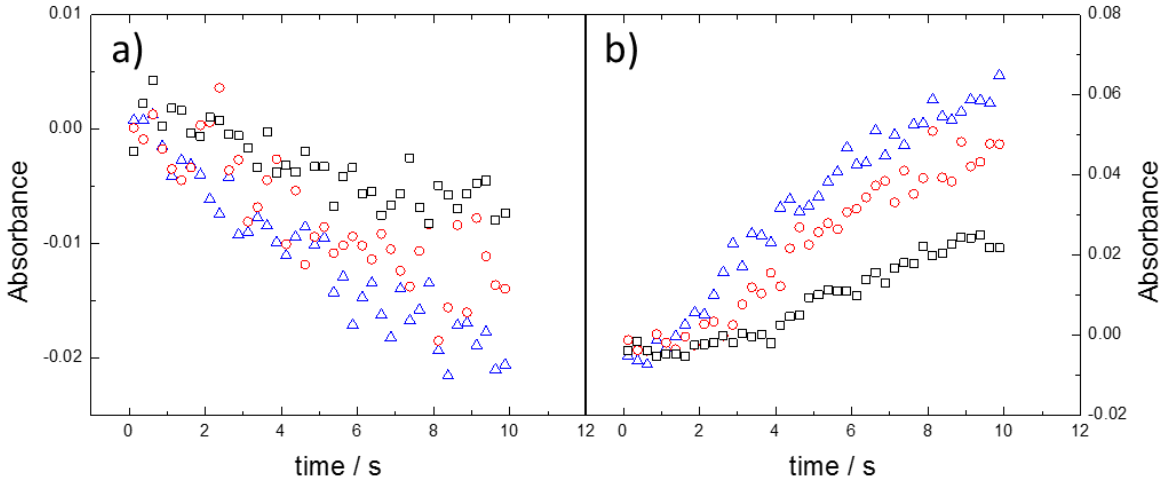

Figure 5.4: Absorbance transients for the reduction of 10 mM ferricyanide, (a) ferricyanide (Ox) and (b) ferrocyanide (Red). Experiments were preformed using a 20 µm circular aperture at distances of 25 µm (triangles), 45 µm (circles) and 65 µm (squares).

Using the improved measurement procedure (particularly the use of blade apertures instead of circular apertures) the IR signal at the closest spot position shows a much starker change in concentration (Figure 5.5, black squares). The increased S/N also gives the transients for ferricyanide a more defined curve that can be simulated with greater accuracy. This indicates that the size of the aperture does have an effect on the reported IR signal simply because the circular apertures sample a greater range of concentrations but report only the mean concentration change.

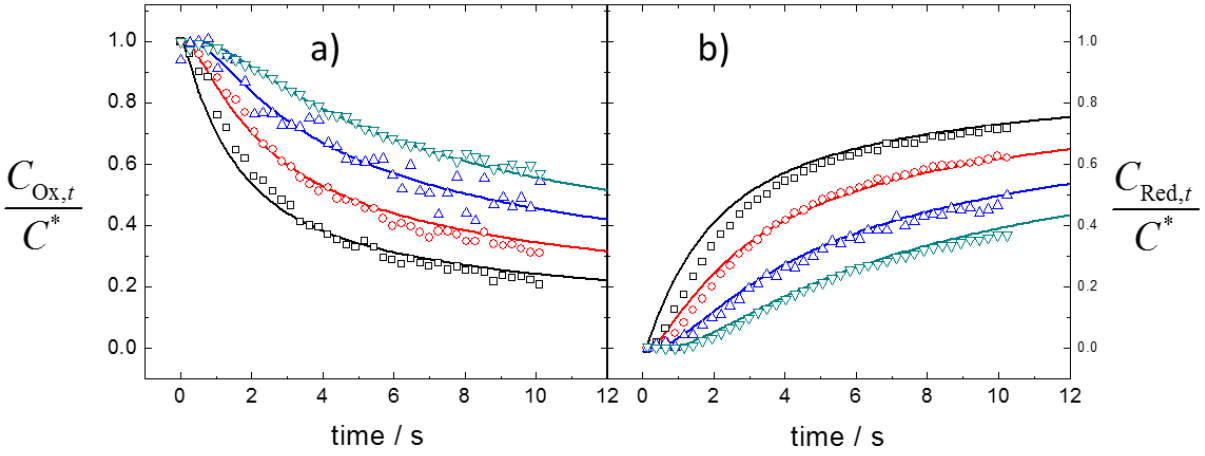

Figure 5.5: Experimental (points) and simulated (lines) concentrations transients for the reductions of 10 mM ferricyanide, (a) ferricyanide (Ox) and (b) ferrocyanide (Red). Concentrations have been normalized by the initial concentration of Ox. Experiments were performed with the closest edge of the beam at distances of 15 µm (squares), 30 µm (circles), 45 µm (triangles) and 65 µm (down triangles).

The simulated results seen in Figure 5.5 were produced using the procedure detailed in Chapter 4.8. The optical fringes between the two windows were used to determine the cell height (the inter-window cavity was 38 µm) and the distance between the window and the top of the Pt foil working electrode (~25 µm). The distance between the top calcium fluoride (CaF_2) and the electrode varied slightly depending on the location on the Pt foil electrode that was measured. This indicates that the Pt foil surface was uneven, which is not surprising given the fact that attachment of the foil was done by gluing the foil onto the CaF_2 window using cyanomethacrylate adhesive. While it is conceivable to simulate the diffusion using an electrode of variable height, it is expected that the overall effect would be minimal and as such the electrode thickness was set to a constant height of 25 µm.

Using these values for the boundary conditions in Table 4.3 the simulated curves used to fit the experimental data are shown as the solid lines in Figure 5.5. This resulted in diffusion coefficients of $D_{Ox} = 4.4 \times 10^{-6}$ cm^2 s^{-1} (ferricyanide) and $D_{Red} = 3.6 \times 10^{-6}$ cm^2 s^{-1} (ferrocyanide). These diffusion coefficients were determined using the procedure outlined in Chapter 4.10 where the diffusion coefficient of the initial redox species present is adjusted to fit the experimental

curves. Comparison of the simulated concentration transients and experimental concentration transients show that distances of 30, 45 and 60 μm demonstrate good agreement for both the ferricyanide and ferrocyanide species. The curves at the 15 μm distance shows good agreement at long times but at short times the experimental signal is lower than that predicted by simulation. The discrepancy between the simulated concentration transients and the experimental concentration transients can be attributed to two factors. The first factor is that deviations from the expected concentration profile have been previously noted in diffusion layer mapping studies where the large concentration gradient produces a refractive index gradient causing angular divergence of the beam.*(4)* The other factor was described previously in Chapter 4.7; where the evolution of the diffusion layer at distances close to the electrode and at short times results in the sampling of various concentrations as the IR beam passed through the SEC as described in Figure 4.8b. While both are thought to be factors that contribute to the difference between the experimental results and the simulated results at the 15 μm spot, it is believed that the discrepancies are primarily caused by the convoluted diffusion profile produced by the electrode's particular geometry. This is due to the fact that the divergence of the optical path cause by refractive index gradients is path dependent and with such a small optical path length its contribution should to be minimal.*(15)*

The absolute diffusion coefficients determined for ferri and ferrocyanide obtained by SIR studies are lower by about ~ 30 – 40% than those previously obtained by electrochemical methods.*(16)* However, the ratio between the two diffusion coefficients is in good agreement with the literature values. The systematically low diffusion coefficients predicted by SIR studies here will be discussed, analyzed and reconciled in Chapter 7.

5.3: Summary and Conclusion

Preliminary experiments showed that a change in the IR signal with respect to time for both ferricyanide and ferrocyanide could be followed in the SEC and produced the expected trends. However, the reported IR signal for ferricyanide was quite noisy with only the general trend being distinguishable.

Refinements to the measurement resulted in data quality. The increase in S/N was such that the concentration transients at the various distances from the electrode for both the ferricyanide and

ferrocyanide could be resolved. Simulation of the experimental concentration transients was performed in order to extract the diffusion coefficients of both ferricyanide and ferrocyanide. The simulation resulted in diffusion coefficients of $D_{Ox} = 4.4 \times 10^{-6}$ cm^2 s^{-1} and $D_{Red} = 3.6 \times 10^{-6}$ cm^2 s^{-1} of ferricyanide and ferrocyanide respectively. These diffusion coefficients are lower than the reported literature values, this discrepancy will be discussed in Chapter 7.

5.4: References

1. Engstrom, R. C.; Weber, M.; Wunder, D. J.; Burgess, R.; Winquist, S. Measurements within the diffusion layer using a microelectrode probe. *Anal. Chem.* **1986,** *58*, 844-848.

2. Jan, C. C.; McCreery, R. L. High-resolution spatially resolved visible absorption spectrometry of the electrochemical diffusion layer. *Anal. Chem.* **1986,** *58*, 2771-2777.

3. Amatore, C.; Bonhomme, F.; Bruneel, J. -.; Servant, L.; Thouin, L. Mapping dynamic concentration profiles with micrometric resolution near an active microscopic surface by confocal resonance Raman microscopy. Application to diffusion near ultramicroelectrodes: first direct evidence for a conproportionation reaction. *J Electroanal Chem* **2000,** *484*, 1-17.

4. Amatore, C.; Chovin, A.; Garrigue, P.; Servant, L.; Sojic, N.; Szunerits, S.; Thouin, L. Remote Fluorescence Imaging of Dynamic Concentration Profiles with Micrometer Resolution Using a Coherent Optical Fiber Bundle. *Anal. Chem.* **2004,** *76*, 7202-7210.

5. Cannan, S.; Douglas Macklam, I.; Unwin, P. R. Three-dimensional imaging of proton gradients at microelectrode surfaces using confocal laser scanning microscopy. *Electrochemistry Communications* **2002,** *4*, 886-892.

6. Peng, S.; Liu, Z.; Sun, T.; Ma, Y.; Ding, X. Spatially Resolved In Situ Measurements of the Ion Distribution Near the Surface of Electrode in a Steady-State Diffusion in an Electrolytic Tank with Confocal Micro X-ray Fluorescence. *Anal. Chem.* **2014,** *86*, 362-366.

7. Amatore, C.; Szunerits, S.; Thouin, L.; Warkocz, J. Monitoring Concentration Profiles In Situ with an Ultramicroelectrode Probe. *Electroanalysis* **2001,** *13*, 646-652.

8. Rosendahl, S. M.; Borondics, F.; May, T. E.; Burgess, I. J. Step-Scan IR Spectroelectrochemistry with Ultramicroelectrodes: Nonsurface Enhanced Detection of Near Femtomole Quantities Using Synchrotron Radiation. *Anal. Chem. (Washington, DC, U. S.)* **2013,** *85*, 8722-8727.

9. Pharr, C. M.; Griffiths, P. R. Step-Scan FT-IR Spectroelectrochemical Analysis of Surface and Solution Species in the Ferricyanide/Ferrocyanide Redox Couple. *Anal. Chem.* **1997,** *69*, 4665-4672.

10. Pons, S.; Datta, M.; McAleer, J. F.; Hinman, A. S. Infrared spectroelectrochemistry of the Fe(CN)64−/Fe(CN)63− redox system. *Journal of Electroanalytical Chemistry and Interfacial Electrochemistry* **1984,** *160*, 369-376.

11. Korzeniewski, C.; Severson, M. W.; Schmidt, P. P.; Pons, S.; Fleischmann, M. Theoretical analysis of the vibrational spectra of ferricyanide and ferrocyanide adsorbed on metal electrodes. *J. Phys. Chem.* **1987,** *91*, 5568-5573.

12. Ngamchuea, K.; Eloul, S.; Tschulik, K.; Compton, R. G. Advancing from Rules of Thumb: Quantifying the Effects of Small Density Changes in Mass Transport to Electrodes. Understanding Natural Convection. *Anal. Chem.* **2015,** *87*, 7226-7234.

13. Volgin, V. M.; Davydov, A. D. Numerical simulation of natural convection of electrolyte solution with three types of ions in the electrochemical cell with vertical electrodes. *Russian J. Electrochem.* **2010,** *46*, 1360-1372.

14. Selman, J. R.; Newman, J. Free-Convection Mass Transfer with a Supporting Electrolyte. *J. Electrochem. Soc.* **1971,** *118*, 1070-1078.

15. Pawliszyn, J. Spectroelectrochemical sensor based on Schlieren optics. *Anal. Chem.* **1988,** *60*, 1751-1758.

16. Bard, A. J.; Faulkner, L. R. *Electrochemical Methods :Fundamentals and Applications*; Wiley: New York, 2001.

6: Diffusion Layer Mapping Part 2: Oxidation of Hydroquinone

6.1: Introduction

In the previous chapter the evolution of the diffusion layer for the reduction of ferricyanide, which is a simple one electrode redox process was examined. This chapter looks at extending the use of the diffusion layer mapping methodology (as described in Chapter 4) to follow the evolution of the diffusion layers produced during a more complex redox reaction. Furthermore, the results in Chapter 5 show a significant discrepancy between literature values of the diffusion coefficients and those determined by SIR studies. To determine if the discrepancy is systematic, the method was applied to a second electrochemical system.

The 1,4-benzoquinone (BQ)/hydroquinone (HQ) redox couple was chosen to extend SIR studies. This redox system was chosen due to the fact that unlike the ferri/ferrocyanide redox couple it undergoes a two electron, two proton redox process (see Figure 6.1). While the redox chemistry of the BQ/HQ redox couple is much more complicated, it is still well characterized. Laviron performed a theoretical treatment of the pH effects on the kinetic and thermodynamic factors affecting the electron and proton transfer mechanism*(1, 2)* and Smith and co-workers have elucidated the role of buffer and protic solvents during quinone redox chemistry.*(3, 4)*

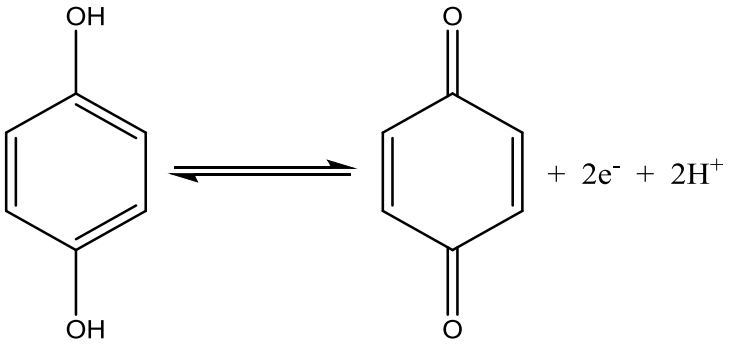

Figure 6.1: Oxidation of HQ to BQ.

These studies highlight the need for the use of buffers for SIR studies as the oxidation of HQ would cause the acidification in the area around the electrode due to the release of protons. The acidification will cause shifts in the formal potential as well as change the proton transfer kinetics*(1-3)*, which can be avoided by the use of buffered solution.*(3)* As such, a buffered solution was used in all SIR studies to ensure reproducible electrochemistry.

Aside from the BQ/HQ redox couple being well studied electrochemically, it has also been used in IR spectroscopic*(5-7)* and IR spectroelectrochemical studies.*(8-12)* Of particular interest is the study by Jin *et al*, who have used time resolved IR measurements to follow the formation and decay of BQ/HQ reaction intermediates in aprotic solvents*(12)*

6.2: Results and Discussion

6.2.1: Molar Extinction Coefficients

While there have been extensive spectroscopic studies*(5-12)* of the BQ/HQ redox couple there is little reported on the molar extinction coefficient in the IR. To the author's knowledge, the only reported IR molar extinction coefficients have been by Yang *et al*, who report molar extinction coefficients for benzoquinone and the intermediates of its reduction in acetonitrile.*(10)* In order to utilize equations 4.4 and 4.5 from Chapter 4.9.1, the molar extinction coefficients are needed. These values must first be obtained from independent measurements.

Before the molar extinction coefficients could be determined, a spectral analysis of BQ and HQ in the D_2O electrolyte solution within the SEC cell was done to determine the IR peaks that would be used to monitor the loss of HQ and production of BQ during SIR studies. The molar extinction coefficients were determined in D_2O due to the overlap of the signal from HQ with the IR-active modes of water. The use of D_2O causes a shift of those modes to regions outside where the IR signal for HQ should appear. Figure 6.2 shows the absorbance spectra of both HQ and BQ in the D_2O electrolyte solution. HQ exhibits a strong peak at 1512 cm^{-1}, corresponding to the benzene ring stretching.*(13, 14)* The spectra of BQ exhibits a strong peak at 1658 cm^{-1}, corresponding to the carbonyl stretch as well as a weak peak at 1315 cm^{-1}, corresponding to the C-H stretching of the ring.*(5, 14)* The peak at 1315 cm^{-1} is far too weak to be used to follow the production of BQ in SIR studies. The strong peak at 1512 cm^{-1} for HQ and 1658 cm^{-1} for BQ provide good IR signals to monitor the change of both BQ and HQ during SIR studies. Also present in the spectra is a large downward going band that is a result of the H-O-D.*(15)* This band arises due to the exchange of a labile hydrogen from the phosphate buffer species and the D_2O solvent. This IR signal from the H-O-D bending mode overlaps other vibrations for BQ and HQ that would be present in that region.*(5, 14)* The H-O-D bending mode perturbs the baseline

near the ring vibration of HQ and requires that no phosphate buffer be used when determining the molar extinction values.

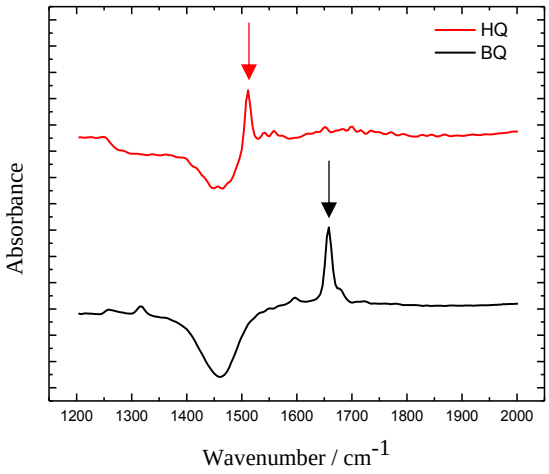

Figure 6.2: Spectra of 15 mM HQ (red) and 15 mM BQ (black) in 0.1M NaF and 20 mM, pH 8 phosphate buffer solution in the SEC cell at a resolution of 8 cm^{-1}.

The molar extinction coefficients BQ and HQ at 1658 cm^{-1} and 1512 cm^{-1} respectively are shown in Figure 6.3 and given in Table 6.1.

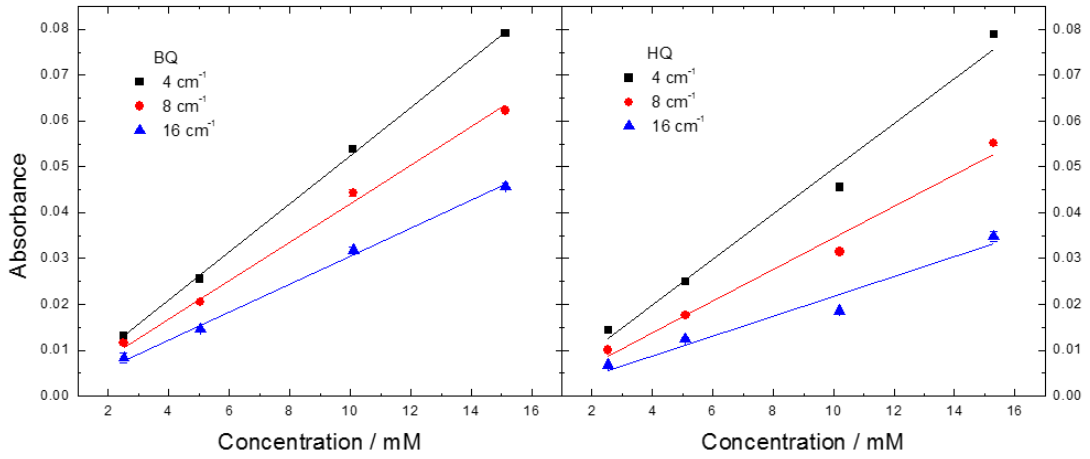

Figure 6.3: Absorbance versus concentration curves for benzoquinone (BQ) and hydroquinone (HQ) at resolutions of 4, 8 and 16 cm^{-1}. Note: the ratios of the molar extinction coefficients are not the same at each resolution due to the presence of a shoulder on the BQ signal that changes with resolution.

Spectral Resolution (cm^{-1})	Molar Extinction Coefficients ($M^{-1}cm^{-1}$)	
	Benzoquinone	Hydroquinone
4	1116	1054
8	893	734
16	650	461

Table 6.1: Calculated molar extinction coefficients for BQ and HQ.

The data for both BQ and HQ show linear trends, which indicates that Beer's law is applicable within the concentration ranges used here.

The concentration *versus* absorbance at resolutions of 16 cm^{-1}, 8 cm^{-1} and 4 cm^{-1} show good agreement with Beer's law and the resulting molar extinction coefficients as expected show an increase with decreased resolution. A resolution of 8 cm^{-1} was chosen for use during SIR experiments for the oxidation of HQ, as it greatly decreased the noise present in the spectra caused by water vapour, but still resulted in a strong signal for both BQ and HQ.

6.2.2: Diffusion Layer Mapping

The SIR studies for the oxidation of HQ to BQ was much more technically challenging due to the instability of BQ and HQ in solution. Both HQ and BQ degrade in solution over time to produce highly conjugated products that cause discolouration of the solutions.*(16-19)* It was found here that solutions of HQ showed a much lower rate of degradation than BQ solutions. Thus, the electrochemical oxidation of HQ was chosen for SIR studies. The number of repeated time resolved measurements (Chapter 4.7) taken during a SIR study was lowered from 256 to 64, as this allows for a time resolved measurement to be completed in ~ 1.2 hour, while still ensuring a sufficient signal to noise ratio at a concentration of 5 mM of HQ. It was also found that the life time of the HQ solution could be extended to last the entire time needed to perform an entire SIR study by placing the HQ solution in a glass electrochemical cell, purging it with nitrogen, and keeping it covered. To further mitigate degradation, the syringe containing the HQ solution was refilled after each time resolved measurement during a SIR study, and the length of tubing between the syringe pump and the SEC was minimized (Figure 4.6). Upon refilling the syringe,

the pump was left on for ~2 minutes to replace some of the old solution within the tube to the SEC with fresh solution. It would be ideal to replace all the fluid from the syringe to the SEC, but this would require a long time to pump enough solution, in which time the solution would have decayed. The other option would be to use new tubing after every syringe refill. While this is possible, it can displace the alignment of the SEC under the microscope.

SIR studies for the oxidation of BQ also differ from the SIR studies of the reduction of ferricyanide in that the SEC with the inlaid band electrode (Figure 4.1c) was used along with resolution 8 cm^{-1} instead of 4 cm^{-1}. The normalized concentration *versus* time curves with the "best-fit" simulated data overlaid are shown in Figure 6.4.

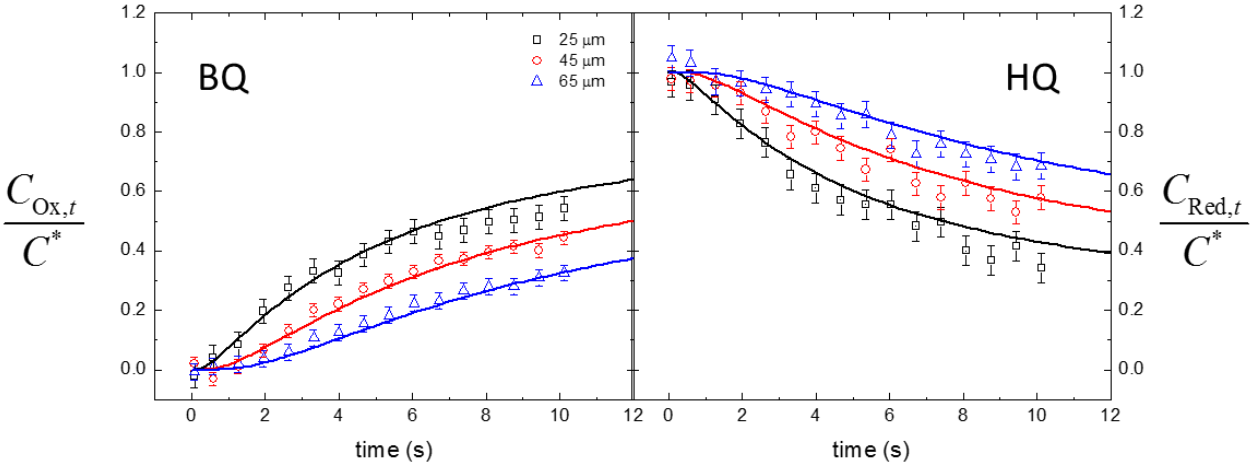

Figure 6.4: Experimental (points) and simulated (lines) concentrations transients for the oxidation of 5 mM hydroquinone, (a) benzoquinone (Ox) and (b) hydroquinone (Red). Concentrations have been normalized by the initial concentration of Red. Experiments were performed with the closest edge of the beam at distances of 25 µm (squares), 45 µm (circles), 65 µm (triangles).

The resulting concentration transients again show the expected trend with the change in concentration being most pronounced at distances close to the electrode. The experimental data is also in very good agreement with the simulated data. The simulation of the experimental data results in diffusion coefficients of $D_{Ox} = 4.1 \times 10^{-6}$ cm^2 s^{-1} and $D_{Red} = 4.7 \times 10^{-6}$ cm^2 s^{-1} for BQ and HQ respectively. The nature of the differences in the diffusion coefficients is thought to

arise from differences in the hydrogen bonding between HQ, BQ and the solvent. These diffusion coefficients are lower than those determined for BQ and HQ in H_2O solution of 12.7 x 10^{-6} cm^2 s^{-1} *(20)* and 7.5 x 10^{-6} cm^2 s^{-1} *(21)* respectively. The decrease in diffusion coefficients is expected due to the increased density of D_2O over water. Again the "validity" of diffusion coefficients determined by SIR will be discussed in the next chapter.

It is important to note that the concentration transients produced in SIR studies are not just dependent on the diffusion coefficients of the species, but also depend on, the cell height and the distance that the IR measurement was made from the electrode. This makes a direct comparison between the BQ/HQ and ferri/ferrocyanide transients impossible. It is this dependency on numerous variables that gives rise to the fact the BQ/HQ transients here show a lower concentration change than the ferri/ferrocyanide transients even though they have larger diffusion coefficients.

6.3: Summary and Conclusions

In this chapter, spectral analysis of BQ and HQ was first done to determine the IR signals that can be used to monitor the change in concentration of BQ and HQ. The molar extinction coefficients for BQ and HQ at various resolutions have been determined.

This chapter has shown that SIR studies using the BQ/HQ redox couple are more technically challenging due to the instability of HQ in solution over time. This required the number of repeated time resolved measurements in a SIR study to be lowered and for the HQ solution within the setup to be refreshed between individual time resolved measurements.

The study of this system has highlighted the need for the appropriate choice of solvent and electrolyte for SIR studies to avoid overlap of solvent IR signals with the IR signals of the analytes. It also gives insight into the limits of SIR studies in the fact that some systems may not be stable enough to be examined by SIR studies due to the long times that are required to complete a full SIR study or the fact that it may be too technically demanding to be feasible.

Nevertheless, SIR studies have been successfully extended from the simple one electron transfer of the ferri/ferrocyanide redox system to the two electron, two proton transport HQ/BQ redox system. The diffusion coefficients of BQ and HQ in the D_2O electrolyte have been determined

to be D_{Ox} = 4.0 x 10^{-6} cm^2 s^{-1} and D_{Red} = 4.5 x 10^{-6} cm^2 s^{-1} respectively, which as expected are lower than the diffusion coefficients reported for BQ and HQ in aqueous solution (H_2O). The examination of the diffusion coefficients produced from SIR studies will be examined in the next chapter.

6.4: References

1. Laviron, E. Electrochemical reactions with protonations at equilibrium: Part VIII. The 2 e, 2H+ reaction (nine-member square scheme) for a surface or for a heterogeneous reaction in the absence of disproportionation and dimerization reactions. *J. Electroanal. Chem.* **1983,** *146*, 15-36.

2. Laviron, E. Electrochemical reactions with protonations at equilibrium: Part X. The kinetics of the p-benzoquinone/hydroquinone couple on a platinum electrode. *J. Electroanal. Chem.* **1984,** *164*, 213-227.

3. Quan, M.; Sanchez, D.; Wasylkiw, M. F.; Smith, D. K. Voltammetry of Quinones in Unbuffered Aqueous Solution: Reassessing the Roles of Proton Transfer and Hydrogen Bonding in the Aqueous Electrochemistry of Quinones. *J. Am. Chem. Soc.* **2007,** *129*, 12847-12856.

4. Staley, P. A.; Lopez, E. M.; Clare, L. A.; Smith, D. K. Kinetic Stabilization of Quinone Dianions via Hydrogen Bonding by Water in Aprotic Solvents. *J. Phys. Chem. C* **2015,** *119*, 20319-20327.

5. Shong, B.; Wong, K. T.; Bent, S. F. Reaction of Hydroquinone and p-Benzoquinone with the Ge(100)-2 x 1 Surface. *J. Phys. Chem. C* **2012,** *116*, 4705-4713.

6. Cyran, J. D.; Nite, J. M.; Krummel, A. T. Characterizing Anharmonic Vibrational Modes of Quinones with Two-Dimensional Infrared Spectroscopy. *J Phys Chem B* **2015,** *119*, 8917-8925.

7. Akai, N.; Kawai, A.; Shibuya, K. Water assisted photo-oxidation from hydroquinone to p-benzoquinone in a solid Ne matrix. *J. Photochem. Photobiol. A.* **2011,** *223*, 182-188.

8. Babaei, A.; McQuillan, A. J. An in situ UV-vis and IR spectroelectrochemical study of the deposition of a hydroquinone anion salt on platinum electrodes from dichloromethane solutions. *J Electroanal Chem* **1999,** *462*, 266-272.

9. Bauscher, M.; Maentele, W. Electrochemical and infrared-spectroscopic characterization of redox reactions of p-quinones. *J. Phys. Chem.* **1992,** *96*, 11101-11108.

10. Jin, B.; Li, L.; Huang, J.; Zhang, S.; Tian, Y.; Yang, J. IR Spectroelectrochemical Cyclic Voltabsorptometry and Derivative Cyclic Voltabsorptometry. *Anal. Chem.* **2009,** *81*, 4476-4481.

11. Wang, J.; Xie, H.; Jin, B. Investigation on Electrochemical Redox of Hydroquinone-Fourier Transform Infrared Spectroelectrochemistry Techniques. *Chinese Journal of Analytical Chemistry* **2013,** *41*, 1006-1012.

12. Jin, B.; Liu, P.; Wang, Y.; Zhang, Z.; Tian, Y.; Yang, J.; Zhang, S.; Cheng, F. Rapid-Scan Time-Resolved FT-IR Spectroelectrochemistry Studies on the Electrochemical Redox Process. *J Phys Chem B* **2007,** *111*, 1517-1522.

13. Kubinyi, M.; Billes, F.; Grofcsik, A.; Keresztury, G. Vibrational spectra and normal coordinate analysis of phenol and hydroquinone. *J. Mol. Struct.* **1992,** *266*, 339-344.

14. Nonella, M. Structures and Vibrational Spectra of p-Benzoquinone in Different Oxidation and Protonation States: A Density Functional Study. *J Phys Chem B* **1997,** *101*, 1235-1246.

15. Socrates, G. *Infrared Characteristic Group Frequencies*; Wiley: Chichester; Toronto, **1980**.

16. Shindo, H.; Huang, P. M. Catalytic Polymerization of Hydroquinone by Primary Minerals. *Soil Sci.* **1985,** *139*, 505-511.

17. Zagorskii, A. L.; Kalnin'sh, K. K.; Toropov, D. K. Structure and Absorption Spectra of Polyhydroquinones. *Russian Journal of Applied Chemistry* **2005,** *78*, 656-662.

18. Cataldo, F. On the structure of macromolecules obtained by oxidative polymerization of polyhydroxyphenols and quinones. *Polym. Int.* **1998,** *46*, 263-268.

19. Barron, E. S. G. The Rate of Autoxidation of Oxidation-Reduction Systems and its Relation to their Free Energy. *J. Biol. Chem.* **1932,** *97*, 287-302.

20. Ahn, S. D.; Somasundaram, K.; Nguyen, H. V.; Birgersson, E.; Lee, J. Y.; Gao, X.; Fisher, A. C.; Frith, P. E.; Marken, F. Hydrodynamic Voltammetry at a Rocking Disc Electrode: Theory versus Experiment. *Electrochim. Acta* **2016,** *188*, 837-844.

21. Ferreira, T. L.; Paixao, Thiago R. L. C.; Richter, E. M.; El Seoud, O. A.; Bertotti, M. Use of Microdevices To Determine the Diffusion Coefficient of Electrochemically Generated Species: Application to Binary Solvent Mixtures and Micellar Solutions. *J Phys Chem B* **2007,** *111*, 12478-12484.

7: Diffusion Coefficient Analysis

7.1: Introduction

Both the ferri/ferrocyanide redox couple and the BQ/HQ redox couple are well studied systems and while diffusion coefficients for both have been determined*(1-4)* they are not directly applicable to these studies. This is due to fact that the solution composition for the ferri/ferrocyanide used here involved the use of different supporting electrolyte.*(1, 2)* The previously determined diffusion coefficients are also not directly applicable for the BQ/HQ redox system owing to the fact that D_2O instead of H_2O was used as the solvent in this work. To the author's knowledge there have been no reported values for the diffusion coefficients for either BQ or HQ with D_2O as the solvent. Therefore, this needed to be determined independently.

In this chapter the diffusion coefficients of ferricyanide, ferrocyanide, BQ and HQ will be determined using hydrodynamic linear sweep voltammetry (HLSV), the details of which are given in Chapter 4.2. The diffusion coefficients determined by this purely electrochemical technique will be compared to those determined by SIR studies to validate its' ability to monitor the evolution of diffusion layers during electrochemical reactions.

7.2: Diffusion Coefficient Analysis

First the diffusion coefficients for ferricyanide and ferrocyanide will be discussed. The initial steps for determining diffusion coefficients was to preform HLSV experiments at the same conditions used by Arvia *et al* (0.1 M KCl electrolyte)*(2)* and compare the values. These initial studies using HLSV produced diffusion coefficients that were lower that the literature values determined previously by HLSV for ferricyanide and ferrocyanide of 6.77×10^{-6} cm^2 s^{-1} and 5.88×10^{-6} cm^2 s^{-1} respectively. The determination of the diffusion coefficients using HLSV by Arvia *et al* do not discuss the determination of the electrode area, which lead to the investigation of the effect of the electrode area on the diffusion coefficients. In the analysis of the diffusion coefficients by HLSV, the resulting slope of the Levich plot is equal to:

$$slope = 0.620nFAD^{2/3}\nu^{-1/6}C \quad (7.3)$$

Only the electrode area (A) has to be determined independently, as all other quantities are known. It was found that if the geometric area of the electrode was substituted for the electrochemical surface area (ECSA), as determined by H UPD in the methodology used here (Chapter 4.2) that the resulting diffusion coefficients were 7.2 x 10^{-6} cm^2 s^{-1} and 6.5 x 10^{-6} cm^2 s^{-1} for ferricyanide and ferrocyanide respectively. These values are in excellent agreement with the literature values for ferricyanide and ferrocyanide stated above.*(2)* This suggests that previous studies to determine the diffusion coefficient for ferricyanide and ferrocyanide have not accurately taken into account the area of the electrode. When the ECSA of the electrode is used rather than the geometric area, lower diffusion coefficients are obtained.

When 0.1 M NaF was used instead of KCl the resulting diffusion coefficients determined using the actual area of the electrode show good agreement with the diffusion coefficients determined by SIR studies. The consistency in the diffusion coefficients between SIR studies and HLSV using the actual area supports the need to be able to accurately determine the electrode area when electrochemical techniques are employed. Beyond this, it also indicates that the methodology developed here for diffusion layer mapping produces a diffusion limited electrochemical reaction with no other mass transport present, resulting in the ability to extract the diffusion coefficients of the redox species.

Analytes	*Conditions*	*Diffusion Coefficient (10^{-6} cm^2 s^{-1})*	
		SIR Study	RDE
Ferricyanide	0.1 M KCl + 1 mM		5.1
Ferrocyanide	analytes		4.6
Ferricyanide	0.1 M NaF + 10 mM	4.5	4.1
Ferrocyanide	analytes	3.6	3.7
Benzoquinone	0.1 M NaF + 1 mM		6.0
Hydroquinone	analytes in H_2O		6.1
Benzoquinone	0.1 M NaF + 5 mM	4.1	3.7
Hydroquinone	analytes in D_2O	4.7	4.2

Table 7.1: Diffusion coefficients of ferricyanide, ferrocyanide, benzoquinone and hydroquinone using various electrolytes and solvents. The error on RDE diffusion coefficients is expected to be ~10%.

As in the case of ferricyanide and ferrocyanide, the diffusion coefficients of BQ and HQ were determined by HLSV in water and compared to literature values. Although the literature values of the diffusion coefficient for BQ in H_2O could not be found, the closely related orthoquinone (catechol) has a reported diffusion coefficient of 6.61×10^{-6} cm^2 s^{-1}.*(5)* Other studies have also reported the diffusion coefficients for catechols, which are substituted with small groups as 6.0×10^{-6} cm^2 s^{-1}.*(6)* The values for BQ measured by HLSV are therefore quite consistent with the literature values for the closely related molecules. Like the values for BQ determined here by HLSV the diffusion coefficient of HQ shows agreement with the literature value of 7.5×10^{-6} cm^2 s^{-1}.*(3)* While the values for BQ and HQ determined here are lower, the disparity could be attributed to differences in the electrolyte used here as compared to the literature.

As expected, the diffusion coefficients of both species decreased by ~ 30% in D_2O due to its higher density compared to H_2O. Most importantly, the diffusion coefficients for HQ and BQ as determined by SIR are within 10-15% of the electrochemically determined values.

In this chapter, the diffusion coefficients of BQ or HQ needed to be independently determined in order to verify the ability of SIR to monitor the diffusion layer, as no values for the diffusion coefficients of either BQ or HQ have previously been reported in D_2O. The resulting diffusion coefficients as determined by the purely electrochemical HLSV technique and SIR studies resulted in diffusion coefficients that were within 10-15% of each other, indicating the validity of SIR to monitor the evolution of electrochemical diffusion layers.

The self-consistency of the diffusion coefficients for the BQ/HQ redox system indicated that the same level of agreement should have been obtained for the ferri/ferrocyanide system. Instead, diffusion coefficients that were ~30% lower than the previously reported values were obtained. While it was thought that the differences in electrolyte could cause shifts in the diffusion of the redox species, this could not account for that large a discrepancy. This chapter reconciles the differences in the diffusion coefficients for ferricyanide and ferrocyanide. It was found that the literature values for the diffusion coefficients previously determined by HLSV for ferri/ferricyanide were erroneous. This error is a result of the fact that the geometric area of the electrode was used instead of the ECSA, as no method to determine the ECSA had been developed. By using the ECSA the results by HLSV and SIR show excellent agreement with each other.

7.3: Summary and Conclusions

Here the diffusion coefficient of ferricyanide and ferrocyanide have been determined by HLSV. It was found that earlier studies to determine the diffusion coefficients did not accurately account for the entire electrochemical active electrode area, which resulted in an over estimation of the diffusion coefficients. This is a rather remarkable result for ferricyanide and ferrocyanide as this redox couple has been a standard go to simple redox system, partly due to the fact that the diffusion coefficients are considered well established within the electrochemical community. For example, the diffusion coefficients of ferricyanide and ferrocyanide listed are in Bard and Faulkner as tabulated data in much the same way as reduction potentials. However, further inspection of the diffusion coefficients reported in the literature revealed that the original measurements were made in the 1950's before the Pt-H UPD method of determining the electrode area was known.

These studies have accurately accounted for the electrochemical active area, which results in lower diffusion coefficients than the literature values. These lower diffusion coefficients produced by using the electrochemical active area show good agreement with the coefficients determined by SIR studies.

The diffusion coefficient determined for BQ and HQ by HLSV in water are comparable to the literature values and diffusion coefficients determined SIR studies also show good agreement to the values determined by HLSV in D_2O.

This study of the diffusion coefficients has shown that the methodology developed here results in a diffusion limited electrochemical reactions within the SEC. The resulting diffusion layers can be monitored by spatially and temporally monitored using SIR, with that ability to extract quantitative information.

7.4: References

1. Bard, A. J.; Faulkner, L. R. *Electrochemical Methods: Fundamentals and Applications*, 2nd ed.; John Wiley and Sons Inc: New York, New York, 2001.

2. Arvía, A. J.; Bazán, J. C.; Carrozza, J. S. W. The diffusion of ferro- and ferricyanide ions in aqueous potassium chloride solutions and in solutions containing carboxy-methylcellulose sodium salt. *Electrochim. Acta* **1968,** *13*, 81-90.

3. Ahn, S. D.; Somasundaram, K.; Nguyen, H. V.; Birgersson, E.; Lee, J. Y.; Gao, X.; Fisher, A. C.; Frith, P. E.; Marken, F. Hydrodynamic Voltammetry at a Rocking Disc Electrode: Theory versus Experiment. *Electrochim. Acta* **2016,** *188*, 837-844.

4. Ferreira, T. L.; Paixao, Thiago R. L. C.; Richter, E. M.; El Seoud, O. A.; Bertotti, M. Use of Microdevices To Determine the Diffusion Coefficient of Electrochemically Generated Species: Application to Binary Solvent Mixtures and Micellar Solutions. *J Phys Chem B* **2007,** *111*, 12478-12484.

5. Sharma, L. R.; Kalia, R. K. Hydrodynamic voltammetry at the tubular graphite electrode. Determination of diffusion coefficients of aromatic amino and phenolic compounds. *J. Chem. Eng. Data* **1977,** *22*, 39-41.

6. Deakin, M. R.; Wightman, R. M. The kinetics of some substituted catechol/o-quinone couples at a carbon paste electrode. *Journal of Electroanalytical Chemistry and Interfacial Electrochemistry* **1986,** *206*, 167-177.

Chapter 8: Conclusions and Future Work

8.1: Conclusions

Purely electrochemical techniques cannot provide molecular information regarding the identity of the species within the diffusion layer created by and electrochemical reaction. The inherent difficulty in spatially probing the area near electrodes via spectroscopic techniques is positioning the radiation close to the electrode without obscuring it, while also allowing sufficiently high resolution such that many regions near the electrode can be distinguished.

The Burgess group has previously used the small illumination spots available with SIR to monitor electrochemical reactions at ultramicroelectrodes,*(1)* but until now have not taken advantage of the small spot size for spatial resolution. This thesis has focused on utilizing the small spot size capabilities of SIR for spatial resolution in order to monitor diffusion layers. To do so, the IR beam must be situated within the area adjacent to the electrode where the diffusion layer develops but not be significantly attenuated or blocked. Two SEC cells have been designed and presented in this thesis that have overcome these challenges; the first SEC used a Pt foil overlaid on the CaF_2 window of the SEC (Figure 4.2b), while the second employs an embedded band electrode (Figure 4.2c). The SEC with the embedded band electrode provides a much more desirable configuration, as diffusion at inlaid band electrodes has been previously described.*(2)* The inlaid band electrode also eliminated edge effects that cannot be easily quantified or accounted for when using the raised Pt foil electrode.

Other than the need to create a SEC that allowed for the passage of the SIR beam adjacent to the electrode, reproducible electrochemistry was needed to ensure that there was no significant change in the relative concentration of the electroactive species within the SEC over the entire duration of a SIR study. To avoid this, the solution within the SEC needed to be replaced after every electrochemical reaction that was triggered. A fully automated pumping system was developed and used as it allowed for the solution within the SEC to be exchanged and minimized the time needed to refill the cell between the IR measurements.

Whereas in previous reflection based studies reflection of the IR light off the electrode*(3)* was used and only the spot size was of interest, in this case the nature of the spot is of interest due to

the nature of the SIR beam, which consists of the two parallel ellipsoids with a roughly Gaussian distribution.*(4)* The non-homogenous nature of the IR beam can cause skewing of the reported IR signal if "hot spots" are present. To minimize this effect, the IR beam was defocused to produce a single spot that showed more homogenous illumination and blade apertures rather than circular apertures were employed. The blade aperture increased the spatial resolution by allowing the distance normal to the electrode to be minimized. It also allowed for the positioning of the apertures such that the most homogenous illumination area could be selected. These refinements in the methodology resulted in an increase in the S/N and increased the spatial resolution. This is advantageous as only the first 100 μm away from the electrode edge are expected to give a significant enough change in IR signal to be followed.

Here, the diffusion space around an electrode for two redox systems was studied. The first was the simple one electron transfer of the ferri/ferrocyanide redox couple, the second was the two electron, two proton transfer of the BQ/HQ redox couple. The goal of studying both of these redox systems was to verify the ability of SIR studies to monitor the evolution of diffusion layers as well as determine if quantitative information about the redox species could be obtained. In the systems studied here, the diffusion coefficients of the redox species can be extracted by numerically simulating the experimental data. As a comparison, hydrodynamic linear sweep voltammetry (HLSV) was done to determine the diffusion coefficients of the redox species independently to see if the diffusion coefficient measurements were consistent. For the ferri/ferrocyanide redox couple, the diffusion coefficients from SIR studies and HLSV are consistent, however, these values were inconsistent with the previously reported literature values. As mentioned earlier, this divergence from the literature values was primarily due to the fact that in the literature studies the geometric area of the electrode was used to determine the diffusion coefficient instead of the electrochemically active area of the electrode. This is quite a remarkable result due to the fact that the diffusion coefficients of ferricyanide and ferrocyainde are considered to be well established. This, and the fact that this redox couple displays simple well-described electrochemical behaviour along with readily identifiable spectroscopic signals, has resulted in this redox couple being widely used in electrochemical studies. Many of the studies like this one have used this ideal behaviour of the ferri/ferrocyanide redox couple for the purposes of technique development, as is the case here and as a probe to aid in measurement and analysis.*(5, 6)* The fact that the results presented here have brought to light a discrepancy with

established values could question the validity of previous electrochemical studies using ferri/ferrocyanide. One convenient method for determining electrode areas is to measure voltammetric currents from the ferri/ferrocyanide redox couple and apply the Randles-Sevcik equation. It is quite common to see this method implemented using the diffusion coefficients listed in text books such as Bard and Faulkner [ref]. Clearly the results of this thesis call into question this practice and indicate that electrochemical areas determined in such a fashion are most likely in error by roughly 30%.

In the case of the BQ/HQ redox couple, no known diffusion coefficients of either BQ or HQ in D_2O solvent were previously reported, and as such they needed to be determined independently. The study of diffusion coefficients of BQ and HQ by HLSV and SIR studies were within 10-15%. The discrepancy between the diffusion coefficients determined by SIR studies and HLSV may be due to accelerated decay of the solution used in HLSV that arises from the fact that both HQ and BQ were present in solution and BQ appears to be less stable.

A method has been developed here where a diffusion limited reaction is produced such that the IR beam can be positioned adjacent to the working electrode, resulting in the ability to spatially and temporally monitor the evolution of the resulting diffusion layer produced during an electrochemical reaction. This is evidenced by the consistency of the diffusion coefficients of all the species studied here as determined by the IR based SIR studies and the purely electrochemical HLSV. This spatiotemporal monitoring has resulted in the ability to extract the diffusion coefficients of the redox species. This is a first step towards using this method to studying more complex electrochemical reactions with the ability to monitor the growth/decay of reactant, intermediates and products.

Previous diffusion layer mapping methods, such as SECM and Raman microscopy have been successful in monitoring diffusion produced by electrode processes and are capable of monitoring and analyzing reactions within the diffusion layer. *(7, 8)* However, they have not found widespread application in studying complex electrochemical processes, this is due to the fact that in many cases the methods cannot detect the molecules of interest.

The technique developed here offers a more versatile method that greatly broadens the breadth of electrochemical systems that can be studied. This method is much better tool to study

electrochemical processes of both scientific and industrial interest such as fuel cell reactions (e.g. methanol oxidation) and complex bioelectrochemical conversions (e.g. intracylcization of dopamine).*(9, 10)* Application of the methodology developed herein can provide a full understanding of the processes occurring in the vicinity of the electrode and potentially lead to the development of improved processes.

8.2: Future Work

The methodology developed here is open to improvement. One area that will require further refinement is the design of the SEC. While the current SEC design fulfills optical requirements and the embedded electrode allows for more accurate modeling of the temporal-evolving concentration gradient, there are limitations. It is suspected that the SEC based on the current design will be limited to the 36x objective and in order to reach compatibility with higher magnification objectives, a radically new SEC design is needed. This redesign is required due to the small working distance of higher magnification lenses. Miller *et al* have developed an optical flow cell that is compatible with the 72x objective and is a promising starting point for future possible SECs.*(11)* The ability to couple SEC with these high magnification objective will allow a truly diffusion limited spot to be used.

The current cell is also limited by the fact that it cannot handle solution with high or low pH due to the materials used in its construction, in particular the cyanomethacrylate adhesive. A design based on the cell used by Miller *et al* could be used to overcome this by eliminating the use of adhesives altogether. This would increase the variability of electrochemical reactions that could be studied by SIR studies.

Another aspect of the SEC that could be addressed to improve SIR studies would be to have the working electrode oriented parallel to the focused beams so that the blade apertures could be oriented over one of the elliptical IR spots. This would eliminate the need to defocus the beam to produce a homogenous IR beam spot, however implementing the correct orientation is not trivial and requires the ability to precisely orient the SEC. This could be achieved through the use of a rotation stage to hold the SEC.

As mentioned above, the current SEC is compatible with the 36x objectives, but only the 15x objectives were used here. A beneficial study would be to use the 36x objectives and repeat the SIR studies using the ferri/ferrocyanide redox couple. This study would indicate whether or not increased photon throughput due to the increased focusing of the IR beam would allow for the same signal to noise level to be reached in a smaller amount of time. This could also determine if the use of higher magnification objectives are truly advantageous.

Other than improvements to the measurements of diffusion layers, there is a need to quantify the fitting of the simulated data to the experimental data. The fitting of the simulated curves presented here has been done by eye (solid lines Figures 5.5 and 6.4). While this has produced diffusion coefficients that show good agreement with those produced by HLSV, the diffusion coefficients determined by simulations are still very much qualitative in nature. As such, for further use of this technique a mathematical fitting of the simulated data to the experiment via least-squares regression is necessary. This type of analysis will give a more accurate and reliable diffusion coefficient. However, implementing a fitting routine of this nature is not an "out-of-the-box" optimizing via computer program. Significant resources would be need to be devoted to build a successful routine.

Beyond the improvements in the SEC and refinements in the methodology, the expansion of the use of SIR studies to electrochemical reactions of greater complexity is of great interest. In particular, the Burgess group has immediate plans to study EC type reactions where information about the kinetics and nature of the coupled chemical reaction are not defined. Simulations of the SEC diffusion space for a simple EC reaction (Figure 8.1) are given in Figure 8.2 and show that the formation and decay of the intermediate can be followed at different distances from the electrode.

$$A + e^- \rightarrow B$$

$$B \rightarrow C$$

Figure 8.1: Example of an EC type reaction.

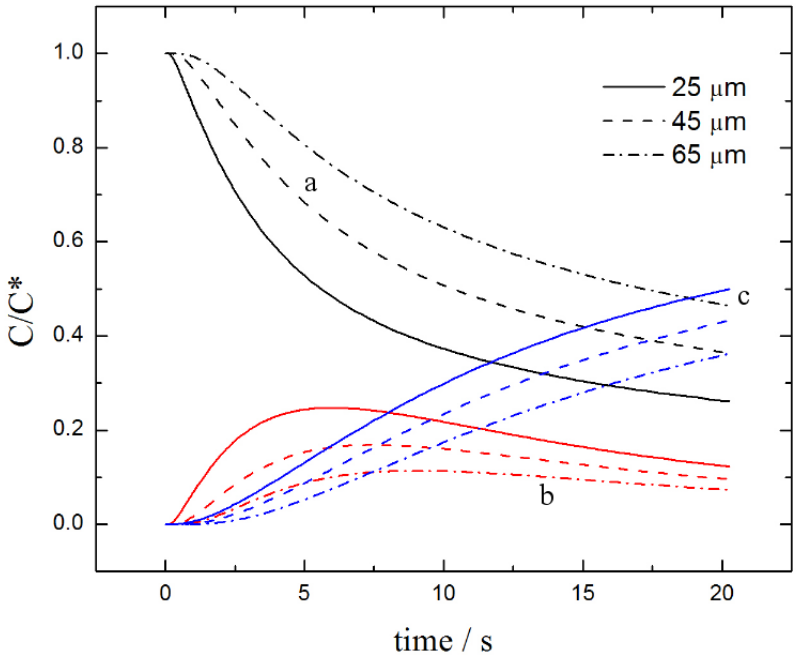

Figure 8.2: Simulation of an EC type electrochemical with the reactant (black, a), intermediate (red, b) and product (blue, c) concentrations shown at various distances from the electrode.

The oxidation of hydroxylamine at gold electrodes offers an EC type reaction system where the reactants and products have clearly distinguishable IR signatures for both products and reactants. The coupled chemical reaction should also be such that it can be monitored effectively by SIR studies.*(12)* This makes the oxidation of hydroxylamine ideal for the verification of SIR studies ability to analyze EC type electrochemical reactions. The validation of SIR studies to examine EC type reactions would open up this methodology to study a number of electrochemical reaction of greater interest.

Beyond this, Gross *et al* have eluded to another aspect of using the spatial resolution of SIR*(13)* as it could easily be translated in order to study electrochemical reaction that involve the flow of solution across the electrode instead of the quiescent solutions studied here.

8.3: References

1. Rosendahl, S. M.; Borondics, F.; May, T. E.; Burgess, I. J. Step-Scan IR Spectroelectrochemistry with Ultramicroelectrodes: Nonsurface Enhanced Detection of Near Femtomole Quantities Using Synchrotron Radiation. *Anal. Chem.* **2013,** *85*, 8722-8727.

2. Bard, A. J.; Faulkner, L. R. *Electrochemical Methods: Fundamentals and Applications*, 2nd ed.; John Wiley and Sons Inc: New York, New York, 2001.

3. Rosendahl, S. M. *Advances in in-Situ Spectroelectrochemical Fourier Transform Infrared Spectroscopy*2013.

4. May, T.; Ellis, T.; Reininger, R. Mid-infrared spectromicroscopy beamline at the Canadian Light Source. *Nuclear Instruments and Methods in Physics Research Section A: Accelerators, Spectrometers, Detectors and Associated Equipment* **2007,** *582*, 111-113.

5. Li, W.; Qian, D.; Li, Y.; Bao, N.; Gu, H.; Yu, C. Fully-drawn pencil-on-paper sensors for electroanalysis of dopamine. *J Electroanal Chem* **2016,** *769*, 72-79.

6. Emery, S. B.; Hubbley, J. L.; Roy, D. Time resolved impedance spectroscopy as a probe of electrochemical kinetics: The ferro/ferricyanide redox reaction in the presence of anion adsorption on thin film gold. *Electrochim. Acta* **2005,** *50*, 5659-5672.

7. Engstrom, R. C.; Weber, M.; Wunder, D. J.; Burgess, R.; Winquist, S. Measurements within the diffusion layer using a microelectrode probe. *Anal. Chem.* **1986,** *58*, 844-848.

8. Amatore*, C.; Bonhomme, F.; Bruneel, J.; Servant*, L.; Thouin, L. Mapping dynamic concentration profiles with micrometric resolution near an active microscopic surface by confocal resonance Raman microscopy. Application to diffusion near ultramicroelectrodes: first direct evidence for a conproportionation reaction. *J Electroanal Chem* **2000,** *484*, 1-17.

9. Matsuda, S.; Kitamura, F.; Takahashi, M.; Ito, M. Dynamic aspects of methanol oxidation on Pt electrodes by time resolved infrared reflection absorption spectroscopy. *Journal of Electroanalytical Chemistry and Interfacial Electrochemistry* **1989,** *274*, 305-312.

10. Engstrom, R. C.; Meaney, T.; Tople, R.; Wightman, R. M. Spatiotemporal description of the diffusion layer with a microelectrode probe. *Anal. Chem.* **1987,** *59*, 2005-2010.

11. Gelfand, P.; Smith, R. J.; Stavitski, E.; Borchelt, D. R.; Miller, L. M. Characterization of Protein Structural Changes in Living Cells Using Time-Lapsed FTIR Imaging. *Anal. Chem.* **2015,** *87*, 6025-6031.

12. Fromondi, I.; Scherson, D. (Bi)Sulfate Adsorption on Quasiperfect Pt(111) Facets from Acidic Aqueous Electrolytes as Monitored by Optical Techniques. *J. Phys. Chem. C* **2007,** *111*, 10154-10157.

13. Gross, E.; Shu, X.; Alayoglu, S.; Bechtel, H. A.; Martin, M. C.; Toste, F. D.; Somorjai, G. A. In Situ IR and X-ray High Spatial-Resolution Microspectroscopy Measurements of Multistep Organic Transformation in Flow Microreactor Catalyzed by Au Nanoclusters. *J. Am. Chem. Soc.* **2014,** *136*, 3624-3629.

Appendix

A: Matlab script

```
%
%--------------------------------------------------------------------%
clear variables
close all
clc
%--------------------------------------------------------------------%
%

%Sets path to retrieve rapid scan single channel spectra
path = 'C:\Users\ladna\Desktop\Data\CLS\Analysis\2015-07-24-Analysis\2015-07-
24-matlab\Rapidscan-65um-4.9mMHQ-0.5MNaF-PBS20mM-pH8-matlab\';

search_path = sprintf('%s*.mat',path);

file_count = 0;
files = dir(search_path);
%The sniftir and DeltaABS matrices must be set so the same number of rows
%as the spectra (same length as the wavenumber points) and the columns must
be set
%to the number of data points (# of individual spectra gathered in the
%rapid-scan measurement)
sniftir = zeros(1271,60);
DeltaABS = zeros (1271,60);

%Loop that co-adds the spectra. Note: the # of loops must be equal to the #
%of columns of the snifter and DeltaABS matrices
for file = files'
    filename = sprintf('%s%s',path,file.name);
    temp = load(filename);
    data = temp.Sc;

    for j=1:1:60
        temp_sniftir = (data(:,j+2)-data(:,2))./data(:,2);
        sniftir(:,j) = sniftir(:,j)+temp_sniftir;
    end;

    file_count = file_count+1;
end;

for i= 1:1:60
    sniftir(:,i) = sniftir(:,i)./file_count;
end;

wavenum = temp.Sc (:,1);

%converts snifter spectra into absrobance spectra and extracts areas of
%interest
DeltaABS = -log10((sniftir+1));
```

```
ABS1658 = DeltaABS(800:885,:);
ABS1512 = DeltaABS(885:950,:);

%output of absorbance data
dlmwrite ('Absorbance1658.dpt', ABS1658);
dlmwrite ('Absorbance1512.dpt', ABS1512);
```

B: LabVIEW program